



# Distinct synovial tissue macrophage subsets regulate inflammation and remission in rheumatoid arthritis

Stefano Alivernini<sup>1,2,3,4</sup> , Lucy MacDonald<sup>1,4,11</sup> , Aziza Elmesmari<sup>1,4,11</sup>, Samuel Finlay<sup>1,4,11</sup>, Barbara Tulusso<sup>2</sup> , Maria Rita Gigante<sup>2</sup>, Luca Petricca<sup>2</sup>, Clara Di Mario<sup>3</sup>, Laura Bui<sup>5</sup>, Simone Perniola<sup>3</sup> , Moustafa Attar<sup>6</sup> , Marco Gessi<sup>5</sup>, Anna Laura Fedele<sup>2</sup>, Sabarinadh Chilaka<sup>4</sup>, Domenico Somma<sup>4</sup>, Stephen N. Sansom<sup>1,6</sup> , Andrew Filer<sup>1,7,8</sup> , Charles McSharry<sup>4</sup> , Neal L. Millar<sup>4</sup> , Kristina Kirschner<sup>9</sup> , Alessandra Nerviani<sup>10</sup> , Myles J. Lewis<sup>10</sup> , Costantino Pitzalis<sup>10</sup> , Andrew R. Clark<sup>17</sup>, Gianfranco Ferraccioli<sup>3</sup> , Irina Udalova<sup>1,6</sup> , Christopher D. Buckley<sup>1,6,7,8</sup> , Elisa Gremese<sup>1,2,3</sup>, Iain B. McInnes<sup>1,4</sup> , Thomas D. Otto<sup>1,4</sup>  and Mariola Kurowska-Stolarska<sup>1,4</sup> 

**Immune-regulatory mechanisms of drug-free remission in rheumatoid arthritis (RA) are unknown. We hypothesized that synovial tissue macrophages (STM), which persist in remission, contribute to joint homeostasis. We used single-cell transcriptomics to profile 32,000 STMs and identified phenotypic changes in patients with early/active RA, treatment-refractory/active RA and RA in sustained remission. Each clinical state was characterized by different frequencies of nine discrete phenotypic clusters within four distinct STM subpopulations with diverse homeostatic, regulatory and inflammatory functions. This cellular atlas, combined with deep-phenotypic, spatial and functional analyses of synovial biopsy fluorescent activated cell sorted STMs, revealed two STM subpopulations (MerTK<sup>pos</sup>TREM2<sup>high</sup> and MerTK<sup>pos</sup>LYVE1<sup>pos</sup>) with unique remission transcriptomic signatures enriched in negative regulators of inflammation. These STMs were potent producers of inflammation-resolving lipid mediators and induced the repair response of synovial fibroblasts in vitro. A low proportion of MerTK<sup>pos</sup> STMs in remission was associated with increased risk of disease flare after treatment cessation. Therapeutic modulation of MerTK<sup>pos</sup> STM subpopulations could therefore be a potential treatment strategy for RA.**

Rheumatoid arthritis is characterized by breach of tolerance to modified self-proteins and chronic synovitis. Current therapies adequately benefit only ~50% of patients; half then relapse after treatment cessation<sup>1–3</sup>. Although rare, long-term drug-free remission suggests that articular immune homeostasis can be reinstated<sup>4</sup>, the mechanisms maintaining remission are poorly characterized. A recent study showing a potential role of ILC2-derived IL-9 in the resolution of experimental arthritis suggests that disease remission might be an active process<sup>5</sup>. A better understanding of mechanisms of remission could inform development of RA and other immune-mediated disease therapeutics.

The immune cells that predominate in synovial tissue of patients in disease remission are STMs, suggesting that they may have a role in reinstating synovial homeostasis. The healthy synovial membrane consists of lining-layer fibroblasts and resident macrophages, and sublining connective tissue and fibroblasts<sup>6</sup>. In mice, embryonic precursors populate the synovium during embryogenesis, proliferate in situ and maintain immune homeostasis<sup>7–9</sup>. Murine Trem2<sup>pos</sup> lining-layer macrophages are long lived, locally renewing

and form a protective epithelial-like barrier that is disrupted during experimental arthritis, and this disruption of synovial distribution is also seen in patients with RA<sup>9</sup>. RA synovitis includes influx of inflammatory macrophages<sup>10–12</sup>, which are probably differentiated from blood-derived monocytes<sup>7,13–15</sup> and are the main producers of pathogenic tumor necrosis factor (TNF)<sup>4,11,16,17</sup>. However, human STM ontogeny remains unresolved.

Recent single-cell transcriptome sequencing (scRNA-seq) analyses have shown that synovial fibroblasts<sup>18–21</sup> and macrophages<sup>19,22</sup> from patients with active RA and osteoarthritis are heterogeneous. The distinct biology of different synovial fibroblast clusters may have important implications for therapies aimed at modulation of inflammation or tissue repair<sup>18</sup>. While inflammatory synovial macrophages has been exploited with great success<sup>23</sup>, the potential therapeutic use of targeting STMs involved in tissue resolution and repair remains unclear. Our understanding of the biology of these cells has been hampered by a lack of sampling from healthy and remission synovium<sup>19,22</sup>, and the absence of robust functional characterization of synovial tissue-derived STMs<sup>19,22</sup>. Our earlier

<sup>1</sup>Research into Inflammatory Arthritis Centre Versus Arthritis (RACE). <sup>2</sup>Division of Rheumatology, Fondazione Policlinico Universitario A. Gemelli IRCCS, Rome, Italy. <sup>3</sup>Institute of Rheumatology, Università Cattolica del Sacro Cuore, Rome, Italy. <sup>4</sup>Institute of Infection, Immunity, and Inflammation, University of Glasgow, Glasgow, UK. <sup>5</sup>Division of Pathology, Fondazione Policlinico Universitario A. Gemelli IRCCS, Rome, Italy. <sup>6</sup>The Kennedy Institute of Rheumatology, University of Oxford, Oxford, UK. <sup>7</sup>Institute of Inflammation and Ageing, University of Birmingham, Birmingham, UK. <sup>8</sup>NIHR Birmingham Biomedical Research Centre, University Hospitals Birmingham NHS Foundation Trust, University of Birmingham, Birmingham, UK. <sup>9</sup>The Institute of Cancer Sciences, University of Glasgow, Glasgow, UK. <sup>10</sup>Centre for Experimental Medicine and Rheumatology, William Harvey Research Institute, Queen Mary University of London, London, UK. <sup>11</sup>These authors contributed equally: Lucy MacDonald, Aziza Elmesmari, Samuel Finlay. ✉e-mail: [stefano.alivernini@unicatt.it](mailto:stefano.alivernini@unicatt.it); [thomasdan.otto@glasgow.ac.uk](mailto:thomasdan.otto@glasgow.ac.uk); [mariola.kurowska-stolarska@glasgow.ac.uk](mailto:mariola.kurowska-stolarska@glasgow.ac.uk)

studies<sup>2,4,24,25</sup> demonstrated that, although most synovial inflammation resolves in RA in sustained clinical and ultrasound remission<sup>2,4</sup>, clusters of synovial tissue macrophages persist, predominantly in the lining layer<sup>4</sup>. In this study we used scRNA-seq, multiparameter flow cytometry, immunofluorescent staining and micrococulture of STM with synovial fibroblasts to explore the phenotypic and functional changes in synovial tissue macrophage subpopulations spanning health, inflammation and disease remission, and uncovered STM-dependent mechanisms that actively maintain remission.

## Results

**MerTK<sup>pos</sup>CD206<sup>pos</sup> STMs are associated with remission maintenance.** To determine the phenotypic spectrum of human STMs, we investigated their relative composition from 45 treatment-naïve active RA, 31 treatment-resistant active RA, 36 sustained clinical and ultrasound remission RA (Supplementary Table 1) and 10 healthy donors, using pan macrophage markers (CD11b and CD64), along with expression of CD163, MerTK and CD206, which were previously reported to be expressed on healthy STMs<sup>11,26</sup>, and murine mature immune-homeostatic tissue macrophages<sup>27–29</sup> (Methods). Healthy donor STMs were mostly MerTK<sup>pos</sup>CD206<sup>pos</sup>. This population of STMs was also substantially increased in patients in disease remission compared to those with active RA, who had fewer of these STMs and significantly increased MerTK<sup>neg</sup>CD206<sup>neg</sup> STMs (Fig. 1a). The CD163<sup>pos</sup> subpopulation of MerTK<sup>pos</sup>CD206<sup>pos</sup> STMs was increased in remission compared to other conditions (Fig. 1b,c). MerTK<sup>pos</sup>CD206<sup>pos</sup>, CD163<sup>pos</sup>CD206<sup>pos</sup> and MerTK<sup>pos</sup>CD163<sup>pos</sup> STM frequencies correlated negatively with disease activity score 28/C-reactive protein (DAS28/CRP; Fig. 1d), systemic disease activity index, synovial hypertrophy and vascularity (Supplementary Figs. 1a,b and 2a,b).

We validated the relationship between STM populations and degree of disease remission using highly stringent Boolean criteria for remission<sup>30</sup> (Methods). Among 36 patients with RA in DAS28-defined sustained remission, 11 also met Boolean remission criteria at the time of synovial biopsy. MerTK<sup>pos</sup>CD206<sup>pos</sup> STM frequency patterns were consistent across two different definitions of remission. However, patients with Boolean remission exhibited increased MerTK expression-density on MerTK<sup>pos</sup>CD206<sup>pos</sup> STMs (Fig. 1e) and had increased frequencies of CD163-expressing STMs compared with DAS28-defined remission (Fig. 1f–h and Extended Data Fig. 1a–d).

Next, we investigated the clinical significance of the relative proportions of MerTK<sup>pos</sup> and MerTK<sup>neg</sup> STMs by monitoring subsequent occurrence of flare after treatment withdrawal. All 36 patients with RA that achieved sustained clinical and ultrasound remission had received identical treatment (TNF inhibitor + methotrexate (MTX)) (Methods) before synovial biopsy. Twenty-two patients with RA consented to taper and then discontinue biological treatment following biopsy collection. Of these, 11 patients flared within 6 months of treatment modification (mean  $\pm$  s.e.m.,  $3.7 \pm 0.38$  months) while 11 maintained remission ( $21.45 \pm 2.44$  months at the time of manuscript submission). Those who maintained remission had higher relative proportions of MerTK<sup>pos</sup>CD206<sup>pos</sup> STMs at the time of synovial tissue biopsy compared to those who flared (Fig. 1i–j and Extended Data Fig. 1e–i). We hypothesized that the STM phenotypic profile may provide a biomarker predictive of disease flare after treatment modification. Therefore, we examined whether the proportions of individual and/or combined STM populations could predict flare in RA in remission using logistic regression analysis. The proportions of the MerTK<sup>neg</sup>CD206<sup>neg</sup> population or MerTK<sup>pos</sup>CD206<sup>pos</sup>CD163<sup>pos</sup> subpopulation per se were insufficient to predict flare. However, the ratio of MerTK<sup>pos</sup>CD206<sup>pos</sup> to MerTK<sup>neg</sup>CD206<sup>neg</sup>  $\leq 2.5$  and a proportion of MerTK<sup>pos</sup>CD206<sup>pos</sup> STMs  $\leq 47.5\%$  emerged as independent factors predicting disease flare at the time of treatment tapering and discontinuation (odds ratios 16.2 (95% confidence interval,

2.61–100.45) and 13.5 (95% confidence interval, 2.26–80.79), respectively) (Fig. 1k and Extended Data Fig. 1j–k).

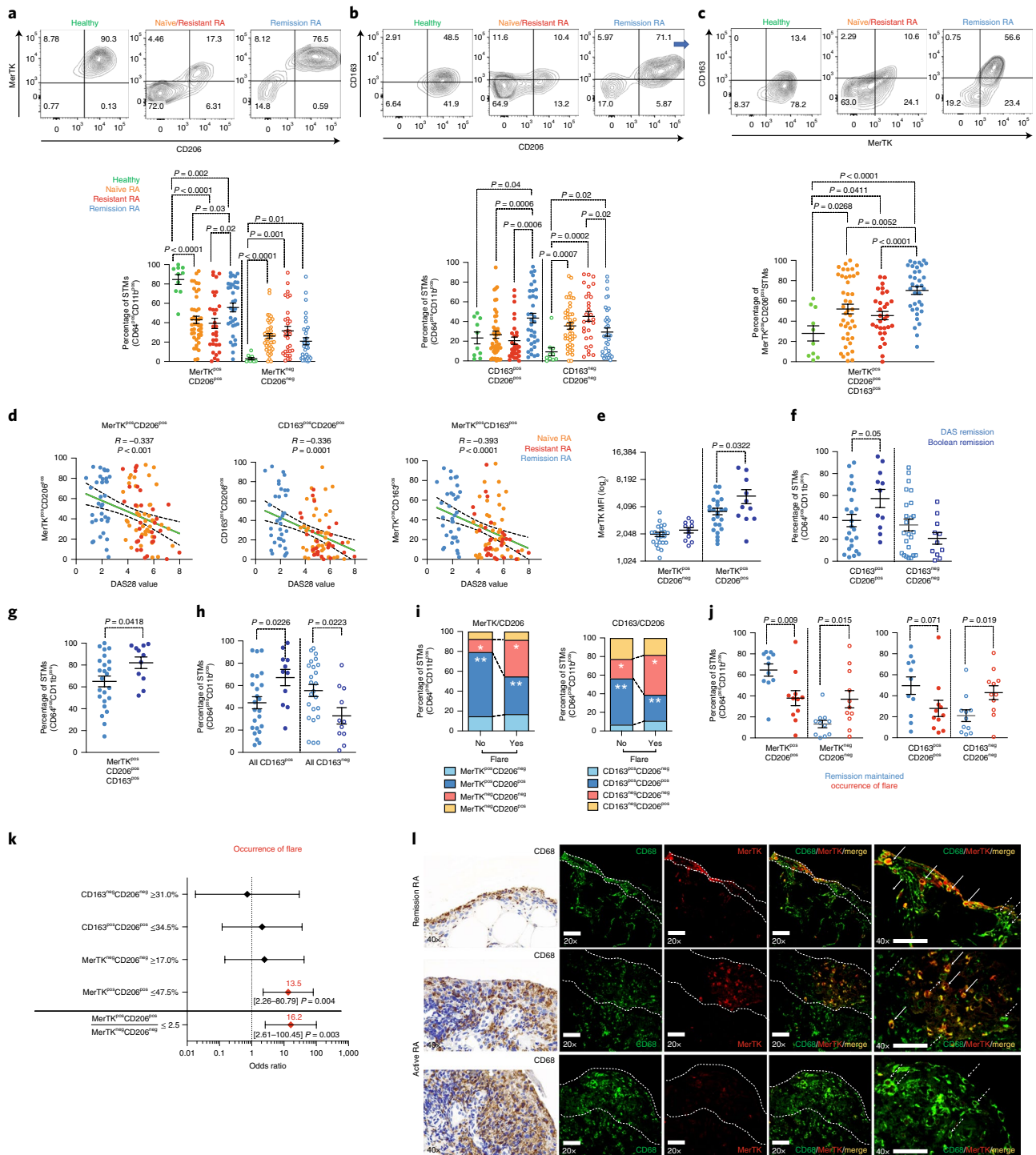
Next, we used immunohistochemistry/immunofluorescence (IHC/IF) to explore the synovial tissue localization of MerTK<sup>pos</sup> STMs. In accordance with flow cytometry (Fig. 1a), the majority of STMs (CD68<sup>pos</sup>) in remission were MerTK<sup>pos</sup> and formed a tight lining layer whereas in active RA many lining-layer CD68<sup>pos</sup> cells lacked MerTK but, if present, these were dispersed in the sublining layer (Fig. 1l).

Together, these data suggest that the relative proportions of MerTK<sup>pos</sup>CD206<sup>pos</sup> versus MerTK<sup>neg</sup>CD206<sup>neg</sup> STM populations characterize distinct clinical phases of RA.

**Heterogeneity of MerTK<sup>pos</sup>CD206<sup>pos</sup> and MerTK<sup>neg</sup>CD206<sup>neg</sup> STM populations.** To better understand the heterogeneity and change in patterns of human MerTK<sup>pos</sup>CD206<sup>pos</sup> and MerTK<sup>neg</sup>CD206<sup>neg</sup> STM populations during development and resolution of arthritis, we performed unbiased scRNA-seq, followed by validation with flow cytometry and immunofluorescent IHC staining, of CD11b<sup>pos</sup>CD64<sup>pos</sup> STMs from patients with treatment-naïve RA, treatment-resistant RA and RA in sustained remission. For comparison, we included STMs from healthy and pathological control (autoantibody-negative, undifferentiated peripheral arthritis<sup>31</sup>) (Extended Data Fig. 2a,b and Supplementary Table 2). Initial scRNA-seq of whole synovium provided unbiased confirmation that CD11b and CD64 markers captured the entirety of the STM compartment. Some of these STMs also expressed CD1c (a dendritic cell (DC) marker), and these STMs were also included in STM sorting and subsequent scRNA-seq (Extended Data Fig. 2c). In total, we analyzed 32,141 STMs (>5,000 per condition) and identified nine distinct STM clusters (Fig. 2a and Supplementary Tables 2–4), each characterized by the expression of 63–432 unique genes (Fig. 2b,c).

We next examined the developmental relationship between these nine clusters using diffusion map analysis (Fig. 2d), hierarchical clustering analysis (Fig. 2e) and gene expression of MerTK, CD163 and CD206 (Fig. 2f). Collectively, these approaches classified the STMs into four subpopulations: TREM2<sup>pos</sup>, FOLR2<sup>high</sup>, HLA<sup>pos</sup> and CD48<sup>pos</sup>. MerTK<sup>pos</sup> STMs comprise the subpopulations TREM2<sup>pos</sup> and FOLR2<sup>high</sup>, and MerTK<sup>neg</sup> STMs comprise subpopulations HLA<sup>pos</sup> and CD48<sup>pos</sup> (taxonomy proposed in Fig. 2g). The TREM2<sup>pos</sup> subpopulation contains two of the nine described clusters, TREM2<sup>low</sup> and TREM2<sup>high</sup>, the latter being further distinguished by coexpression of TIMD4 and CD163. The FOLR2<sup>high</sup> subpopulation contains three clusters, defined as ID2<sup>pos</sup>, LYVE1<sup>pos</sup> or ICAM1<sup>pos</sup>. The HLA<sup>pos</sup> subpopulation of MerTK<sup>neg</sup>STMs contains two clusters distinguished by either an interferon signature (ISG15<sup>pos</sup>CLEC10A<sup>low</sup> cluster) or antigen-presenting-cell signature (CLEC10A<sup>high</sup>HLA<sup>high</sup> cluster). Finally, the CD48<sup>pos</sup> subpopulation contains two clusters enriched in expression of either alarmins (S100A12<sup>pos</sup>) or osteopontin (SPP1<sup>pos</sup>CD9<sup>pos</sup> cluster). The SPP1<sup>pos</sup> and ISG15<sup>pos</sup> clusters were previously noted in the synovium of active RA<sup>19</sup>.

To discover condition-specific STM profiles and genes indicative of mechanisms of homeostasis, pathogenesis and resolution of arthritis, we next compared differences in the relative proportions of the nine clusters and their unique Gene Ontology (GO) pathway signatures between clinical states (Fig. 2h and Supplementary Fig. 3a). As expected, healthy synovium contains predominantly MerTK<sup>pos</sup> STMs comprising TREM2<sup>pos</sup> and FOLR2<sup>high</sup> subpopulations. GO and ingenuity pathway analysis revealed that both subpopulations are enriched in complement and defensin pathways (contrasting with MerTK<sup>neg</sup> STMs), suggesting efferocytosis and antimicrobial functions (Extended Data Fig. 3a). They also show high expression of genes of retinoic acid production (for example, *ALDH1A1*) driving regulatory T-cell differentiation<sup>32</sup> and the B7-related coinhibitory molecule *VSIG4*, which inhibits T-effector cells<sup>33</sup>, suggesting a role in the local regulation of adaptive immunity. Healthy synovium



**Fig. 1 | MerTK<sup>pos</sup>CD206<sup>pos</sup> STMs are associated with remission maintenance.** **a–c**, Expression of MerTK, CD206 and CD163 on STMs distinguishes two main populations: MerTK<sup>pos</sup>CD206<sup>pos</sup> and MerTK<sup>neg</sup>CD206<sup>pos</sup>. CD163 was found exclusively on MerTK<sup>pos</sup>CD206<sup>pos</sup> STMs. One-way ANOVA with Tukey's correction or two-sided Mann-Whitney was used. Representative and quantitative data are presented. **d**, Two-tailed Spearman's correlation between DAS28 and the frequencies of MerTK<sup>pos</sup>CD206<sup>pos</sup>, CD163<sup>pos</sup>CD206<sup>pos</sup> and MerTK<sup>pos</sup>CD163<sup>pos</sup> STMs. Dashed lines represent 95% confidence intervals. For **a–c**, healthy (n = 10); for **a–d**, naïve RA (n = 43), resistant RA (n = 30) and RA in remission (n = 36). **e**, Comparison of MerTK expression. **f–h**, Distribution of CD163<sup>pos</sup>CD206<sup>pos</sup> (**f**), MerTK<sup>pos</sup>CD163<sup>pos</sup>CD206<sup>pos</sup> (**g**) and total CD163<sup>pos</sup> STMs (**h**) between RA in DAS-based remission (n = 24) and Boolean remission (n = 11). Two-sided Mann-Whitney was used. **i**, Comparison of STM distribution in patients with RA who maintained remission (n = 11) and those who flared (n = 11); CD163/CD206: \*P < 0.0001, \*\*P = 0.0032; two-way ANOVA with Sidak's correction. **j**, Relative proportions of MerTK<sup>pos</sup>CD206<sup>pos</sup>- and CD163<sup>pos</sup>CD206<sup>pos</sup>-positive and -negative STMs in patients in remission (n = 11) versus flare (n = 11), two-sided Mann-Whitney test. **k**, Odds ratio of occurrence of flare in remission RA (n = 22, log-rank test, 95% confidence interval in parentheses). **l**, Representative IHC images (three independent experiments) of CD68 (brown) and IF staining of CD68 (green), MerTK (red) and nuclei (blue) in synovium of RA in remission (n = 6) and with naïve active disease (n = 6). The dotted lines mark lining/sublining areas, white arrows indicate CD68<sup>pos</sup>MerTK<sup>pos</sup> STMs and white dashed arrows indicate CD68<sup>pos</sup>MerTK<sup>neg</sup> STMs. Scale bars, 100 μm. Data in **a–k** are derived from at least 22 independent experiments. Data in **a–c**, **e–h** and **j** are mean ± s.e.m., with values for individual patients plotted.

had the highest proportion of the TREM2<sup>high</sup> cluster compared with RA. TREM2<sup>high</sup> STMs have a distinct transcriptome indicative of phagocytosis—for example, high expression of scavenger receptors (for example, *TIMD4*), lipid-binding proteins (for example, *APOE*) and components of the phagosome—together suggesting a role in clearing of microbes, apoptotic cells and oxysterols. Their high expression of *MERTK* and *LILRB5*, which inhibit TLR/cytokine<sup>34</sup>- and integrin/FcγR<sup>35</sup>-driven activation, respectively, suggests that they restrain inflammation. Early undifferentiated arthritis (UPA) showed increased proportions of the MerTK<sup>pos</sup>TREM2<sup>low</sup> cluster, which was closely related by transcriptomics to TREM2<sup>high</sup> STMs, had increased oxidative phosphorylation and cytoskeletal pathways and may represent an early activation phenotype of the protective TREM2<sup>high</sup> STMs.

Treatment-naïve and -resistant active RA had reduced MerTK<sup>pos</sup> clusters (TREM2<sup>high</sup> and LYVE1<sup>pos</sup>) and increased proportions of MerTK<sup>neg</sup>CD48<sup>neg</sup>SPP1<sup>pos</sup> and MerTK<sup>neg</sup>CD48<sup>neg</sup>S100A12<sup>pos</sup> clusters (Fig. 2h and Supplementary Fig. 3a), with transcriptomes suggesting proinflammatory phenotypes (Extended Data Fig. 3b). The top marker of the SPP1<sup>pos</sup> cluster (osteopontin) has proinflammatory and bone-resorbing properties<sup>36</sup> and high levels of glycolytic enzymes, cytoskeletal proteins and integrins, suggesting an activated and migratory phenotype. The S100A12<sup>pos</sup> cluster is characterized by abundance of the inflammation-triggering alarmins S100A8/9/12, which are chemoattractants for neutrophils and inducers of monocyte and fibroblast production of TNF and IL-6, respectively<sup>37</sup>. In sustained remission RA, the SPP1<sup>pos</sup> cluster was absent but the S100A12<sup>pos</sup> cluster persisted (Fig. 2h).

Patients with RA in sustained remission were characterized by an increase in the MerTK<sup>pos</sup>FOLR2<sup>high</sup>LYVE1<sup>pos</sup> cluster. LYVE1 plays a role in perivascular localization<sup>38</sup>, and this cluster expresses genes related to collagen turnover, antiprotease enzymes, coagulation factors and regulators of vascular endothelial growth factor (Extended Data Fig. 3a) which, collectively, suggest a role in synovial tissue remodeling and homeostasis.

The proportions of clusters MerTK<sup>neg</sup>CLEC10a<sup>high</sup>, MerTK<sup>pos</sup>ID2<sup>pos</sup> and MerTK<sup>pos</sup>ICAM1<sup>pos</sup> were similar in healthy and RA synovial tissues (Fig. 2h). MerTK<sup>pos</sup>ID2<sup>pos</sup> STMs may be the human equivalent of mouse macrophage colony-stimulating factor (M-CSF)-driven in situ precursors of resident STMs<sup>9</sup> (Extended Data Fig. 4a,b), given their high expression of both *M-CSF-R* and *ID2*, which encodes a driver of self-renewing hemopoietic stem cells<sup>39</sup> (Extended Data Fig. 4c). The CLEC10a<sup>high</sup> cluster is enriched in antigen-presentation pathway genes, DC markers<sup>40</sup> and DC transcription factors (for example, *NR4A3*<sup>41</sup>), suggesting that this population represents synovial tissue-resident antigen presenting cells (Extended Data Fig. 3b). We also found increased expression of HBEGF, which was shown to promote synovial fibroblast invasiveness in active RA<sup>22</sup>, in this cluster in early inflammation (Supplementary Fig. 3b,c). The MerTK<sup>pos</sup>ICAM1<sup>pos</sup> STMs form a small cluster (~0.025% of all STMs and similar across all joint

conditions) that is characterized by high expression of proinflammatory cytokine genes (for example, *TNF*) (Fig. 2b,c), which suggests that they may form the first line of defense against pathogens in the joint (Fig. 2h).

To orthogonally validate the scRNA-seq classification of STM clusters, we next investigated the expression of markers of the most prominent subpopulations/clusters by multiparameter flow cytometry of additional RA and healthy synovial tissues, in conjunction with the initial STM MerTK classification (Fig. 2g). The majority of STMs from healthy and remission RA, but only ~50% of STMs from active RA, were MerTK<sup>pos</sup>FOLR2<sup>pos</sup> (Extended Data Fig. 5a–c), in agreement with scRNA-seq data and initial phenotyping (Fig. 1). Patients with active RA showed a decrease in the proportion of the TREM2<sup>pos</sup> subpopulation (defined as MerTK<sup>pos</sup>TREM2<sup>pos</sup>) and LYVE1<sup>pos</sup> cluster (defined as MerTK<sup>pos</sup>LYVE1<sup>pos</sup>) compared to healthy synovium. These proportions were restored in patients in sustained disease remission to levels similar to (TREM2<sup>pos</sup>), or significantly higher than (LYVE1<sup>pos</sup>), those in healthy tissue (Fig. 2i and Extended Data Fig. 5d). Regarding the MerTK<sup>neg</sup> STM population (CD48<sup>pos</sup>; Methods) (Fig. 2j and Extended Data Fig. 5e), clusters SPP1<sup>pos</sup> (identified as CD48<sup>pos</sup>CD9<sup>pos</sup>CLEC10a<sup>neg</sup>) and S100A12<sup>pos</sup> (identified as CD48<sup>pos</sup>CD9<sup>neg</sup>CLEC10a<sup>neg</sup>) were scarce in health and remission (SPP1<sup>pos</sup> cluster), abundant in active RA and present but reduced in sustained disease remission (cluster S100A12<sup>pos</sup>) (Fig. 2k and Extended Data Figs. 5f,g and 6a,b). We also investigated the signature expression of these STM clusters in an independent pathobiology of early arthritis cohort (PEAC)<sup>42,43</sup> (Methods). Analysis confirmed that expression of SPP1 and S100A9, the top two markers of clusters MerTK<sup>neg</sup>SPP1<sup>pos</sup> and MerTK<sup>neg</sup>S100A12<sup>pos</sup>, correlated positively with disease activity (Fig. 2l). These findings validated the classification of STM subpopulations based on scRNA-seq (Fig. 2g) and corroborate their proportional differences in health, synovitis and remission.

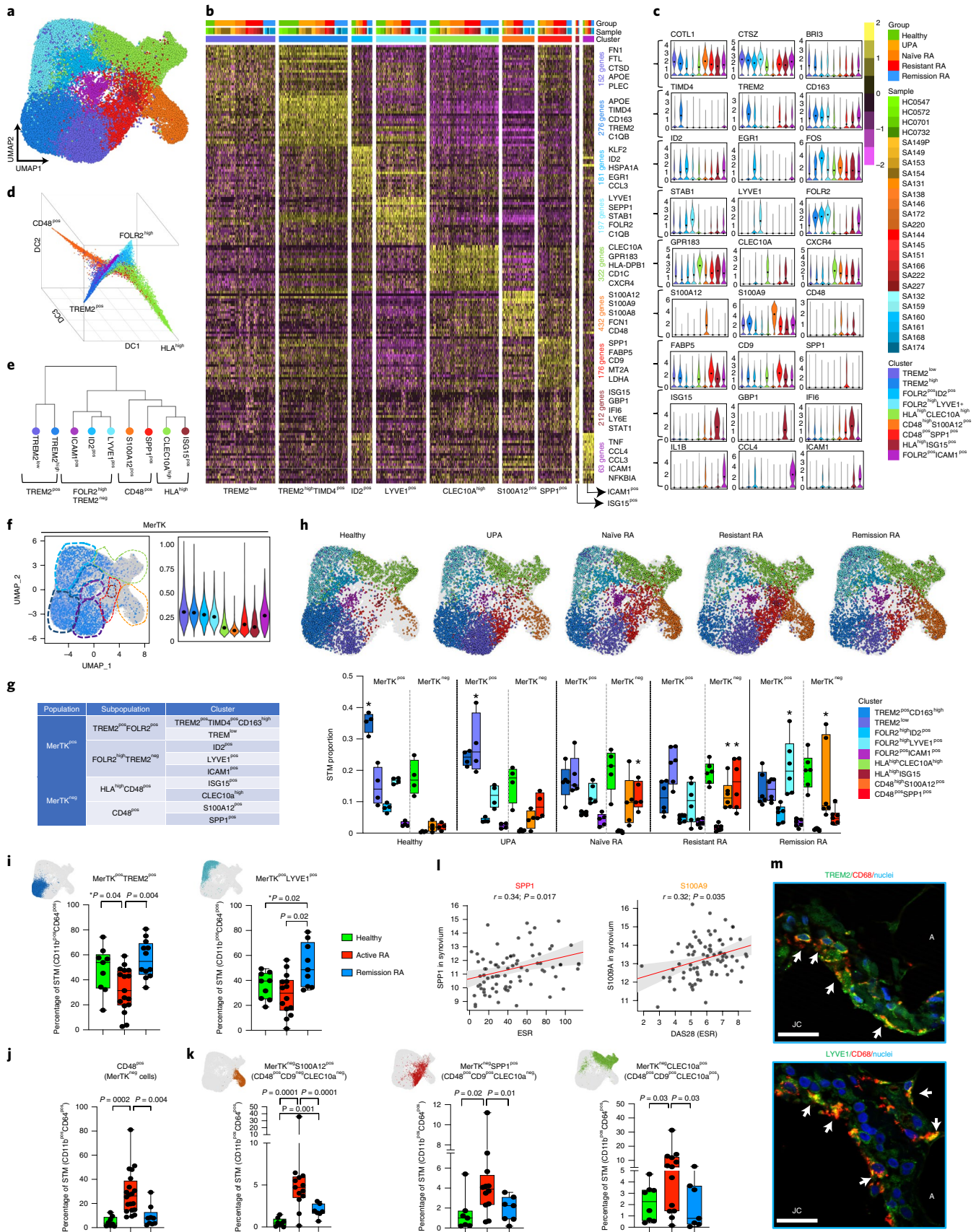
The scRNA-seq analysis showed similar proportions of the MerTK<sup>neg</sup>CLEC10a<sup>high</sup> cluster between clinical conditions; however, flow cytometry revealed increased CLEC10a<sup>pos</sup>CD48<sup>pos</sup>CD9<sup>pos</sup> STMs in active RA compared with health and remission RA (Fig. 2k), suggesting a minor phenotype requiring further characterization.

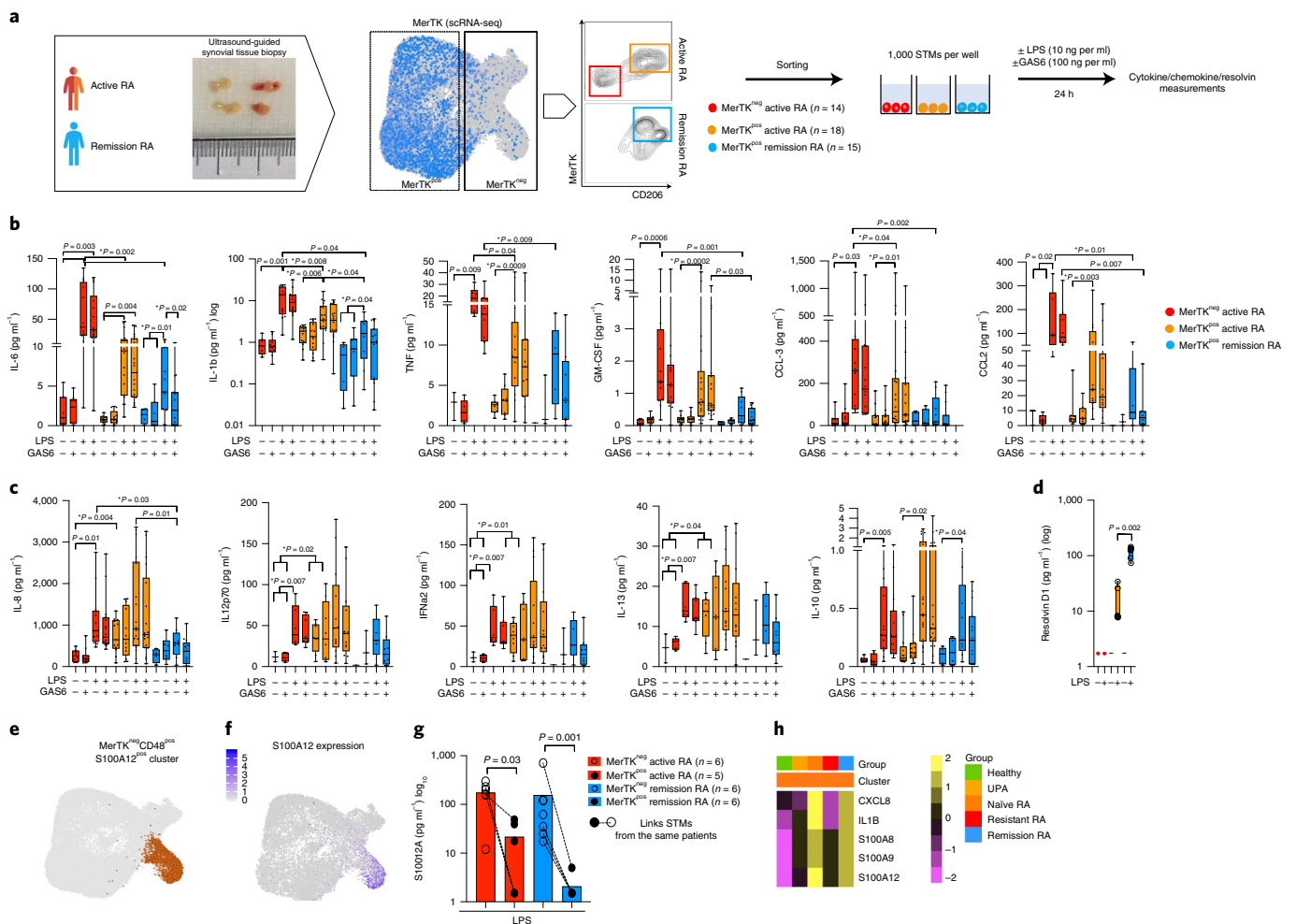
Next, we investigated the tissue distribution of STM clusters, as categorized by scRNA-seq, by fluorescence IHC (Methods) and found MerTK<sup>pos</sup>TREM2<sup>pos</sup> STMs forming a neat lining layer in healthy and remission RA synovium that was disrupted and dispersed in both layers in active RA (Fig. 1m and Extended Data Fig. 7a–c), consistent with recent findings<sup>9</sup>. Hierarchical clustering of the average expression of orthologous genes of human and mouse STMs confirmed that TREM2<sup>high</sup> STMs were homologs of mouse<sup>9</sup> lining layer Trem2<sup>pos</sup>Cx3cr1<sup>pos</sup> STMs, and expressed similar tight-junction genes, suggesting that human TREM2<sup>high</sup> STMs have comparable barrier functions (Extended Data Fig. 4a–d). The MerTK<sup>pos</sup>LYVE1<sup>pos</sup>FOLR2<sup>high</sup> cluster was also localized predominantly in the lining layer in both healthy and remission RA, while in active RA this cluster was localized around blood vessels

**Fig. 2 | scRNA-seq defines heterogeneity within MerTK<sup>pos</sup>CD206<sup>pos</sup> and MerTK<sup>neg</sup>CD206<sup>neg</sup> STM populations.** **a**, UMAP of nine STM clusters identified by scRNA-seq analysis. **b**, Heatmap of the top 20 DEGs per cluster. Top cluster markers and the total number of genes characterized in each cluster are provided. **c**, Violin plots representing log-normalized expression values of STM cluster markers; medians marked by black dots and cluster identity by individual coloring. **d**, Relationship between clusters embedded in the top three diffusion map components. **e**, Hierarchical clustering of STMs. **f**, MerTK expression in the nine STM clusters. **g**, Proposed classification of human STMs. **h**, Split UMAP and dot plots of relative changes in STM clusters between groups. Significant differences (\**P* < 0.05) between the given condition and at least two other conditions in two-way ANOVA with Tukey's correction. Precise *P* values are given in Supplementary Fig. 3a. **a–h**, Data from healthy (*n* = 4), UPA (*n* = 4), naïve active RA (*n* = 5), treatment-resistant RA (*n* = 6) and RA in remission (*n* = 6) in five independent experiments. **i–k**, Flow cytometry validation of scRNA-seq clusters in synovial tissues from healthy (*n* = 9), active RA (*n* = 14–17) and remission (*n* = 9–12). **i**, TREM2<sup>pos</sup>MerTK<sup>pos</sup> and LYVE1<sup>pos</sup>MerTK<sup>pos</sup>. **j**, MerTK<sup>neg</sup>CD48<sup>pos</sup>. **k**, MerTK<sup>neg</sup>CD48<sup>pos</sup>S100A12<sup>pos</sup>, MerTK<sup>neg</sup>CD48<sup>pos</sup>SPP1<sup>pos</sup> and MerTK<sup>neg</sup>CD48<sup>pos</sup>CLEC10a<sup>pos</sup> cluster. One-way ANOVA with Dunn's correction or two-sided Mann-Whitney test; each patient is represented by one dot. **l**, Two-tailed Spearman's correlation between synovial expression of S100A9 and SPP1 with disease activity in the PEAC cohort (*n* = 90). **m**, Representative confocal microscopy of TREM2 or LYVE1 (green) and CD68 (red) from synovial tissue of RA in remission. White arrows indicate double-positive cells (TREM2<sup>pos</sup>CD68<sup>pos</sup> and LYVE1<sup>pos</sup>CD68<sup>pos</sup>). Scale bars, 50 μm. A, adipocytes; JC, joint cavity.

in the sublining layer (Fig. 1m and Extended Data Fig. 8a–c). FOLR2<sup>high</sup>LYVE1<sup>pos</sup> STMs transcriptionally closely resembled mouse resident interstitial Relm $\alpha$ <sup>pos</sup> STMs<sup>9</sup> (Extended Data Fig. 4a–d).

The MerTK<sup>neg</sup>CLEC10a<sup>pos</sup> cluster was exclusively located in the sublining layer adjacent to lining-layer TREM2<sup>pos</sup> STMs in all synovial tissues (Extended Data Fig. 9a–c). Not all CLEC10a<sup>pos</sup> cells



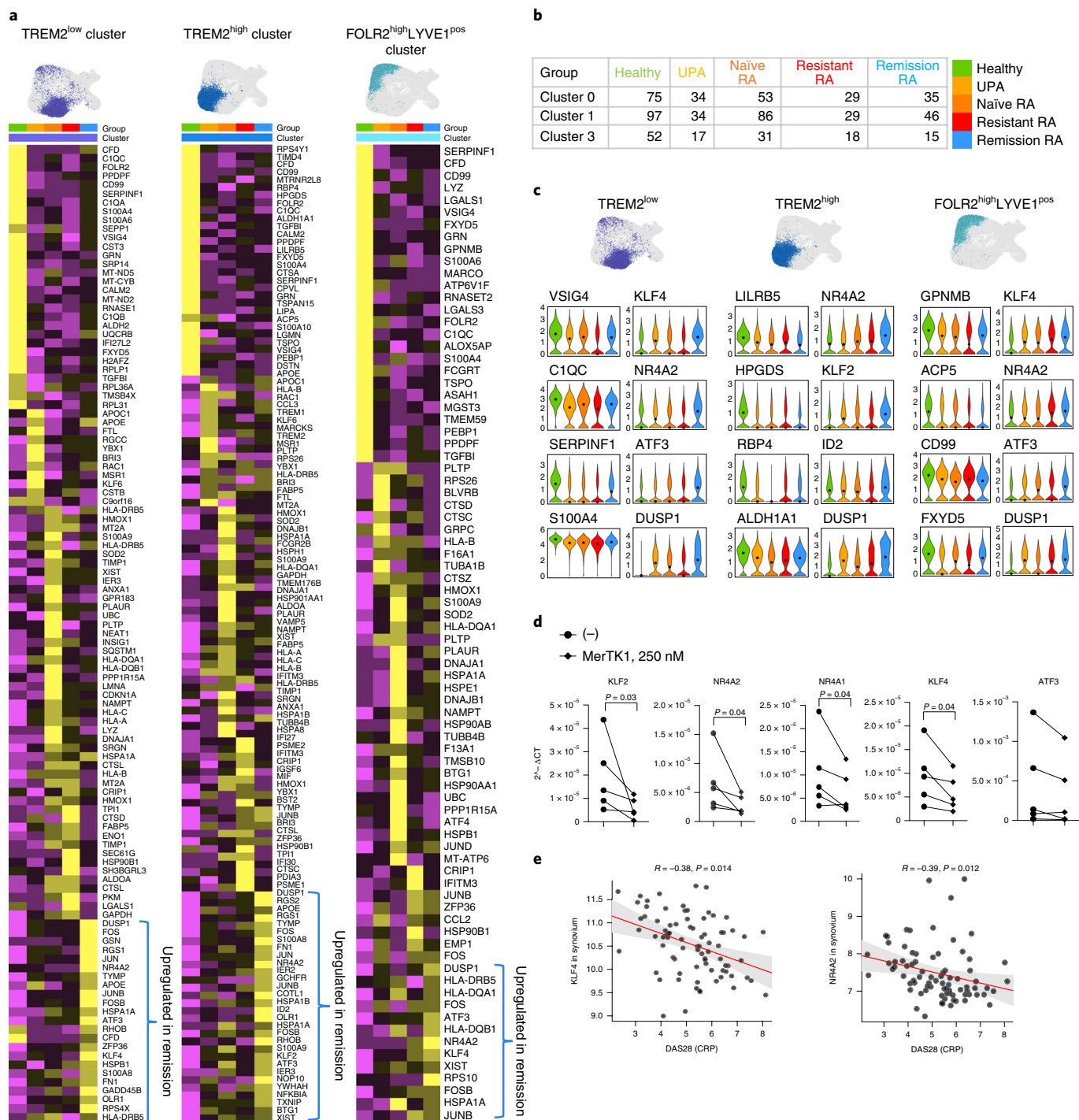


**Fig. 3 | MerTK<sup>neg</sup>CD206<sup>neg</sup> and MerTK<sup>pos</sup>CD206<sup>pos</sup> STM populations have distinct pro- and anti-inflammatory phenotypes.** **a**, Overview of sorting strategy for MerTK<sup>pos/neg</sup> STMs ( $n = 47$ ). **b, c**, In vitro production of pro-inflammatory (**b**) and immune (**c**) mediators. IL-6, IL-1 $\beta$ , GM-CSF, CCL3, IL-8 and IL-10 from active RA (MerTK<sup>neg</sup> STMs,  $n = 15$  and MerTK<sup>pos</sup> STMs,  $n = 18$ ) and RA in remission ( $n = 14$ ). TNF, CCL2, IL-12, IFN $\alpha$ 2 and IL-13 from active RA (MerTK<sup>neg</sup> STMs,  $n = 8$  and MerTK<sup>pos</sup> STMs,  $n = 14$ ) and RA in remission ( $n = 8$ ). Exact  $P$  values are shown, One-way ANOVA (Kruskal-Wallis) with Dunn's correction or two-sided Mann-Whitney (marked with \* when two conditions compared). **d**, Resolvin D1 production by MerTK<sup>neg</sup> from active RA ( $n = 7$ ), MerTK<sup>pos</sup> from active RA ( $n = 6$ ) and MerTK<sup>pos</sup> STMs from RA in remission ( $n = 6$ ). Two-sided Mann-Whitney, exact  $P$  values shown. **b–d**, Box plots with median, 25th/75th percentiles and whiskers from minimum to maximum, and individual values plotted. **e, f**, UMAPs illustrating cluster MerTK<sup>neg</sup>CD48<sup>pos</sup>S100A12<sup>pos</sup> (**e**) and S100A12 mRNA expression in this cluster (**f**) from healthy ( $n = 4$ ), UPA ( $n = 4$ ) and naïve active RA ( $n = 5$ ), treatment-resistant RA ( $n = 6$ ) and RA in remission ( $n = 6$ ). **g**, Production of S100A12 by LPS-stimulated MerTK<sup>neg</sup>CD206<sup>neg</sup> and MerTK<sup>pos</sup>CD206<sup>pos</sup> STMs sorted from active RA ( $n = 6$ ) or remission RA ( $n = 6$ ). Mean  $\pm$  s.e.m., two-sided Mann-Whitney, exact  $P$  values shown, two independent experiments. **h**, Heatmap showing proinflammatory mediators differentially expressed in the cluster MerTK<sup>neg</sup>CD48<sup>pos</sup>S100A12<sup>pos</sup> between conditions in the patient cohort as in **f**.  $P < 0.05$ , MAST with Bonferroni. US, ultrasound-guided.

were CD68<sup>pos</sup>, consistent with our earlier scRNA-seq data suggesting that CLEC10a is a marker for tissue-resident DCs (CD68<sup>neg</sup>) and interferon-signature (ISF15<sup>pos</sup>) STMs. The clusters MerTK<sup>neg</sup>S100A12<sup>pos</sup> and SPP1<sup>pos</sup> were restricted to the sublining layer, and were abundant in active RA and scarce in healthy and remission RA, confirming scRNA-seq and fluorescent activated cell sorter (FACS) data (Extended Data Fig. 9d–i). Collectively, these data systematically map the heterogeneity in MerTK<sup>neg</sup> and MerTK<sup>pos</sup> STM populations spanning different clinical states.

**MerTK<sup>neg</sup>CD206<sup>neg</sup> and MerTK<sup>pos</sup>CD206<sup>pos</sup> populations have distinct proinflammatory and resolving mediator profiles.** To evaluate MerTK<sup>pos</sup> and MerTK<sup>neg</sup> STM functions, we performed ex vivo stimulations using lipopolysaccharide (LPS), which binds TLR4 and elicits proinflammatory cytokine secretion and/or GAS6 to activate MerTK (Fig. 3a; Methods). In response to LPS stimulation, MerTK<sup>neg</sup> STMs produced significantly more

proinflammatory cytokines than MerTK<sup>pos</sup> STMs from either active or remission RA (Fig. 3b). Following stimulation, all STM populations produced similar concentrations of tissue-remodeling cytokines and the anti-inflammatory cytokine IL-10, irrespective of clinical state (Fig. 3c). The inflammation-resolving lipid mediator resolvin D1 was released only by MerTK<sup>pos</sup> STMs, and concentrations were significantly higher in culture supernatants of STMs from disease remission (Fig. 3d). The production of resolvin by MerTK<sup>pos</sup> STMs was consistent with this population, including the TREM2<sup>pos</sup> cluster, which is enriched in pathways of lipid mediator production (Extended Data Fig. 3a). Moreover, addition of GAS6 reduced LPS-induced production of proinflammatory cytokines by MerTK<sup>pos</sup> STMs from remission RA (Fig. 3b), suggesting a GAS6/MerTK negative feedback mechanism in remission MerTK<sup>pos</sup>CD206<sup>pos</sup> STMs. This, together with the higher ratio of resolvin and IL-10 to proinflammatory cytokines produced by remission MerTK<sup>pos</sup>CD206<sup>pos</sup> STMs, suggests they may promote resolution.



**Fig. 4 | MerTK<sup>pos</sup> STM clusters from patients in remission have a unique regulatory signature. a**, Heatmaps illustrating scaled expression of the top 30 marker genes of each condition within clusters TREM2<sup>low</sup>, TREM2<sup>high</sup> and FOLR2<sup>high</sup>LYVE1<sup>pos</sup>. Rows include genes and columns show pseudo-bulk expression per condition within each cluster. All genes were expressed in at least 60% of cells in that condition, with average log fold-change  $\geq 0.25$  ( $P < 0.05$  MAST, corrected for multiple comparison with Bonferroni). **b**, Numbers of genes differentially expressed between conditions for each cluster. **c**, Violin plots representing log-normalized expression values of top DEGs of clusters TREM2<sup>pos</sup> and FOLR2<sup>pos</sup> in healthy or remission STMs, with medians marked by black dots and cluster identity by color. **a–c**, STM samples from healthy ( $n = 4$ ), UPA ( $n = 4$ ), naïve active RA ( $n = 5$ ), treatment-resistant RA ( $n = 6$ ) and RA in remission ( $n = 6$ ). **d**, Transcription factors identified in clusters TREM2<sup>pos</sup> and FOLR2<sup>pos</sup> in remission are inhibited in macrophages incubated with MerTK inhibitor ( $n = 5$  independent samples in three independent experiments); paired two-sided  $t$ -test, exact  $P$  values are given. **e**, Synovial tissue expression of *KLF4* and *NRA42* in PEAC cohort negatively correlates with DAS28 ( $n = 90$ ). Two-tailed Spearman's correlation; gray-shaded area, 95% confidence interval;  $R$  and  $P$  values shown.

scRNA-seq revealed that the CD48<sup>pos</sup>S100A12<sup>pos</sup> subpopulation of MerTK<sup>neg</sup> STMs may persist in remission. Consistent with their high *S100A12/8/9* expression, only MerTK<sup>neg</sup> STMs produced high levels of alarmins after LPS stimulation,

which was irrespective of clinical state (Fig. 3e–h). Collectively, our in vitro stimulation data suggest that MerTK<sup>neg</sup> and MerTK<sup>pos</sup> STMs have distinct proinflammatory and tissue-resolving properties.

**MerTK<sup>pos</sup> STM clusters from patients in remission have a unique regulatory signature.** To investigate the molecular signature underlying the resolving phenotype of remission MerTK<sup>pos</sup> STM clusters, we compared their transcriptomic profiles across health, joint inflammation and resolution. We observed that the transcriptomes of MerTK<sup>pos</sup> STM clusters from healthy donors and remission RA differed significantly from MerTK<sup>pos</sup> STM clusters from active RA. These included lower expression of genes of glycolytic pathways and higher expression of scavenger receptors (Supplementary Fig. 4). The MerTK<sup>pos</sup> clusters in remission had an additional regulatory transcriptomic signature not present in MerTK<sup>pos</sup> STMs in healthy or active RA (Fig. 4a–c). This signature is characterized by upregulation of transcription factors (*KLF2*, *KLF4*, *NR4A1*, *NR4A2*, *ATF3*) and dual-specificity phosphatase 1 (*DUSP1*). Murine studies suggest these are negative regulators of inflammation that reinstate tissue homeostasis<sup>44–48</sup>. We confirmed that this remission-specific transcriptomic signature is linked to upstream activation of MerTK by demonstrating that their expression was reduced by a MerTK inhibitor (Fig. 4d). Subsequent validation of this signature in the independent PEAC cohort<sup>42</sup> confirmed that *KLF4* and *NR4A2* expression in RA synovium correlated negatively with disease activity (Fig. 4e). Together with the mediator profile, these data suggest that MerTK<sup>pos</sup> STM clusters in remission RA have regulatory functions characterized by a unique set of transcription factors.

**MerTK<sup>neg</sup>CD206<sup>neg</sup> and MerTK<sup>pos</sup>CD206<sup>pos</sup> STMs induce inflammatory and repair responses, respectively, in primary fibroblast-like synoviocytes (FLS).** We next tested the resolving versus inflammatory roles of FACS-sorted CD206<sup>pos</sup>MerTK<sup>pos</sup> and CD206<sup>neg</sup>MerTK<sup>neg</sup> STMs from RA biopsies in modulating the synovial tissue environment, by ex vivo micrococulture with RA biopsy-derived FLS (Fig. 5a; Methods). Based on the scRNA-seq immune-stromal gene panel (Methods), FLS cultured per se exhibited four distinct activation states (phenotypes): FLS cluster 1 (FLS1) expressed extracellular matrix proteins (for example, *COL1A1* and *COL1A2*) and genes of the TGFβ pathway (*TGFBI* and *TGFB3*); FLS2 expressed cell adhesion molecules (for example, *ITGB2* and *SELPLG*); FLS3 expressed receptors for TGF-β and resolvin (for example, *CMKLR1* and *TGFBRI*); and FLS4 expressed high levels of glycolytic enzymes and proliferation markers (for example, *LDHA*, *PGK1*, *ENO1* and *PCNA*) (Fig. 5b,c).

Following coculture with proinflammatory MerTK<sup>neg</sup>CD206<sup>neg</sup> STMs, but not with MerTK<sup>pos</sup>CD206<sup>pos</sup> STMs, an additional fifth cluster (FLS5) emerged characterized by high expression of cartilage- and bone-destructive mediators (for example, matrix metalloproteinases *MMP1/3* and *RANKL*), proinflammatory cytokines (for example, *IL-6*) and chemokines that recruit neutrophils (for example, *CXCL8*), monocytes (for example, *CCL2*) and T cells (for example, *CCL20*). This FLS5 cluster was further enhanced by pretreatment of MerTK<sup>neg</sup>CD206<sup>neg</sup> STMs with LPS (Fig. 5d–f). This increase in the expression of inflammatory mediators in FLS cocultured with MerTK<sup>neg</sup>CD206<sup>neg</sup>, but not with MerTK<sup>pos</sup>CD206<sup>pos</sup>, STMs was also evident at the pseudobulk

level (mean gene expression per sample) (Fig. 5g,h). In contrast to proinflammatory MerTK<sup>neg</sup>CD206<sup>neg</sup> STMs, MerTK<sup>pos</sup>CD206<sup>pos</sup> STMs—especially those isolated from biopsies of patients in sustained RA disease remission—induced FLS repair responses including increased expression of collagen genes (for example, *COL1A*) and TGF-β response genes (for example, *TGFBI*) (Fig. 5i). Together, these data suggest counter-regulatory modulation of synovitis by MerTK<sup>neg</sup>CD206<sup>neg</sup> and MerTK<sup>pos</sup>CD206<sup>pos</sup> STM populations.

To examine the role of MerTK in macrophage-mediated changes in FLS we used surrogate human monocyte-derived macrophages (MoM), which have M-CSF-driven expression of MerTK and an LPS-induced inflammatory phenotype (Supplementary Fig. 5a–f). Pretreatment of these macrophages with a MerTK inhibitor (Methods) increased FLS expression of *MMP1/3/14* and *IL-6*. Transcriptomic analysis of FLS from the cocultures revealed 82 differentially expressed genes (DEGs) under macrophage MerTK regulation. String-pathway analysis highlighted the proinflammatory cytokine pathway (15 of 216 genes,  $P=4.10^{-15}$ ) and the proinflammatory chemokine pathway (9 of 48 genes,  $P=1.79^{-12}$ ). In contrast, repair mediators (for example, *FGF14*) and extracellular matrix (for example, *COL21a*) were downregulated (Supplementary Fig. 5g and Supplementary Dataset). These data suggest that macrophage membrane MerTK restrains the proinflammatory (cytokine) and tissue-destructive properties (MMP) of synovial fibroblasts.

**scRNA-seq FLS transcriptomic profiles reflect local interaction with MerTK<sup>pos</sup>CD206<sup>pos</sup> or MerTK<sup>neg</sup>CD206<sup>neg</sup> STMs.** To investigate whether the transcriptome of remission FLS indicates in vivo interaction with MerTK<sup>pos</sup>CD206<sup>pos</sup> STMs, we compared scRNA-seq (10x Genomics; Methods) of synovial fibroblasts from remission and active RA. Unsupervised clustering (13,949 FLS) confirmed the current classification<sup>18–20</sup> and distinguished one lining-layer FLS cluster expressing MMPs and four sublining-layer clusters (*HLA<sup>high</sup>*, *THY1<sup>high</sup>*, *THY1<sup>pos</sup>CXCL14<sup>pos</sup>* and *THY1<sup>pos</sup>CD34<sup>pos</sup>*) expressing collagens and immune mediators (Fig. 6a,d). The relative proportions of these clusters were similar in active and remission RA (Fig. 6e), but their transcriptomes differed (Fig. 6f–h). The expression of proinflammatory mediators induced by MerTK<sup>neg</sup>CD206<sup>neg</sup> STMs and negatively regulated by MerTK was reduced in lining-layer remission FLS compared to those from active RA, including metalloproteinases (*MMP1/3*) and chemokines (*CXCL1/8*). In contrast, mediators of tissue repair and resolution (for example, *IGFBP5/6*, *AXL*) were increased, suggesting a transcriptomic signature of a ‘resolved/repair’ phenotype potentially induced by interaction with MerTK<sup>pos</sup>CD206<sup>pos</sup> STMs.

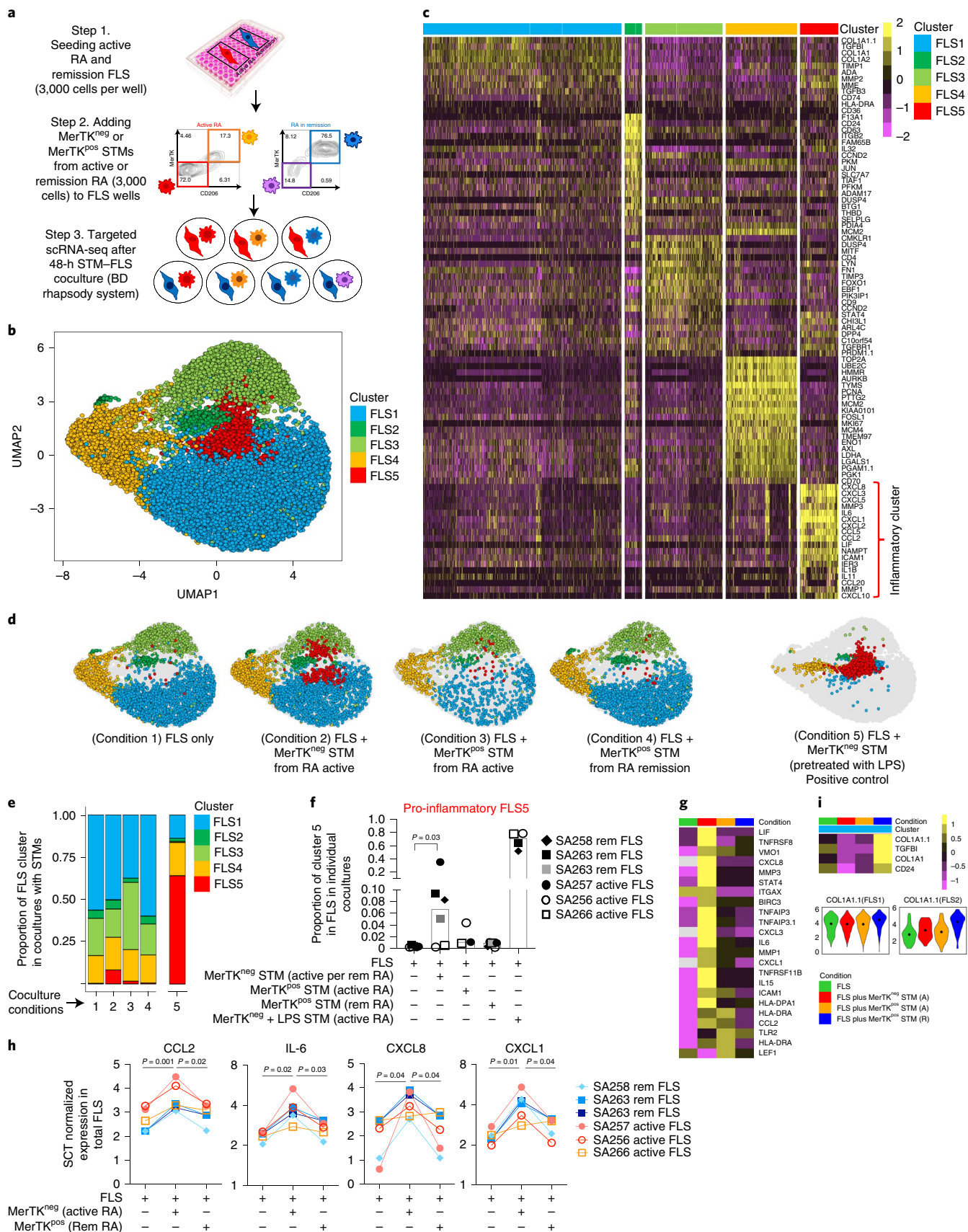
Given our earlier data showing that GAS6 regulates the function of remission MerTK<sup>pos</sup>CD206<sup>pos</sup> STMs (Fig. 3b), we investigated synovial sources of GAS6 in this scRNA-seq dataset. Sublining FLS clusters expressed GAS6 messenger RNA abundantly in the *THY1<sup>pos</sup>CXCL14<sup>pos</sup>* cluster (Fig. 6e), and this expression was increased in remission compared to active RA (Fig. 6i), suggesting increased GAS6 in tissue niches of resolving synovitis. Experimentally, in vitro production of GAS6 was abundant in cultures of primary FLS lines

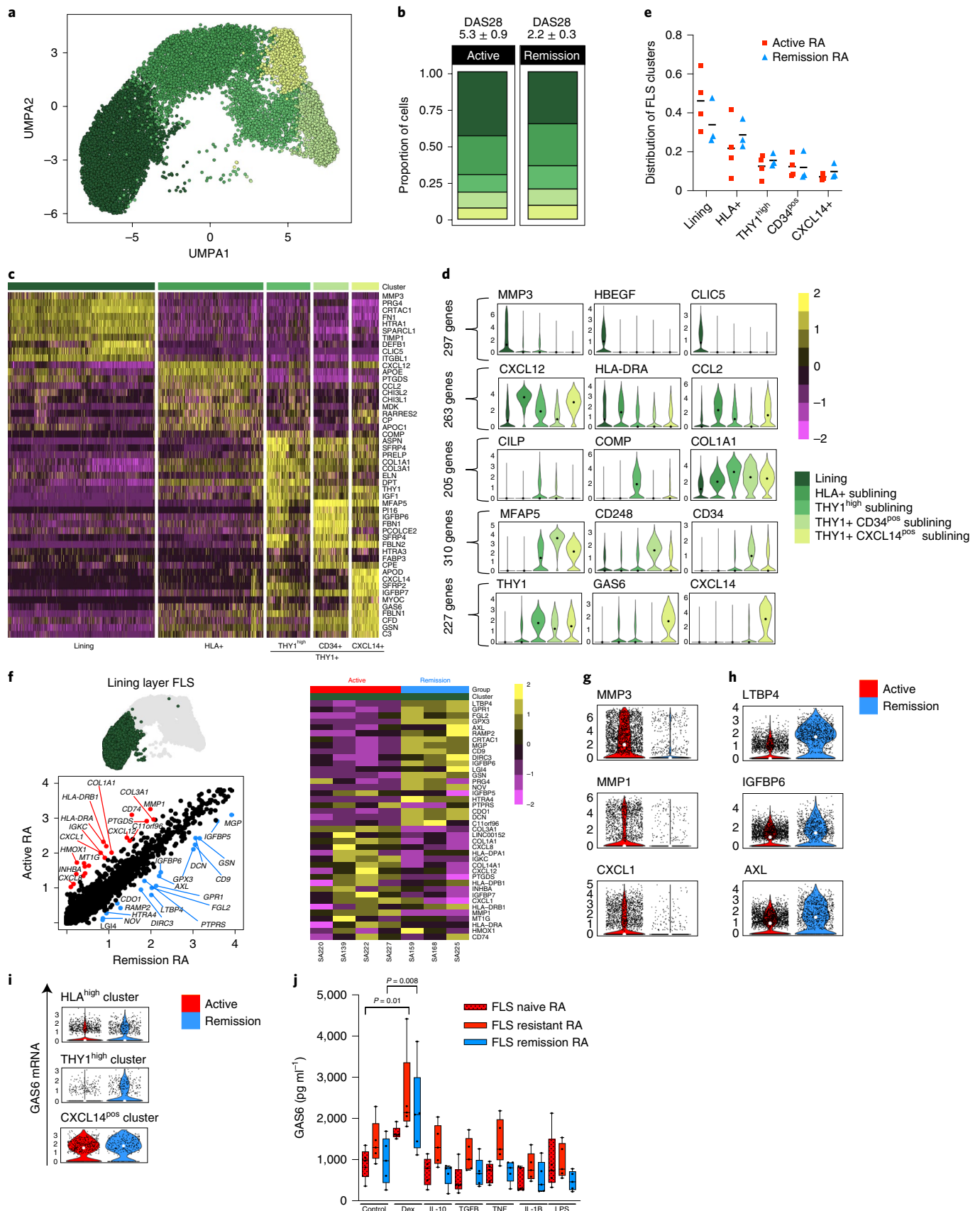
**Fig. 5 | MerTK<sup>neg</sup>CD206<sup>neg</sup> and MerTK<sup>pos</sup>CD206<sup>pos</sup> STMs induce inflammatory and repair responses, respectively in FLS.** **a**, Schematic of STM–FLS coculture experiments. STM–FLS cocultures ( $n=6$ ) were performed in three independent experiments. **b**, UMAP of five clusters of FLS from all cocultures. **c**, Heatmap of the top 20 DEGs per cluster. All genes are expressed in at least 40% of cells in each cluster ( $P < 0.05$  MAST, with Bonferroni). **d–f**, Change in FLS cluster distribution across conditions illustrated by split UMAP (**d**) and bar (**e**) and dot plots (**f**). Kruskal–Wallis test with Dunn’s. Each symbol represents FLS from an individual RA patient ( $n=5$ ) cocultured with sorted MerTK<sup>neg</sup> or MerTK<sup>pos</sup> STMs from active RA ( $n=3$ ) or remission RA ( $n=3$ ). **g**, Heatmap of the top DEGs in total FLS ( $n=6$ , pseudobulk RNA analysis;  $P < 0.05$  MAST, with Bonferroni) induced by MerTK<sup>neg</sup> STMs versus MerTK<sup>pos</sup> STMs in active RA. **h**, Representative genes differentially expressed in FLS following coculture with MerTK<sup>neg</sup> from patients with active RA as compared to MerTK<sup>pos</sup> STM from remission RA ( $n=6$ , pseudobulk RNA analysis; two-sided paired  $t$ -test,  $P$  values are shown). **i**, Heatmap ( $n=6$ ) of scaled expression of the top DEGs in FLS1, induced by MerTK<sup>pos</sup> STMs from RA in disease remission compared to other conditions ( $P < 0.05$ , MAST corrected with Bonferroni). Violin plots show log-normalized expression values of *Col1a* in FLS1 and 2; shape of the violin represents the density of the data at different expression values, with medians marked by dots and colors representing unique coculture conditions. A, active; R, remission.



from biopsies of patients with RA (Fig. 6j), and short interfering RNA-mediated deletion of *GAS6* in FLS increased its proinflammatory phenotype following contact with MerTK-expressing

macrophages (Supplementary Fig. 6a–f). Thus, *GAS6* derived from sublining FLS may contribute to the homeostatic regulatory functions of lining-layer MerTK<sup>pos</sup> macrophages.





## Discussion

This study provides a comparative description of the functional biology of human synovial tissue macrophages. Integrated scRNA-seq,

deep-phenotypic, spatial and functional analyses demonstrated that STMs consist of two populations that can be further subdivided into nine clusters with distinct properties. MerTK<sup>neg</sup>CD206<sup>neg</sup> STM

**Fig. 6 | scRNA-seq FLS transcriptomic profiles reflect local interaction with MerTK<sup>pos</sup>CD206<sup>pos</sup> or MerTK<sup>neg</sup>CD206<sup>neg</sup> STM. a–i**, FLS from active RA ( $n=4$ ) and RA in remission ( $n=3$ ). **a**, UMAP visualization of heterogeneity of human FLS. **b**, relative proportion of cells within each cluster per clinical group. **c**, Top 10 DEGs per cluster. All genes are expressed in at least 40% of cells per cluster ( $P < 0.05$ , MAST with Bonferroni). **d**, Violin plots of the top cluster markers, median value represented by a black dot and cluster identity by color. **e**, Cluster distribution between active and remission RA; each point represents an individual patient and the black line represents the mean. **f**, DEGs in the lining-layer FLS of remission RA compared to active RA. Scatterplot illustrates pseudobulk expression of each DEG, and the top 20 genes for each condition are annotated. Heatmap shows pseudobulk expression of these top 20 DEGs. All genes are expressed in at least 60% of cells per group;  $P < 0.05$  MAST with Bonferroni. **g,h**, Violin plots showing genes for MMPs and chemokines (**g**) and anti-inflammatory mediators (**h**) in lining-layer FLS. **i**, Violin plots of GAS6 in distinct sublining FLS clusters. **g–i**, Violin plots: median values represented by white dots while conditions identified by color. **j**, GAS6 production by primary FLS from biopsies of patients with RA (treatment-naïve, treatment-resistant and RA in remission). Each dot represents a separate FLS line ( $n=5$  per condition in five independent experiments); two-way ANOVA with Tukey's test. Box plots show median with 25th/75th percentiles and whiskers from minimum to maximum, and individual values are plotted.

clusters produce proinflammatory cytokines and alarmins, and induce inflammatory responses in synovial fibroblasts. In contrast, MerTK<sup>pos</sup>CD206<sup>pos</sup> STM clusters from patients with RA in sustained disease remission produce lipid mediators that resolve inflammation and induce a repair phenotype of FLS. This is consistent with our previous finding of increased collagen deposition in remission synovium<sup>3</sup>. Thus, intercellular crosstalk between MerTK<sup>pos</sup>CD206<sup>pos</sup> STMs and synovial fibroblasts during remission may govern and maintain joint immune homeostasis.

The MerTK<sup>pos</sup>CD206<sup>pos</sup> STMs, predominant in healthy and remission synovium, are composed of TREM2<sup>pos</sup> and FOLR2<sup>pos</sup>LYVE1<sup>pos</sup> clusters. Their respective transcriptomes suggest complementary roles in controlling local immune response and homeostasis, consistent with the ex vivo function of MerTK<sup>pos</sup>CD206<sup>pos</sup> STMs and the in vivo joint-protective functions of their recently identified murine counterparts<sup>9</sup>. Their murine counterparts differentiate from locally proliferating precursors<sup>9</sup>, and human synovial macrophage proliferation in situ was recently reported<sup>49</sup>, introducing the potential for therapy-directed expansion of MerTK<sup>pos</sup>CD206<sup>pos</sup> STMs to reinstate and maintain synovial homeostasis. In remission RA, the resolution signature of MerTK<sup>pos</sup>CD206<sup>pos</sup> STM clusters that included negative regulators of inflammation was driven by MerTK activation, potentially by GAS6 produced locally by Thy1<sup>pos</sup> synovial fibroblasts. The protective role for the MerTK pathway was recently supported by an observation of increased joint pathology in global MerTK-deficient mice<sup>50</sup>. Recent murine and human studies have also suggested a protective function for TREM2<sup>pos</sup> resident macrophages in adipose tissues that counteract insulin intolerance and obesity. Our study suggests the TREM2<sup>pos</sup>MerTK<sup>pos</sup> subpopulation as a potential source of resolvins and highlights a broad regulatory role of TREM2<sup>pos</sup> tissue-resident macrophages<sup>51</sup>. Thus, sustained remission appears to be an active process maintained by tissue-resident subpopulations of MerTK<sup>pos</sup>CD206<sup>pos</sup> STMs governing synovial fibroblasts to reinstate and maintain homeostasis.

Our analysis uncovered diversity in STM phenotypes unrecognized by previous studies<sup>19,22</sup>, due to our substantially higher STM numbers and inclusion of STMs from healthy donors and patients with RA in remission. The clusters we identified in our study are consistent with a previously proposed STM classification scheme<sup>17</sup>.

Our findings (Extended Data Fig. 10) may help to generate new therapeutic strategies to exploit STM-based endogenous mechanisms of resolution of synovitis. We provide evidence that therapeutic enhancement of the functions of MerTK<sup>pos</sup>CD206<sup>pos</sup> STM clusters by activation of MerTK with agonists, or of myeloid cell re-education by activation of transcription factors driving a remission STM signature (*KLF2*, *KLF4*, *NR4A1*, *NR4A2* and *ATF3*), could facilitate restoration of synovial homeostasis. In addition, our study provides a resource of new molecular and cellular data specifically associated with remission, with TREM2, LYVE1 and FOLR2 receptors as potential candidates for testing in functional studies.

The absence of serum antibodies to citrullinated proteins (anticitrullinated peptide antibody (ACPA)-negative) in RA has

prognostic value for drug-free remission<sup>1</sup>. However, ACPA seroconversion is rare in clinical practice<sup>52</sup> and a need remains for better prognostic biomarkers of treatment modification<sup>1–3</sup>. With this study we propose that the relative proportions of STM subpopulations in remission RA may provide a biomarker predictive of persistent remission versus disease flare. If validated with additional remission studies, this could potentially be incorporated within personalized protocols for the management of patients with RA in sustained 'cellular' remission to aid management of biologic, kinase-inhibitory or other therapeutic discontinuations.

### Online content

Any methods, additional references, Nature Research reporting summaries, source data, extended data, supplementary information, acknowledgements, peer review information; details of author contributions and competing interests; and statements of data and code availability are available at <https://doi.org/10.1038/s41591-020-0939-8>.

Received: 23 September 2019; Accepted: 12 May 2020;

Published online: 29 June 2020

### References

- Nagy, G. & van Vollenhoven, R. F. Sustained biologic-free and drug-free remission in rheumatoid arthritis, where are we now? *Arthritis Res. Ther.* **17**, 181 (2015).
- Alivernini, S. et al. Tapering and discontinuation of TNF-alpha blockers without disease relapse using ultrasonography as a tool to identify patients with rheumatoid arthritis in clinical and histological remission. *Arthritis Res. Ther.* **18**, 39 (2016).
- Baker, K. F. et al. Predicting drug-free remission in rheumatoid arthritis: a prospective interventional cohort study. *J. Autoimmun.* **105**, 102298 (2019).
- Alivernini, S. et al. Synovial features of patients with rheumatoid arthritis and psoriatic arthritis in clinical and ultrasound remission differ under anti-TNF therapy: a clue to interpret different chances of relapse after clinical remission? *Ann. Rheum. Dis.* **76**, 1228–1336 (2017).
- Rauber, S. et al. Resolution of inflammation by interleukin-9-producing type 2 innate lymphoid cells. *Nat. Med.* **23**, 938–944 (2017).
- Firestein, G. S., Gabriel, S. E., McInnes, I. B. & O'Dell, J. R. *Kelley and Firestein's Textbook of Rheumatology* 2nd edn (Elsevier, 2016).
- Misharin, A. V. et al. Nonclassical Ly6C(–) monocytes drive the development of inflammatory arthritis in mice. *Cell Rep.* **9**, 591–604 (2014).
- Gomez Perdiguero, E. et al. Tissue-resident macrophages originate from yolk-sac-derived erythro-myeloid progenitors. *Nature* **518**, 547–551 (2015).
- Culemann, S. et al. Locally renewing resident synovial macrophages provide a protective barrier for the joint. *Nature* **572**, 670–675 (2019).
- Mandelin, A. M. 2nd et al. Transcriptional profiling of synovial macrophages using minimally invasive ultrasound-guided synovial biopsies in rheumatoid arthritis. *Arthritis Rheumatol.* **70**, 841–854 (2018).
- Kurowska-Stolarska, M. & Alivernini, S. Synovial tissue macrophages: friend or foe? *RMD Open* **3**, e000527 (2017).
- Udalova, I. A., Mantovani, A. & Feldmann, M. Macrophage heterogeneity in the context of rheumatoid arthritis. *Nat. Rev. Rheumatol.* **12**, 472–485 (2016).
- Herenius, M. M. et al. Monocyte migration to the synovium in rheumatoid arthritis patients treated with adalimumab. *Ann. Rheum. Dis.* **70**, 1160–1162 (2011).
- Weiss, M. et al. IRF5 controls both acute and chronic inflammation. *Proc. Natl. Acad. Sci. USA* **112**, 11001–11006 (2015).

15. Yeo, L. et al. Expression of chemokines CXCL4 and CXCL7 by synovial macrophages defines an early stage of rheumatoid arthritis. *Ann. Rheum. Dis.* **75**, 763–771 (2016).
16. Firestein, G. S. & McInnes, I. B. Immunopathogenesis of rheumatoid arthritis. *Immunity* **46**, 183–196 (2017).
17. Kurowska-Stolarska, M. et al. MicroRNA-155 as a proinflammatory regulator in clinical and experimental arthritis. *Proc. Natl Acad. Sci. USA* **108**, 11193–11198 (2011).
18. Croft, A. P. et al. Distinct fibroblast subsets drive inflammation and damage in arthritis. *Nature* **570**, 246–251 (2019).
19. Zhang, F. et al. Defining inflammatory cell states in rheumatoid arthritis joint synovial tissues by integrating single-cell transcriptomics and mass cytometry. *Nat. Immunol.* **20**, 928–942 (2019).
20. Mizoguchi, F. et al. Functionally distinct disease-associated fibroblast subsets in rheumatoid arthritis. *Nat. Commun.* **9**, 789 (2018).
21. Stephenson, W. et al. Single-cell RNA-seq of rheumatoid arthritis synovial tissue using low-cost microfluidic instrumentation. *Nat. Commun.* **9**, 791 (2018).
22. Kuo, D. et al. HBEGF(+) macrophages in rheumatoid arthritis induce fibroblast invasiveness. *Sci. Transl. Med.* **11**, eaau8587 (2019).
23. Smolen, J. S. et al. Rheumatoid arthritis. *Nat. Rev. Dis. Primers* **4**, 18001 (2018).
24. Gremese, E. M., Fedele, A. L., Alivernini, S. & Ferraccioli, G. Ultrasound assessment as predictor of disease relapse in children and adults with arthritis in clinical stable remission: new findings but still unmet needs. *Ann. Rheum. Dis.* **77**, 1391–1393 (2018).
25. Najm, A. et al. Standardisation of synovial biopsy analyses in rheumatic diseases: a consensus of the EULAR Synovitis and OMERACT Synovial Tissue Biopsy Groups. *Arthritis Res. Ther.* **20**, 265 (2018).
26. Singh, J. A., Arayssi, T., Duray, P. & Schumacher, H. R. Immunohistochemistry of normal human knee synovium: a quantitative study. *Ann. Rheum. Dis.* **63**, 785–790 (2004).
27. Davies, L. C., Jenkins, S. J., Allen, J. E. & Taylor, P. R. Tissue-resident macrophages. *Nat. Immunol.* **14**, 986–995 (2013).
28. A-Gonzales, N. et al. Phagocytosis imprints heterogeneity in tissue-resident macrophages. *J. Exp. Med.* **214**, 1281–1296 (2017).
29. Hogg, N., Palmer, D. G. & Revell, P. A. Mononuclear phagocytes of normal and rheumatoid synovial membrane identified by monoclonal antibodies. *Immunology* **56**, 673–681 (1985).
30. Bykerk, V. P. & Massarotti, E. M. The new ACR/EULAR remission criteria: rationale for developing new criteria for remission. *Rheumatology (Oxford)* **51**, vi16–vi20 (2012).
31. Alivernini, S. et al. Synovial predictors of differentiation to definite arthritis in patients with seronegative undifferentiated peripheral inflammatory arthritis: microRNA signature, histological, and ultrasound features. *Front. Med. (Lausanne)* **5**, 186 (2018).
32. Nolting, J. et al. Retinoic acid can enhance conversion of naive into regulatory T cells independently of secreted cytokines. *J. Exp. Med.* **206**, 2131–2139 (2009).
33. Vogt, L. et al. VSIG4, a B7 family-related protein, is a negative regulator of T cell activation. *J. Clin. Invest.* **116**, 2817–2826 (2006).
34. Rothlin, C. V., Ghosh, S., Zuniga, E. I., Oldstone, M. B. & Lemke, G. TAM receptors are pleiotropic inhibitors of the innate immune response. *Cell* **131**, 1124–1136 (2007).
35. van der Touw, W., Chen, H. M., Pan, P. Y. & Chen, S. H. LILRB receptor-mediated regulation of myeloid cell maturation and function. *Cancer Immunol. Immunother.* **66**, 1079–1087 (2017).
36. Kahles, F., Findeisen, H. M. & Brummer, D. Osteopontin: a novel regulator at the crossroads of inflammation, obesity and diabetes. *Mol. Metab.* **3**, 384–393 (2014).
37. Wang, S. et al. S100A8/A9 in Inflammation. *Front. Immunol.* **9**, 1298 (2018).
38. Lim, H. Y. et al. Hyaluronan receptor LYVE-1-expressing macrophages maintain arterial tone through hyaluronan-mediated regulation of smooth muscle cell collagen. *Immunity* **49**, 326–341 (2018).
39. Freeman, C. L. et al. Cytokine release in patients with CLL treated with obinutuzumab and possible relationship with infusion-related reactions. *Blood* **126**, 2646–2649 (2015).
40. Villani, A. C. et al. Single-cell RNA-seq reveals new types of human blood dendritic cells, monocytes, and progenitors. *Science* **356**, eaah4573 (2017).
41. Boulet, S. et al. The orphan nuclear receptor NR4A3 controls the differentiation of monocyte-derived dendritic cells following microbial stimulation. *Proc. Natl Acad. Sci. USA* **116**, 15150–15159 (2019).
42. Humby, F. et al. Synovial cellular and molecular signatures stratify clinical response to csDMARD therapy and predict radiographic progression in early rheumatoid arthritis patients. *Ann. Rheum. Dis.* **78**, 761–772 (2019).
43. Lewis, M. J. et al. Molecular portraits of early rheumatoid arthritis identify clinical and treatment response phenotypes. *Cell Rep.* **28**, 2455–2470 (2019).
44. Vattakuzhi, Y., Abraham, S. M., Freidin, A., Clark, A. R. & Horwood, N. J. Dual-specificity phosphatase 1-null mice exhibit spontaneous osteolytic disease and enhanced inflammatory osteolysis in experimental arthritis. *Arthritis Rheum.* **64**, 2201–2210 (2012).
45. Roberts, A. W. et al. Tissue-resident macrophages are locally programmed for silent clearance of apoptotic cells. *Immunity* **47**, 913–927 (2017).
46. Koenis, D. S. et al. Nuclear receptor Nur77 limits the macrophage inflammatory response through transcriptional reprogramming of mitochondrial metabolism. *Cell Rep.* **24**, 2127–2140 (2018).
47. Hanna, R. N. et al. NR4A1 (Nur77) deletion polarizes macrophages toward an inflammatory phenotype and increases atherosclerosis. *Circ. Res.* **110**, 416–427 (2012).
48. Mahajan, S. et al. Nuclear receptor Nr4a2 promotes alternative polarization of macrophages and confers protection in sepsis. *J. Biol. Chem.* **290**, 18304–18314 (2015).
49. Wood, M. J. et al. Macrophage proliferation distinguishes 2 subgroups of knee osteoarthritis patients. *JCI Insight* **4**, e125325 (2019).
50. Waterborg, C. E. J. et al. Protective role of the MER tyrosine kinase via efferocytosis in rheumatoid arthritis models. *Front. Immunol.* **9**, 742 (2018).
51. Jaitin, D. A. et al. Lipid-associated macrophages control metabolic homeostasis in a trem2-dependent manner. *Cell* **178**, 686–698 (2019).
52. Boeters, D. M., Burgers, L. E., Toes, R. E. & van der Helm-van Mil, A. Does immunological remission, defined as disappearance of autoantibodies, occur with current treatment strategies? A long-term follow-up study in rheumatoid arthritis patients who achieved sustained DMARD-free status. *Ann. Rheum. Dis.* **78**, 1497–1504 (2019).

**Publisher's note** Springer Nature remains neutral with regard to jurisdictional claims in published maps and institutional affiliations.

© The Author(s), under exclusive licence to Springer Nature America, Inc. 2020

## Methods

**Patient recruitment and management.** One hundred and twelve patients fulfilling the American College of Rheumatology 2010 revised criteria for RA<sup>53</sup> were enrolled and underwent ultrasound-guided synovial tissue biopsy of the knee at the Division of Rheumatology of Fondazione Policlinico Universitario A. Gemelli IRCCS, Università Cattolica del Sacro Cuore, Rome, Italy. These samples comprised the SYNGem cohort. Patients with RA were stratified into naïve to treatment ( $n=45$ ), inadequate responder to MTX (treatment-resistant RA,  $n=31$ ) and those in sustained (minimum 6 months) clinical and ultrasound remission under MTX + TNF inhibitor ( $n=36$ ). Ten healthy donors attending arthroscopy for meniscal tear or cruciate ligament damage and with normal synovium (via magnetic resonance imaging and macroscopically) were included as a control group (University of Glasgow). The study protocol was approved by the Ethics Committee of the Università Cattolica del Sacro Cuore (no. 6334/15) and by the West of Scotland Research Ethics Committee (no. 19/WS/0111). All subjects provided signed informed consent. Demographic, clinical and immunological features of the study RA and healthy cohorts are summarized in Supplementary Tables 1–3. All treatment-resistant RA were taking stable doses of MTX (mean dose,  $15.3 \pm 3.3$  mg per week). All RA in sustained clinical (DAS28 < 2.6 for three sequential determinations, each 3 months apart) and ultrasound remission (Power Doppler negativity at ultrasound assessment for three sequential determinations, each 3 months apart) were selected based on published protocols<sup>54</sup>. For each patient with RA enrolled, clinical and laboratory evaluations included the number of tender and swollen joints of 28 examined, erythrocyte sedimentation rate (ESR), C-reactive protein (CRP) and DAS28. Peripheral blood samples were tested for IgA and IgM-RF (Orgentec Diagnostika) and ACPA (Menarini Diagnostics) using commercial ELISA assay and chemiluminescence immunoassay (CLIA), respectively. After study enrollment, patients with RA in sustained clinical and ultrasound remission ( $n=22$ ) were first tapered on TNF inhibitor (adalimumab 40 mg every 4 weeks or etanercept 50 mg every 2 weeks) for 3 months. After those 3 months, patients who were still in ultrasound remission (power Doppler negative) discontinued TNF inhibitor and were followed up every 3 months while being maintained on stable doses of MTX ( $15.2 \pm 2.9$  mg per week), with follow-up after treatment modification of mean  $\pm$  s.d.  $21.45 \pm 8.09$  months (till submission of the study)<sup>5</sup>. The relapse rate was recorded for each patient in sustained clinical and ultrasound remission after treatment modification<sup>54</sup>.

**Patient selection for scRNA-seq.** Seventeen patients fulfilling the American College of Rheumatology 2010 revised criteria for RA<sup>53</sup> (five treatment-naïve RA, six treatment-resistant RA and six in sustained clinical and ultrasound remission) and four patients with UPA<sup>55</sup> with at least one active knee joint, seronegative for IgA/IgM-rheumatoid factor (RF) and ACPA and naïve to any pharmacological treatment, were enrolled in the study at the Division of Rheumatology of Fondazione Policlinico Universitario A. Gemelli IRCCS, Università Cattolica del Sacro Cuore, Rome, Italy. For each patient with RA or UPA enrolled, clinical and laboratory evaluations included the number of tender and swollen joints at 28 sites, ESR, CRP and DAS28. Peripheral blood samples were tested for IgA and RF (Orgentec Diagnostika) and ACPA (Menarini Diagnostics) using commercial ELISA and CLIA, respectively. Each enrolled patient underwent ultrasound-guided synovial tissue biopsy, and synovial tissue samples were processed following the protocol described below. Four healthy donor synovial tissues were included as control. Demographic, clinical and immunological features of patients and healthy donor samples used for scRNA-seq are summarized in Supplementary Tables 2 and 3.

**Synovial tissue biopsies.** All enrolled patients with RA or UPA underwent ultrasound-guided synovial tissue biopsy of the knee following a published protocol<sup>56</sup> at the Division of Rheumatology of Fondazione Policlinico Universitario A. Gemelli IRCCS, Università Cattolica del Sacro Cuore (SYNGem cohort). Ultrasound evaluation of the knee was performed using an ultrasound machine with a multifrequency linear transducer (MyLab). Using ultrasound viewing, the optimal point of entrance for the biopsy needle was identified on the lateral margin of the suprapatellar recess. Each patient was provided with a face mask and cap, and the procedure was performed under sterile conditions. The skin was disinfected twice with iodine solution, starting from the point of needle entrance and up to 25 cm both proximally and distally. If joint effusion was present, arthrocentesis was performed using the lateral suprapatellar access. The skin, subcutaneous tissue and joint capsule were anesthetized with 10 ml of 2% lidocaine. Next, a 14-g needle (Precisa 1410) was inserted into the joint. Regions of synovial hypertrophy were identified under grayscale guidance to ensure sampling of representative synovial tissue. All synovial tissue specimens obtained (at least eight pieces for histology and 12 for single-cell RNA-seq and functional experiments) were placed on a nonwoven wet sterile gauze for collection. For histology, tissue specimens were fixed in 10% neutral-buffered formalin and embedded in paraffin. Briefly, paraffin-embedded synovial tissue specimens were sectioned at 3  $\mu$ m and then stained with hematoxylin and eosin as follows: deparaffinization in xylene and rehydration in a series of graded ethanol, stained in hematoxylin and counterstained in eosin/phloxine. Finally sections were dehydrated, cleared in xylene and mounted with Bio Mount (Bio-Optica). Slides were examined using a

light microscope (Leica Biosystems DM 2000). The severity of synovitis was graded according to three synovial membrane features—synovial lining cell layer, stromal cell density and inflammatory infiltrate—each ranked on a scale through none (0), slight (1), moderate (2) and strong (3). The values of the parameters were summed and interpreted as follows: 0–1, no synovitis; 2–4, low-grade synovitis; and 5–9, high-grade synovitis<sup>57</sup>.

For MerTK immunohistochemistry, sections were stained with IgG2a mouse anti-human monoclonal antibody for CD68 (clone 514H12; antibody at  $6.7 \mu\text{g ml}^{-1}$ ) (Leica Biosystems) or IgG rabbit anti-human monoclonal antibody for MerTK (clone Y323, Abcam no. ab205718, dilution 1:1,000) by immunostainer BOND MAXIII (Leica Biosystems). Single immunohistochemical staining for CD68 or MerTK was performed as follows: 3- $\mu$ m sections from formalin-fixed, paraffin-embedded tissue blocks were dried at 60 °C for 30 min. Sections were placed in a Bond Max Automated Immunohistochemistry Vision Biosystem (Leica Microsystems) according to the following protocol. Tissues were deparaffinized and pretreated with Epitope Retrieval Solution 1 (citrate buffer) or Solution 2 (EDTA buffer) at 98 °C for 10 min, according to the manufacturer's instructions. After washing, peroxidase blocking was carried out for 10 min using the Bond Polymer Refine Detection Kit DC9800 (Leica Microsystems). Tissues were washed and incubated with the primary antibody for 30 min, incubated with polymer for 10 min, developed with DAB-chromogen and finally counterstained with hematoxylin. Slides were examined under a light microscope (Leica DM 2000).

For MerTK immunofluorescence, 3- $\mu$ m formalin-fixed RA synovial tissue sections were microwaved in citric acid (pH 9.2) and preincubated with phosphate-buffered saline containing 10% bovine serum albumin (BSA) for 30 min. Sections were then stained with primary antibody against CD68 (clone L26 mouse anti-human monoclonal antibody at  $1.2 \mu\text{g ml}^{-1}$ , Leica Biosystems) and anti-MerTK (rabbit IgG polyclonal Cy3-conjugated anti-human MerTK, clone 5770, no. BLOSS bs-0548R-Cy3, dilution 1:100) at 37 °C for 1 h. Sections were rinsed and incubated with secondary conjugated antibody fluorescein isothiocyanate (FITC) conjugated goat anti-mouse IgG H&L (Abcam, no. ab6785, dilution 1:1,000) at room temperature for 1 h. Slides were mounted and scanned on a fluorescent microscope (Nikon).

**Synovial tissue processing for macrophage phenotyping, subset FACS sorting and scRNA-seq.** Fresh synovial tissues were diced into 1–2-mm<sup>3</sup> fragments with a sterile disposable no. 22 scalpel and transferred to a sterile universal container containing 10 ml of sterile RPMI with penicillin/streptomycin 100 U ml<sup>-1</sup> and L-glutamine 2 mM (RPMI medium) in a 1:33 dilution of Liberase at  $0.15 \mu\text{g ml}^{-1}$ , 0.78 Wünsch units ml<sup>-1</sup> (TM Research Grade, Thermolysin, medium, Roche Diagnostics (no. 000000005401127001, Sigma)). Tissue pieces were incubated at 37 °C, 5% CO<sub>2</sub> in a humidified atmosphere for 30–45 min, with rotation on a Miltenyi MACSmix tube-rotator and vigorous shaking by hand twice during this incubation. After incubation, the digested mixture was filtered using an Easy Strain 100  $\mu$ m cell strainer into a 50-ml falcon tube. Residual cell clumps retained on the filter were gently massaged using the rubber end of a 1-ml syringe plunger, to optimize cell retrieval. Complete medium (RPMI with 10% fetal calf serum (FCS) was poured through the filter into the falcon tube up to 40 ml then centrifuged at 1,800 r.p.m. for 10 min at 4 °C, and the supernatant was carefully removed. One milliliter of complete medium was added to gently resuspend the cell pellet, using a wide-opening 1-ml pipette tip to minimize cell damage, then the resuspended cells were transferred to a sterile Eppendorf tube. A 20- $\mu$ l aliquot was used to count the cells. Cells were centrifuged at 1,500 r.p.m. for 5 min at 4 °C. The supernatant was removed, and cells were aliquoted for either STM phenotyping and/or STM FACS sorting as described below, or for subsequent scRNA-seq (cells from 25 patients/healthy donors described above). Cells were added to 1 ml of ice-cold freezing mix (Bambanker, no. 302-14681), immediately frozen at –80 °C and stored in liquid nitrogen.

**Phenotyping and FACS sorting of STM populations.** Digested biopsies were centrifuged at 1,800 r.p.m. for 10 min, resuspended and washed with FACS buffer, and transferred to FACS tubes (BD Biosciences) in a final volume of 3 ml FACS buffer (PBS/2% FSC/2 mM EDTA). An 80- $\mu$ l aliquot was set aside for live–dead gating (unstained cells). For the remainder of the cells, Fixable Viability Dye eFluor 780 (eBioscience) was added at 1:1,000 in PBS and incubated for 20 min at 4 °C. Cells were then washed with FACS buffer. Four tubes were labeled: (1) unstained; (2) live–dead marker only; (3) fluorescence minus one control (FMO) and FMO minus FITC, where cells were stained with antibodies specific for STM but not FITC antibodies against all other lineage-positive cells; and (4) cells stained with antibodies against STMs and FITC antibodies against any unwanted lineage. Staining was performed in a final volume of 500  $\mu$ l with antibody dilution 1:100 for 30 min on ice. All antibodies are listed in Supplementary Fig. 7a. Cells were washed twice with FACS buffer and resuspended in a final volume of 500  $\mu$ l, filtered through an Easy Strain 100- $\mu$ m cell strainer and analyzed or sorted with the use of a FACS ARIAIII (BD Biosciences). Synovial tissue macrophages were gated based on their membrane expression of CD45, CD64, CD11b and HLA-DR after all other cell lineages (FMO–FITC gating), and cell doublets were excluded (dump channel 1). FMO–FITC cells were used to set up a gate to exclude unwanted lineage-positive cells (dump channel). The expression of MerTK, CD163, CD206,

TREM2, FOLR2 and TIM4 was evaluated on gated CD64<sup>pos</sup>CD11b<sup>pos</sup>HLA-DR<sup>pos</sup> STMs (Supplementary Fig. 7b–d). In addition, MerTK<sup>pos</sup>CD206<sup>pos</sup> and MerTK<sup>neg</sup>CD206<sup>neg</sup> STM populations were FACS sorted from 47 synovial biopsies. The cells were sorted into FACS tubes containing 2 ml of complete RPMI1640. Post-sorting purity of macrophages was performed, and all data generated were analyzed using FlowJo software (TreeStar).

**Ex vivo stimulation of sorted STMs.** MerTK<sup>pos</sup>CD206<sup>pos</sup> and MerTK<sup>neg</sup>CD206<sup>neg</sup> STMs were FACS sorted into complete medium and plated into a 96-well, flat-bottom cell-culture plate precoated with collagen (Sigma; bovine collagen at 1:300 dilution). The precoating protocol was as follows: wells were incubated with collagen at 37 °C, 5% CO<sub>2</sub> for 2 h and then washed twice with PBS. STMs were seeded at 1,000 cells per well and stimulated with either LPS (10 ng ml<sup>-1</sup>, Sigma, no. L6529) or human recombinant Gas6 (100 ng ml<sup>-1</sup>, R&D Systems, no. 885-GSB-050), or both in combination, or left unstimulated for 24 h in a total volume of 100 µl. Supernatants were then harvested and assayed using an ultrasensitive 19-plex assay (Meso Scale Discovery), Resolvin D1 (Cayman Chemical, no. 500380) and S10012A (R&D Systems, no. DY 1052-05).

#### Coculture of distinct STM populations with primary synovial fibroblasts.

Synovial tissue biopsies from patients with RA ( $n=6$ ) were digested as described above. Synovial fibroblasts were identified by surface membrane Thy and podoplanin (PDPN)<sup>18</sup>, and PDPN<sup>pos</sup> (lining) plus PDPN<sup>pos</sup>Thy1<sup>pos</sup> (sublining) FLS were FACS sorted into Eppendorf tubes containing 0.5 ml of complete RPMI 1640. FLS were seeded into T25 culture flasks (Merck) with complete RPMI 1640. After attachment to the plastic surface (~1 week), these were harvested and seeded into 96-well plates at 3,000 cells per well, and freshly FACS-sorted MerTK<sup>pos</sup>CD206<sup>pos</sup> or MerTK<sup>neg</sup>CD206<sup>neg</sup> STMs from patients with RA ( $n=3$  with active RA and  $n=3$  in sustained clinical and ultrasound imaging remission) were added to the cocultures. One patient from each group was biopsied together on the same day, so that paired cultures of STM populations from active and remission RA could be compared (Supplementary Table 5). STMs were added to FLS at 3,000 cells per well in two or three technical replicates.

FLS cultured without STMs were used as comparator and, as a positive inflammatory control, FLS cocultured with MerTK<sup>pos</sup>CD206<sup>pos</sup> sorted from patients with active RA and pretreated with LPS (10 ng ml<sup>-1</sup>) for 1 h were used. LPS pretreated MerTK<sup>pos</sup>CD206<sup>pos</sup> were extensively washed before being added to FLS (three times). After 48 h, changes in FLS phenotype during cocultures were investigated using scRNA-seq (BD Rhapsody System), and their associated function investigated by soluble mediators in culture supernatants and quantified by luminex (no. PPX-06/PROCARTAPLEX, Life Technologies; Fig. 4a).

#### Coculture of MoM with synovial fibroblasts in a direct and indirect coculture systems.

CD14<sup>pos</sup> cells were isolated from peripheral blood mononuclear cells using CD14<sup>pos</sup> microbeads and AutoMACSPro (Miltenyi BioTec) according to the manufacturer's protocol. These were differentiated into monocyte-derived macrophages in complete medium containing M-CSF. Briefly, cells were plated at a density of  $1 \times 10^6$  per well in a six-well cell-culture plate in 3 ml of RPMI 1640 complete medium containing M-CSF (PeproTech) at 50 ng ml<sup>-1</sup>. On day 3, the medium was replaced with fresh medium containing M-CSF. On day 6, cells were pretreated with LPS (1 ng ml<sup>-1</sup>) in the presence or absence of the MerTK inhibitor UNC1062 (ref. <sup>58</sup>; 250 µM, Aobious). After 24 h, macrophages were de-attached and labeled with CellTrace Far Red (5 µM, Life Technologies) according to the manufacturer's protocol. These cells were added at  $2 \times 10^3$  per well of a 96-well plate containing  $2 \times 10^5$  primary FLS. Fibroblasts were obtained from ultrasound-guided synovial tissue biopsies (Supplementary Table 6) and had been labeled with CellTracer Violet (5 µM, Life Technologies) 24 h before coculture with macrophages. In experiments designed to demonstrate the role of FLS-derived GAS6 in FLS–MoM interactions, before coculture with STMs, FLS were transfected with 5 pmol of GAS6 siRNA (4390824) or Silencer Select Negative Control (no. 390843) using Lipofectamine RNAiMAX Reagent (Life Technologies) on 2 consecutive days. Twenty-four hours after the last transfection, FLS were washed and labeled with CellTracer Violet. After 24 or 48 h coculture, supernatant was collected for assay of mediators, and macrophages and synovial fibroblasts were de-attached and stained with antibodies against the synovial fibroblast marker PDPN and the macrophage marker CD64 (both at 1:100 dilution; details in Supplementary Fig. 1a). Fibroblasts and macrophages were FACS sorted into RLT buffer (Qiagen) containing 1% β-mercaptoethanol, based on their specific CellTracer staining and cell-type-specific markers, and stored at –80 °C for RNA isolation. The trans-well culture system was then employed (an indirect coculture). CD14<sup>pos</sup> monocytes were plated in a 24-well culture plate in 3 ml of complete medium containing M-CSF (PeproTech) at 50 ng ml<sup>-1</sup>. On day 3, some cells were pretreated with LPS (1 ng ml<sup>-1</sup>) for 4 h and, for others, for the last 2 h, the MerTK-specific inhibitor, UNC106258 (ref. <sup>58</sup>; Aobious) was added at 100 or 250 nM. Cells were then washed with PBS and trans-well inserts (0.4-µm pore size) containing  $3 \times 10^5$  RA synovial fibroblasts were added to the wells to generate a coculture system to test the effect of soluble mediators without direct cell contact. After 48 h, supernatants were collected and cocultured macrophages and fibroblasts were separately lysed in RLT buffer with 1% β-mercaptoethanol (Qiagen) and stored at –80 °C for RNA isolation and RNA-seq. The MMP Luminex panel

(PPX-05/PROCARTAPLEX MMP1, MMP2, MMP3, MMP9 and MMP13-plex) and IL-6 Elisa (both from Life Technologies) were performed on supernatants from direct and trans-well cocultures.

**Evaluation of GAS6 production by synovial fibroblasts.** Fibroblast-like synoviocytes were expanded from biopsies of patients with RA: treatment-naïve, treatment-resistant and in sustained disease remission (Supplementary Table 7) in complete RPMI 1640 medium supplemented with 2 mM Glutamax, 1 mM sodium pyruvate and 1% nonessential amino acid (Life Technologies). FLS at passages 2–3 were seeded in 48-well cell-culture plates at a density of  $30 \times 10^3$  cells per well in complete medium containing 1% FCS. Cells were stimulated with dexamethasone 1 µM or TNF, IL-1β, IL-10, TGFβ or LPS at 10 or 100 ng ml<sup>-1</sup> for 24 and 48 h. GAS6 was quantified in culture supernatants using the Human GAS6 DuoSet ELISA kit (R&D Systems, no. DY885B).

#### Quantitative PCR (qPCR) for MMPs, IL-6, GAS6 and transcription factors.

Ribonucleic acid from macrophages and synovial fibroblasts was isolated using the RNeasy microkit (Qiagen), and complementary DNA was prepared using a High Capacity cDNA Reverse Transcription Kit (Thermo Fisher Scientific). TaqMan mRNA primers/probe assays and TaqMan Gene Expression master mixes (both from Life Technologies) were used for semiquantitative determination of the genes of interest. Data are presented as relative value (1)  $2^{-\Delta Ct}$ , where  $\Delta Ct$  = cycle threshold for 18 S (housekeeping) minus Ct for gene of interest, or (2) fold-change, where  $\Delta Ct$  for selected control condition = 1 or 100%.

We used the following primers/probe TaqMan assays:

```
Hs00231069_m1/ATF3
Hs00374226_m1/NR4A
Hs01117527_g1/NR4A2
Hs01031979_m1/MERTK
Hs00360439_g1/KLF2
Hs00358836_m1/KLF4
Hs01090305_m1/Gas6
Hs00174131_m1/IL-6
Hs00899658_m1/MMP1
Hs00899658_m1/MMP1
Hs00968305_m1/MMP3
Hs00957562_m1/MMP9
Hs01037006_g1/MMP14
```

**scRNA-seq of STM and whole synovial tissues.** Our experiments were performed at two academic centers. The first set of samples (Discovery cohort—Cohort 1) was sequenced at the Oxford Genomics Centre (Oxford University, UK). Synovial tissue myeloid cells were sorted before sequencing, based on positive expression of CD11b<sup>pos</sup> and CD64<sup>pos</sup> and lack of expression of CD3, CD19, CD20, CD56, CD49, CD117 and CD15 as described in phenotyping and FACS sorting of STM subsets section. Typically, 2,000–10,000 synovial tissue macrophages per sample were sorted into qPCR 0.2-ml tubes precoated with FSC and containing 10 µl of PBS/0.02% BSA according to 10x Genomics protocol (available online). Cells were loaded onto a Chromium Controller (10x Genomics) for single-cell partitioning, followed by library preparation using Single Cell 3' Reagent Kit v.2. Single-cell libraries were sequenced on the Illumina HiSeq 4000 system to a minimum depth of 50,000 reads per cell.

We compared the transcriptomic profile of synovial myeloid cells from five subject groups: healthy, patients with UPA, treatment-naïve active RA, treatment-resistant active RA and RA in sustained remission (Extended data Fig. 2a).

We sequenced a second set of samples at Glasgow Polyomics, University of Glasgow (Validation cohort—Cohort 2). These included UPA, treatment-naïve active RA, treatment-resistant active RA and RA in sustained remission. These synovial tissue samples were analyzed for both STMs and FLS (Extended Data Fig. 2b). Detailed demographic, clinical, serological and histological characteristics of patients in both cohorts are provided in Supplementary Tables 2 and 3.

Data from both cohorts were integrated using the following methods: (1) processing raw reads. All steps in primary data analysis, including read alignment and generation of count matrices, were performed using the Cell Ranger (2.1) pipeline. Raw base call files generated by sequencing were previously demultiplexed into FASTQ files per sample. The 'cellranger count' tool mapped the reads against the human genome (hg19) and performed unique molecular identifier counting. (2) Quality control and filtering. The Seurat package (3.0.1)<sup>59</sup> in R was used to create an object (CreateSeuratObject, min.cells=5). Cell filtering involved removal of cells with <500 expressed genes (subset, subset=nFeatures\_RNA>500). We also set thresholds for level of gene expression, including expression of mitochondrial genes (percent.mt). This allows for exclusion of doublets and dying cells (see Supplementary Table 4 for exact values). The data were normalized using Seurat's NormalizeData function. For analysis of synovial macrophages only, these cells were computationally isolated with the subset function from other cell types in Validation cohort samples based on expression of CD14, MARCO, LYZ, CD11b and CD64. The top 2,000 variable genes were then identified for all samples, using the FindVariableFeatures function. (3) Integration. Sample integration was performed following the Seurat vignette, integrating all genes common among samples, using the functions FindIntegrationAnchors

and IntegrateData (see features.to.intergrate to find all common genes). These ‘integrated’ batch-corrected values were then set as the default assay, and gene expression values were scaled before running principle component analysis (PCA). (4) Clustering and dimensional reduction. Uniform manifold approximation and projection (UMAP), based on PCA cell embeddings, was generated from integrated counts batch normalized by Seurat, and the first 12 principle components (PCs) were visualized (RunUMAP). The same PCs were used in determination of the *k*-nearest neighbors for each cell during shared nearest neighbor (SNN) graph construction before clustering at a chosen resolution of 0.5 (FindNeighbors, FindClusters). The Destiny (2.14.0) R package (<https://academic.oup.com/bioinformatics/article/32/8/1241/1744143>) was used to plot a diffusion. A count matrix with the average expression of each cluster was generated before using Seurat’s PlotClusterTree function to generate a dendrogram. (5) Sample filtering. To assess the quality of each sample, we determined the pseudobulk expression of each cluster per sample and performed PCA analysis on the result. Sample SA139 was removed due to low sequencing depth in the macrophages. SA225 was removed due to separation from all other samples in the PCA reduced dimensional space (Supplementary Table 4 and Supplementary Fig. 8a–e). (6) Differential expression analysis. To identify cluster markers and variable genes between conditions of RA, the Seurat function FindAllMarkers was used with the ‘test.use’ function MAST<sup>90</sup>. As recommended in the best practice of Seurat, for differentially expressed (DE) comparison the non-batch normalized counts were used. For identification of cluster markers, we specify that any markers identified must be expressed by at least 40% of cells in the cluster (‘min.pct’ parameter 0.4). A complete list of genes characterizing each of the cluster is provided in Supplementary Dataset. For differential expression analysis between conditions we increased this value to 0.6 to reduce the risk of sample bias. We used the default values for all other parameters. Genes are considered significantly DE if the adjusted  $P < 0.05$  by Bonferroni correction and multiple test correction (multiplied by number of tests). To visualize heatmaps, the pheatmap package was adapted. (7) Pathway analysis. To investigate the function of each of our identified synovial macrophage phenotypes, we performed pathway analysis using StringDB (<https://string-db.org/>) and Ingenuity Pathways Analysis (IPA). Pathways associated with positive DE marker genes were investigated for each cluster. For each cluster, the Reactome pathways were exported and compared between all clusters in a custom Rscript. The script compared the gene ratio (number of observed genes in the pathway divided by total number of genes in the pathways as provided by String-db) as well as the associated false discovery rate of significant pathways of interest. Only pathways with  $P < 0.05$  are listed. Similar approaches were used to analyze FLS scRNA-seq data from the Validation cohort. Raw data can be accessed at EMBL-EBI with the accession number E-MTAB-8322.

**Validation of STM clusters identified by scRNA-seq in flow cytometry.** To validate the clusters identified by scRNA-seq, we developed antibody panels 1 and 2 (Supplementary Table 8), which were used in conjunction with dump panel antibodies (Supplementary Fig. 7a). Tissues from the SynGem cohort (described in Fig. 1) ( $n = 6$  active RA and  $n = 4$  RA in remission), and additional tissue from 13 healthy donors, 11 patients with active RA and nine patients in RA disease remission (Supplementary Table 9), were processed and total STM gating was performed as described above. The clusters were defined in each individual patient by panel 1 and/or panel 2 using FlowJo software (Tree Star). Samples with  $< 500$  STM acquired were excluded from quantitative data analysis. In addition, the CD64<sup>pos</sup>CD11b<sup>pos</sup>HLADR<sup>pos</sup> population from each sample was exported and concatenated to make one .fcs file per subject group. These .fcs files were uploaded to Cytobank ([www.cytobank.org](http://www.cytobank.org)), where the viSNE dimensionality reduction algorithm was applied. This allowed for the visualization of changes in cluster distribution between different conditions using the Cytobank software.

**Immunofluorescence staining for distinct STM markers.** Synovial tissue biopsies from healthy donors ( $n = 5$ ) and patients with RA ( $n = 6$  each—active RA and remission RA) (Supplementary Table 10) were preserved in 10% formalin and embedded in paraffin following standard protocols. For antigen retrieval, tissue-fixed slides were immersed in 0.01 M citrate buffer pH 6.0 (TCS HDS05-100) and boiled in a microwave at full power for 5 min, then on reduced power (30%) for a further 8 min. Slides were left to cool for 15 min before being washed in distilled water for 5 min and then washed twice in TBS/0.025% Triton X-100 (Invitrogen) buffer for 5 min. Sections were then incubated with TBS/1% BSA plus 10% normal human serum and 10% serum of the species in which the secondary antibodies were raised (for example, goat serum) at room temperature for 2 h to minimize nonspecific binding. Sections were then incubated with primary antibodies against TREM2, LYVE1, CLEC10A, S100A12 or osteopontin (SPP1) in combination with antibody against the macrophage marker CD68 or appropriate isotope controls (dilutions provided in Supplementary Table 11) overnight at 4°C. The following day, sections were washed twice for 5 min in TBS/0.025% Triton X-100 and then incubated with secondary antibodies (Invitrogen) diluted in TBS/1% BSA at room temperature for 1 h. After incubation, stained sections were washed three times in TBS and counterstained with mounting media containing DAPI (H-1800-2/VECTASHIELD Vibrance). Sections were visualized with a Zeiss

LSM 880 confocal microscope, using either a water immersion  $\times 40$ /numerical aperture (NA) 1.3 or an oil immersion  $\times 63$ /NA 1.4 objective.

**scRNA-seq and analysis of STM–FLS cocultures.** After 48 h coculture, cells were de-attached using Accutase solution (no. A6964, Merck) according to the manufacturer’s protocol. Cells were transferred to U-bottom 96-well plates and harvested by centrifugation at 200 g for 4 min at 4°C. Supernatant was preserved at  $-80^\circ\text{C}$  for cytokine/chemokine/MMP analysis. Cells from each coculture variant were labeled with unique Tags using a Single-Cell Multiplexing Kit (no. 633781) for 15 min at room temperature.

The following sample Tags were used:

- Sample Tag  
1—ATTCAAGGGCAGCCGCTCACGATTTGGATACGACTGTTGGACCGG  
Sample Tag  
2—TGGATGGGATAAGTGCGTGATGGACCGAAGGGACCTCGTGGCCGG  
Sample Tag  
3—CGGCTCGTGCTGCGTCTCAAGTCCAGAAACTCCGTGTATCTCT  
Sample Tag  
4—ATTGGGAGGCTTTTCGTACCGCTGCCGCCACCAGGTGATACCCGCT  
Sample Tag  
5—CTCCCTGGTGTTCATACCCGATGTGGTGGGCAGAATGTGGCTGG  
Sample Tag  
6—TTACCCGCAGGAAGACGTATACCCCTCGTGCCAGGCGACCAATGC  
Sample Tag  
7—TGTCTACGTCGGACCGCAAGAAGTGAGTCAGAGGCTGCACGCTGT  
Sample Tag  
8—CCCACCAGTTGCTTTGTTCGGACGAGCCCGCACAGCGCTAGGAT  
Sample Tag  
9—GTGATCCGCGCAGGCACACATACCGACTCAGATGGGTTGTCCAGG  
Sample Tag  
10—GCAGCCGCGCTGTCAGAGGCACAGCGGAGACTAGATGAGCCCC  
Sample Tag  
11—CGCGTCCAATTCCGAAGCCCCGCCCTAGGAGTCCCTGCGTGC  
Sample Tag  
12—GCCCATTCATTGCACCCGCCAGTGATCGACCTAGTGAGGCTAAG

Cells were then washed three times with PBS, with centrifugation steps (200g for 4 min at 4°C), after which the Tagged coculture variants were pooled and stained with Fixable Viability Dye eFluor 780 (eBioscience) as described above. Live cells ( $50 \times 10^6$ ) were sorted and immediately (Supplementary Fig. 9a–d) loaded onto the scRNA-seq BD Rhapsody Cartridge using the BD Rhapsody Cartridge Reagent Kit (no. 633731) according to the manufacturer’s protocol. Single-cell cDNA was prepared using the BD Rhapsody cDNA Kit (no. 633773). This was followed by single-cell mRNA and Tag library preparation using BD Rhapsody Targeted mRNA and the Tag Amplification Kit (no. 633774), primers for the BD Rhapsody Immune Response Panel (399 genes; no. 633750) and a custom-made panel that included additional genes expressed by FLS and not represented in the Human Immune Panel (46 genes; Supplementary Dataset). Libraries were sequenced at a depth of  $956,374 \pm 249,958$  (mean  $\pm$  s.e.m.) reads per Tag using Illumina NextSeq 500 (Glasgow Polyomics). Then,  $1,228 \pm 370$  cells (mean  $\pm$  s.e.m.) per Tag were successfully sequenced (Supplementary Dataset). For analysis, the sequencing reads were processed with BD Genomics Rhapsody Analysis Pipeline CWL v.1.8 on the command line. We added 45 genes to the reference gene panel; this tool generated the read count matrix for each condition. The Seurat package (3.1.2)<sup>99</sup> in R was used to create an object from the RSEC\_MolsPerCell.csv file for each sample Tag (CreateSeuratObject, min.cells=3). Fibroblasts were computationally isolated by selecting for cells lacking expression of the PTPRC (CD45) gene, as illustrated in Supplementary Fig. 9e). Seurat implementation of the SCTransform package (0.2.0) was used for normalization and data scaling (SCTransform). Data from each run were integrated using functions compatible with SCTransform normalization (SelectIntegrationFeatures, PrepSCTIntegration, FindIntegrationAnchors, IntegrateData). Principle component analysis of integrated counts, batch normalized by Seurat, was performed (RunPCA) before generating a UMAP (RunUMAP) from the first ten PCs. The same PCs were used in determination of *k*-nearest neighbors for each cell during SNN graph construction, before clustering at a chosen resolution of 0.2 (FindNeighbors, FindClusters). Differential expression was performed using SCT normalized assay (FindAllMarkers, test.use=MAST) to identify cluster markers and variable genes between coculture conditions. Genes are considered significantly DE if the adjusted  $P < 0.05$  by Bonferroni correction, and multiple test correction (multiplied by number of tests). To visualize heatmaps the pheatmap package was adapted. The SCT normalized expression values were also used to perform pseudobulk expression analysis of each sample (AverageExpression) for investigation of previously identified genes of interest. Raw data are accessible at EMBL-EBI with the accession number E-MTAB-8873. The DE genes were confirmed at the protein level using Luminex (no. PPX-06/PROCARTAPLEX, Life Technologies; Supplementary Fig. 9f), as described above for coculture.

**Bulk RNA-seq of synovial fibroblasts cocultured with MoM.** High-quality total RNA (RNA integrity number >8) was used to construct Illumina mRNA sequencing libraries. cDNA synthesis and amplification were performed using a SMART-seq v.4 Ultra Low Input RNA Kit for Sequencing (no. 634890, Takara) starting with 10 ng of total RNA and following the manufacturer's protocol. Next, 10 ng of amplified cDNAs was sheared before preparation of final libraries using the Bioruptor Pico system (Diagenode, 24 cycles of 30/30 s on/off). Dual-indexed Illumina sequencing libraries were prepared using the SMARTer ThruPLEX DNA-seq 48D Kit (no. R400406, Takara) following the manufacturer's protocol. The pooled libraries were sequenced at Edinburgh Genomics (Edinburgh, UK) on a NovaSeq 6000 system using a read length of 100 bases in paired-end mode. The reads were mapped with STAR (v.020201) with default parameter against the human genome version GRCh38, release 91. The read count matrix was constructed with featureCounts (v1.6.4) using default parameters. All differential expression analysis was performed in R using the DESeq2 package. All genes with adjusted  $P < 0.05$  and log fold-change  $> \pm 1.5$  were considered significantly differentially expressed. Raw data are accessible at EMBL-EBI with the accession number [E-MTAB-8316](#).

**Comparison of human and mouse scRNA-seq data.** A recent study by Culemann et al.<sup>9</sup> performed single-cell transcriptional profiling on murine synovial tissue macrophages from the K/BxN serum transfer-induced arthritis model. We downloaded the data ([GSE134691](#)) and integrated these with our human samples from healthy tissue, UPA, naïve active RA and treatment-resistant active RA. This was performed in a stepwise manner, first by disease group, then by species and finally by integration across species, using Seurat's current integration methods (FindIntegrationAnchors, Integrate Data). The combined dataset was then scaled before performing dimensional reduction and clustering using the top 15 PCs at a resolution of 0.3. Cluster marker genes were identified, and clusters were renamed accordingly. In addition, the datasets were subsetted to create separate Seurat objects containing an assay of gene expression normalized across species from the final integration step. The datasets were then clustered and analyzed separately. Orthologs (genes present in both datasets,  $n = 7,954$ ) were also identified using the intersect function in R, and the average expression of such genes was calculated for each dataset using the gene expression values from cross-species normalization. The outputs for each dataset were merged, and a distance matrix (dist function) was generated before performing hierarchical clustering (hclust function). A dendrogram was plotted from the result to demonstrate the relationship between synovial macrophage clusters from different species.

**Analysis of candidate genes in the PEAC cohort.** The detailed methodology and analytical pipeline of synovial tissue bulk RNA-seq from 90 individuals with early treatment-naïve rheumatoid arthritis from the PEAC were described previously<sup>43</sup>. The study was approved by the UK Health Research Authority (no. REC 05/Q0703/198, National Research Ethics Service Committee London) and all patients gave written informed consent. Total RNA (1 µg per sample) was extracted from whole synovial tissue retrieved from an inflamed peripheral joint using the Trizol/chloroform method. Bulk RNA-seq (50 million paired-end 75 base pair reads per sample) was performed on an Illumina HiSeq2500 platform. RNA-seq data were uploaded to ArrayExpress (accession no. [E-MTAB-6141](#)). Data are expressed as regularized log, transformed reads.

**Statistical evaluation of STM phenotyping and culture experiments.** Receiver operating characteristic (ROC) analysis identified the optimal predictive values for MerTK<sup>pos</sup>CD206<sup>pos</sup>, MerTK<sup>neg</sup>CD206<sup>neg</sup>, CD163<sup>pos</sup>CD206<sup>pos</sup> and CD163<sup>neg</sup>CD206<sup>neg</sup> STMs associated with flare in the following groups: (1) patients with RA in sustained clinical and ultrasound remission and who experienced disease flare, and (2) patients with RA in sustained clinical and ultrasound remission and who did not experience disease flare after treatment modification ( $n = 11$  in each group). Logistic regression was performed to determine disease flare occurrence using independent variables: cutoff values discriminating disease flare from sustained remission for MerTK<sup>pos</sup>CD206<sup>pos</sup>, MerTK<sup>neg</sup>CD206<sup>neg</sup>, CD163<sup>pos</sup>CD206<sup>pos</sup> and CD163<sup>neg</sup>CD206<sup>neg</sup> synovial macrophage subpopulations in patients with RA in both clinical and ultrasound remission. The values were expressed as odds ratio and 95% confidence interval, respectively. The Hosmer–Lemeshow test was used to assess the fitting of the model. To assess the correlation coefficient between different clinical parameters and STM subpopulations or STM marker genes, two-sided Spearman's test was used and both  $R$  and  $P$  values, as well as 95% confidence intervals, are reported in the figures.

Differences in individual STM populations or cytokines between more than two joint conditions were evaluated using one-way analysis of variance (ANOVA) with Tukey's correction for multiple comparison, or the Kruskal–Wallis test with Dunn's correction for multiple comparison. To evaluate the influence of individual STMs on FLS clusters, the Kruskal–Wallis test with Dunn's correction for multiple comparisons was used. The two-tailed nonparametric unpaired Mann–Whitney test or paired  $t$ -test was used when two groups were compared. Two-way ANOVA with Tukey's correction for multiple comparison was used to evaluate (1) differences between multiple cell clusters in multiple conditions and (2) GAS6 production from different FLS lines following different stimuli. Statistical tests,

$P$  values and range or precise numbers ( $n$ ) are provided in each figure. When range and  $n$  are provided in the respective figure legends, the exact  $n$  values are provided.

For validation of scRNA-seq-identified STM clusters by flow cytometry, synovial tissue samples from healthy ( $n = 9$ ), active RA ( $n = 17$ ) and RA in remission ( $n = 13$ ) were used to evaluate MerTK<sup>pos</sup>FOLR2<sup>pos</sup> STMs; from healthy ( $n = 9$ ), active RA ( $n = 17$ ) and RA in remission ( $n = 12$ ) to evaluate MerTK<sup>pos</sup>TREM2<sup>pos</sup> STMs; and from healthy ( $n = 9$ ), active RA ( $n = 14$ ) and RA in remission ( $n = 9$ ) to evaluate MerTK<sup>pos</sup>LYVE2<sup>pos</sup> STMs. Synovial tissue samples from healthy ( $n = 8$ ), active RA ( $n = 13$ ) and RA in remission ( $n = 7$ ) were used to evaluate MerTK<sup>neg</sup>CD48<sup>pos</sup>, MerTK<sup>neg</sup>SI100A12<sup>pos</sup> and MerTK<sup>neg</sup>CLEC10a<sup>pos</sup> STMs; and from healthy ( $n = 7$ ), active RA ( $n = 12$ ) and RA in remission ( $n = 7$ ) to evaluate MerTK<sup>neg</sup>SPP1<sup>pos</sup> STMs. The transcriptomic profile of synovial tissues from patients with RA ( $n = 90$ ; PEAC cohort) was used for correlation analysis between STM markers/remission-associated transcription factors and disease activity. Representative IHC/IF staining of STM markers of synovial tissue samples from healthy patients ( $n = 5$ ), those with active RA ( $n = 6$ ) and those in remission with RA ( $n = 6$ ), in three independent experiments with similar results, are shown. STM–FLS cocultures ( $n = 6$ ) were performed with STMs from six different patients with RA and with FLS from five different patients with RA, in three independent experiments.

**Reporting Summary.** Further information on research design is available in the Nature Research Reporting Summary linked to this article.

### Data availability

Ranked lists of STM cluster markers, condition-specific markers of MerTK<sup>pos</sup> STM clusters identified by comparison of two clinical conditions, multiple conditions, STM cluster pathway analysis, FLS cluster markers and DEGs of lining-layer FLS clusters comparing active and remission synovium are provided in the Supplementary Dataset. The list of genes in the custom stromal panel, sample scRNA-seq metrics of FLS cocultured with STM and sequenced with scRNA-seq BD Rhapsody system, and the list of DEGs from FLS–MoM cocultured with MerTK inhibitor, are provided in the Supplementary Dataset. All raw and processed data of STM scRNA-seq, STM–FLS coculture scRNA-seq and MoM–FLS coculture bulk RNA-seq (FLS) were deposited at EMBL-EBI and are available with the following accession numbers: [E-MTAB-8322](#), [E-MTAB-8873](#) and [E-MTAB-8316](#).

### Code availability

The Seurat objects and codes used are available from the corresponding authors upon reasonable request.

### References

- Aletaha, D. et al. 2010 rheumatoid arthritis classification criteria: an American College of Rheumatology/European League Against Rheumatism collaborative initiative. *Ann. Rheum. Dis.* **69**, 1580–1588 (2010).
- Alten, R. et al. Developing a construct to evaluate flares in rheumatoid arthritis: a conceptual report of the OMERACT RA Flare Definition Working Group. *J. Rheumatol.* **38**, 1745–1750 (2011).
- Machado, P. et al. Multinational evidence-based recommendations on how to investigate and follow-up undifferentiated peripheral inflammatory arthritis: integrating systematic literature research and expert opinion of a broad international panel of rheumatologists in the 3E Initiative. *Ann. Rheum. Dis.* **70**, 15–24 (2011).
- Alivernini, S. et al. MicroRNA-155 influences B-cell function through PU.1 in rheumatoid arthritis. *Nat. Commun.* **7**, 12970 (2016).
- Krenn, V. et al. Synovitis score: discrimination between chronic low-grade and high-grade synovitis. *Histopathology* **49**, 358–364 (2006).
- Liu, J. et al. UNC1062, a new and potent Mer inhibitor. *Eur. J. Med. Chem.* **65**, 83–93 (2013).
- Stuart, T. et al. Comprehensive integration of single-cell data. *Cell* **177**, 1888–1902 (2019).
- Finak, G. et al. MAST: a flexible statistical framework for assessing transcriptional changes and characterizing heterogeneity in single-cell RNA sequencing data. *Genome Biol.* **16**, 278 (2015).

### Acknowledgements

We thank the patients and healthy volunteers who participated in this study. We thank D. Vaughan for her outstanding support in cell sorting and phenotyping; D. Riggans (University of Glasgow Mail Room), who facilitated smooth deliveries of clinical samples from Rome to Glasgow and Oxford; A. Corbyn, T. Khoyratty and J. Webber (The Kennedy Institute of Rheumatology, Oxford, UK) for assistance in preparing cells for single-cell sequencing; C. Giampà and O. Parolini (Istituto di Anatomia Umana e Biologia Cellulare, Università Cattolica del Sacro Cuore, Rome, Italy) for support with fluorescent microscopy; J. Galbraith and P. Herzyk (Glasgow Polyomics) for rapid scRNA-seq of samples for the revised version of this manuscript; and L. Lemgruber Soares for help with confocal microscopy. This work was supported by the Research into Inflammatory



Arthritis Centre Versus Arthritis UK, based in the Universities of Glasgow, Birmingham, Newcastle and Oxford (nos. 20298 and 22072) to L.M., S.F., S.N.S., A.F., A.R.C., I.U., C.D.B., T.D.O., I.B.M. and M.K.-S.; linea D1 (no. R4124500654) (Università Cattolica del Sacro Cuore, no. R4124500654, to S.A.); Ricerca Finalizzata Ministero della Salute (no. GR-2018-12366992, to S.A.); Versus Arthritis UK Program (grant no. 21802, to A.R.C., M.K.-S. and A.E.); Versus Arthritis UK (grant no. 22272, to M.K.-S.); Wellcome Trust (no. 204820/Z/16/Z, to T.D.O. and M.K.-S.); and BPF\_Medical Research Trust (to C.M.).

### Author contributions

S.A. and M.K.-S. conceived and oversaw the project, performed scRNA-seq, interpreted all the results and wrote the manuscript with feedback from all authors. S.A. and B.T. performed all synovial biopsies, ran synovial tissue processing/handling and linked clinical information with experimental datasets. L.M. analyzed all scRNA-seq and bulk RNA-seq data, validated scRNA-seq data by flow cytometry, together with M.K.-S., performed STM-FLS cocultures with the scRNA-seq BD Rhapsody system and helped write the manuscript. S.F. performed phenotyping of STMs, stimulation of STMs and the cocultures of MoM with FLS in the trans-well system. A.E. performed phenotyping of STMs, validation of scRNA-seq data with IHC/IF and direct coculture of MoM with FLS. S.A., E.G., M.R.G. and L.P. enrolled the study cohort. S.A., M.R.G., L.P., S.P. and A.L.F. followed all study cohorts and collected clinical and ultrasound data. S.A., M.R.G. and S.P. followed all patients in RA remission for withdrawal study in the SYNGem cohort. C.D.M. and S.P. performed serological assessment for autoantibody positivity of the entire study cohort. L.B. performed MerTK IHC staining of synovial biopsies. M.G. performed semiquantitative assessment of synovitis score in synovial biopsies. M.A. performed 10x Genomics of the Discovery Cohort. S.C. prepared the libraries of

MoM-FLS cocultures. D.S. helped A.E. with validation of scRNA-seq classification of STMs by IF. S.N.S. provided bioinformatic input to scRNA-seq data. A.F. provided protocol for MoM-FLS coculture studies. C.M. helped with interpretation of data and writing of the manuscript. N.L.M. provided healthy synovial tissues. K.K. provided protocol for scRNA-seq. A.N., M.J.L. and C.P. provided data from the PEAC cohort. C.D.B., A.R.C., G.F., E.G. and I.B.M. helped with data interpretation. I.U. provided sorting protocol for scRNA-seq and helped with data interpretation. E.G. and I.B.M. assisted with running of the project. T.D.O. and M.K.-S. supervised all computational analysis in the study. All authors approved the manuscript.

### Competing interests

All authors declare no competing interests.

### Additional information

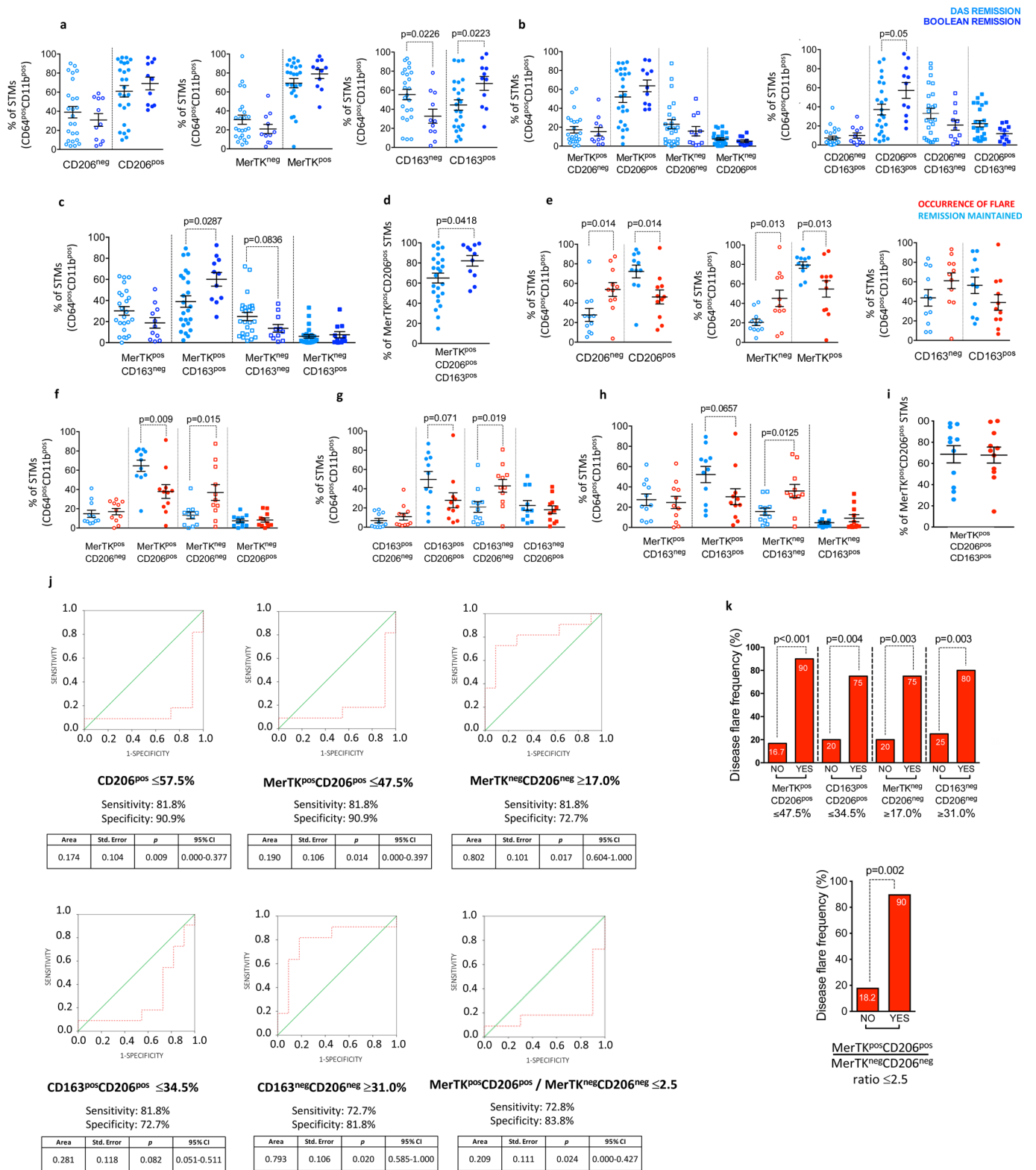
**Extended data** is available for this paper at <https://doi.org/10.1038/s41591-020-0939-8>.

**Supplementary information** is available for this paper at <https://doi.org/10.1038/s41591-020-0939-8>.

**Correspondence and requests for materials** should be addressed to S.A., T.D.O. or M.K.-S.

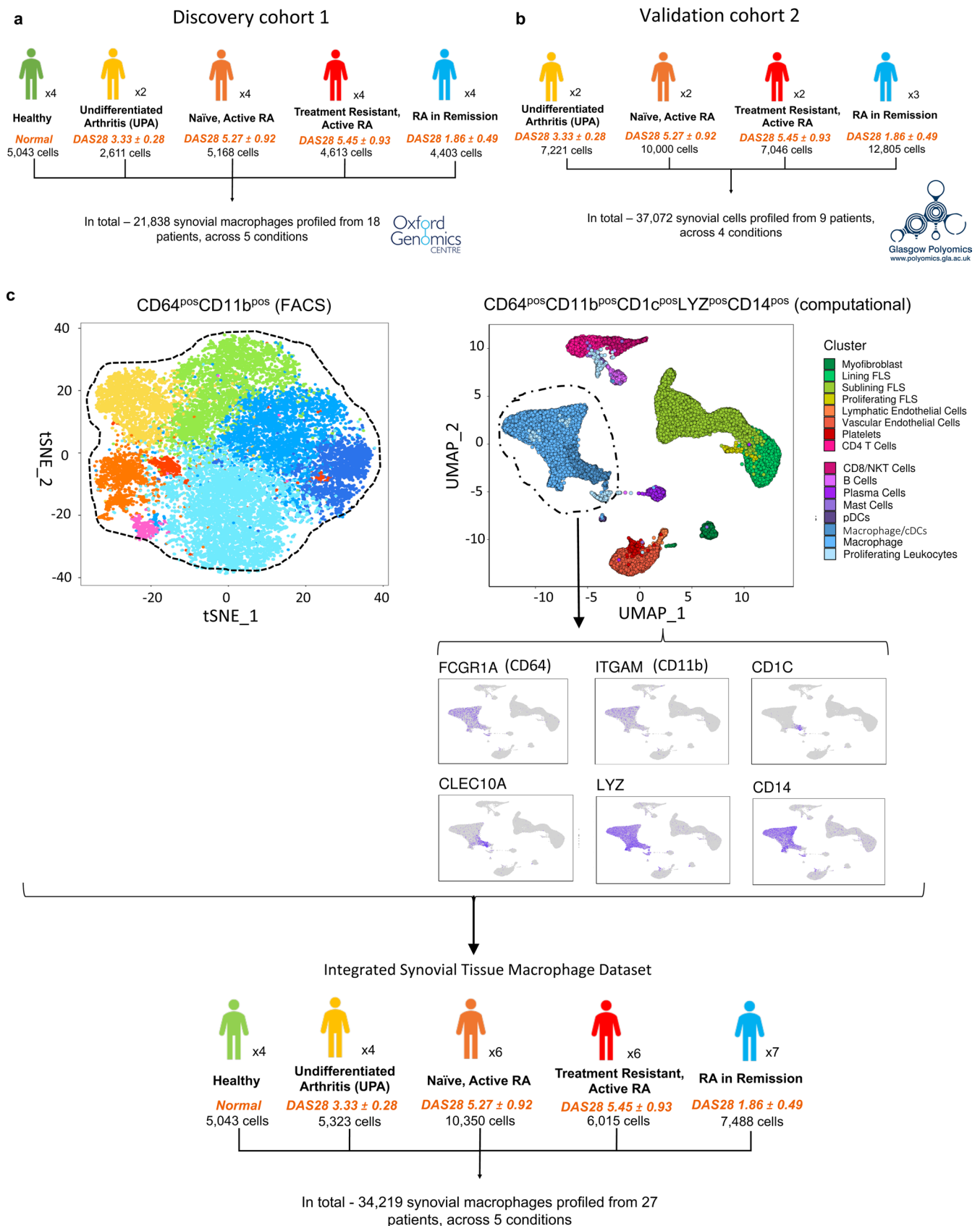
**Peer review information** Saheli Sadanand was the primary editor on this article and managed its editorial process and peer review in collaboration with the rest of the editorial team.

**Reprints and permissions information** is available at [www.nature.com/reprints](http://www.nature.com/reprints).

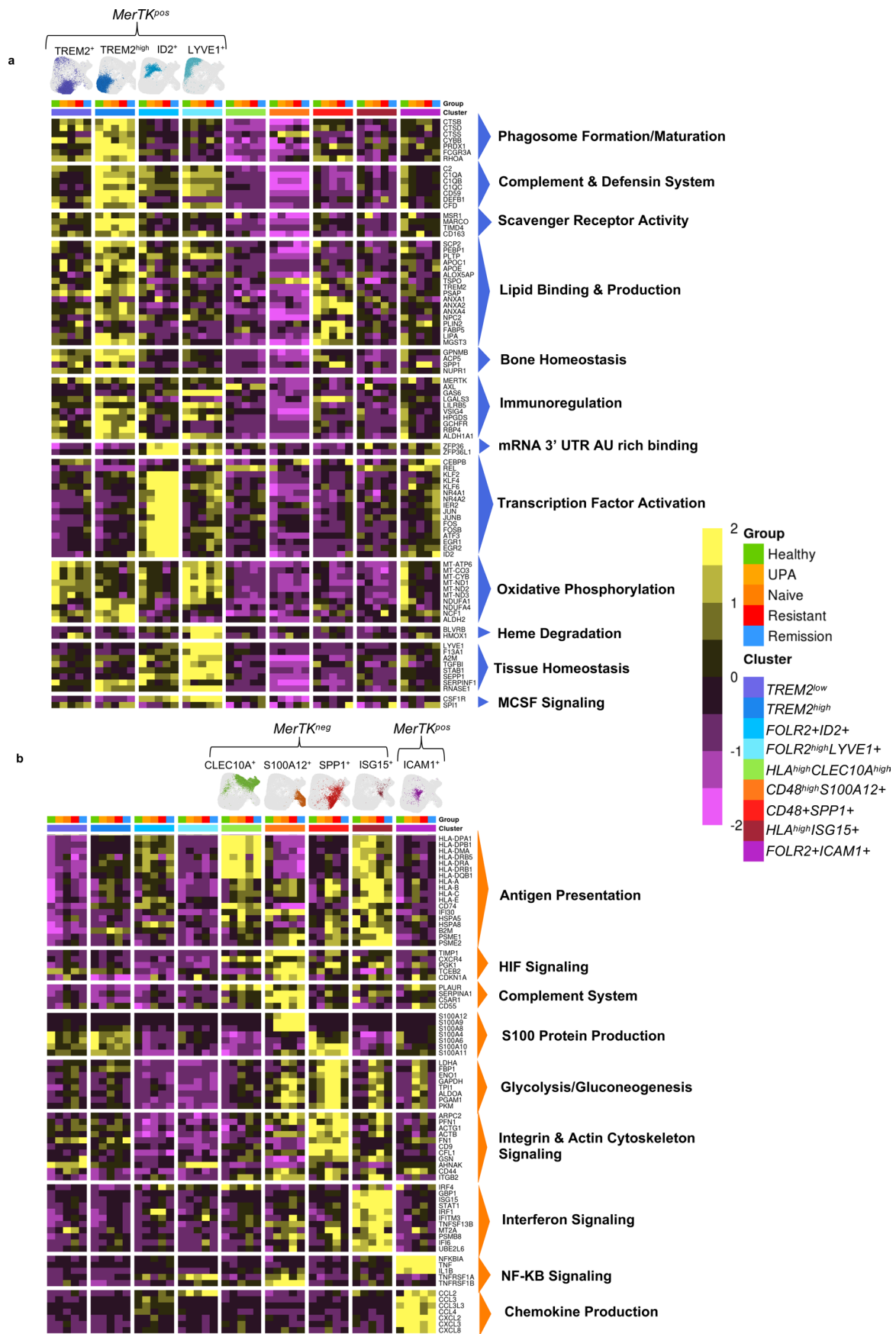


Extended Data Fig. 1 | See next page for caption.

**Extended Data Fig. 1 | A low proportion of MerTK<sup>pos</sup>CD206<sup>pos</sup> STMs in remission was associated with increased risk of disease flare after treatment cessation. a-d**, Comparison of STM distribution between RA patients with disease remission defined by either DAS28 (n = 24) or Boolean criteria (n = 11). Analyses include comparison of STMs: **a**, single-marker positive or negative for CD206 or MerTK or CD163, **b**, double-marker positive or negative for MerTK and CD206, and double-marker positive or negative for CD206 and CD163, **c**, double-marker positive or negative for MerTK and CD163 and **(d)** triple-marker positive for MerTK, CD206 and CD163. **e-i**, Comparison of baseline STM distribution between RA patients in remission who subsequently flared (n = 11) or remained in remission (n = 11) after treatment discontinuation. Analyses include comparison of STMs: **e**, single-marker positive or negative for CD206 or MerTK or CD163, **f**, double-marker positive or negative for either MerTK or CD206, **g**, double-marker positive or negative for either CD163 or CD206, **h**, double-marker positive or negative for either MerTK or CD206 and **(i)** triple-marker positive for MerTK, CD206 and CD163. **j**, ROC curves for optimal cut-off values of STM proportions of CD206<sup>pos</sup>, MerTK<sup>pos</sup>CD206<sup>pos</sup>, MerTK<sup>neg</sup>CD206<sup>neg</sup>, CD163<sup>pos</sup>CD206<sup>pos</sup>, CD163<sup>neg</sup>CD206<sup>neg</sup>, and the MerTK<sup>pos</sup>CD206<sup>pos</sup> to MerTK<sup>neg</sup>CD206<sup>neg</sup> ratio discriminating disease flare in RA in remission (n = 22) described in **e-i**. (Wilson/Brown method) **k**, Comparison of occurrence of flare stratified by the cut-off values for different STM populations (Wilcoxon test.) Data in (a-i) are mean +/-sem, differences in STM populations between remission states were evaluated by Two-tailed Mann-Whitney, p-values provided on graphs.



**Extended Data Fig. 2 | Integration of scRNAseq data.** **a**, Metadata for FACS sorted CD64<sup>pos</sup>CD11b<sup>pos</sup> STMs sequenced in the Discovery Cohort (Cohort 1) at Oxford Genomics Centre. **b**, Metadata for all synovial cell types sequenced in the Validation Cohort (Cohort 2) at Glasgow Polyomics. **c**, Myeloid cells sequenced in Cohort 2 are separated computationally (based on positive expression of CD64, CD11b, CD14, MARCO, CD1c and LYZ), and integrated with synovial macrophages sequenced in the Discovery cohort 1.




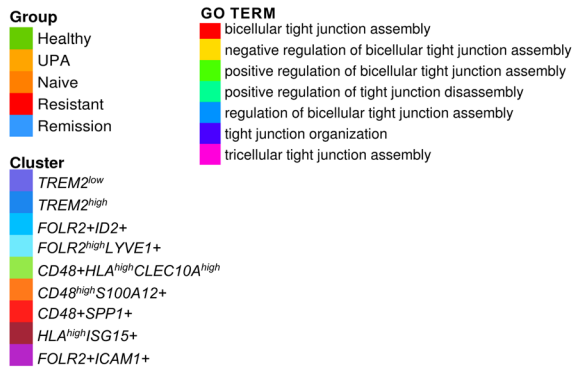
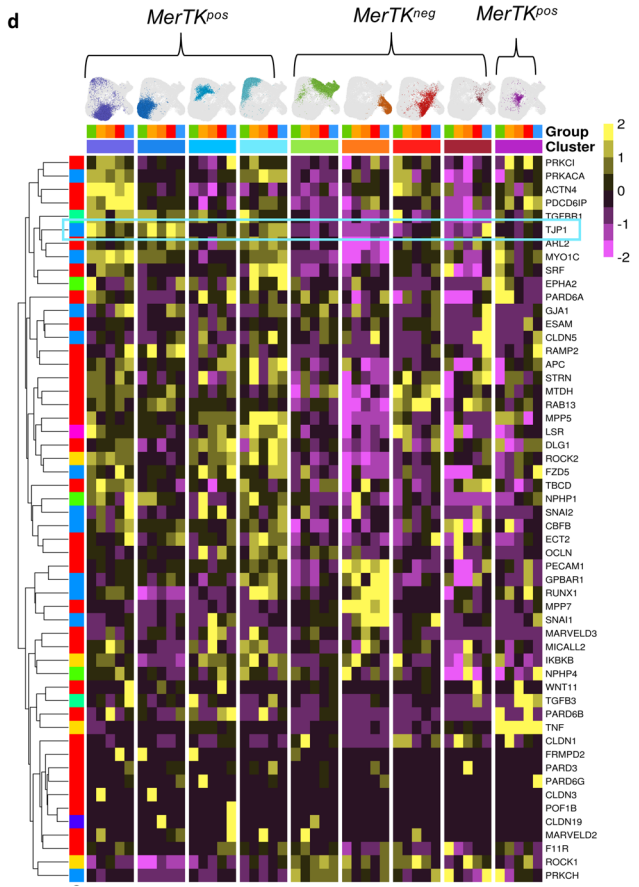
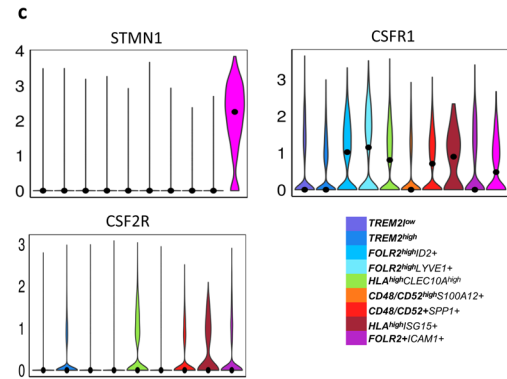
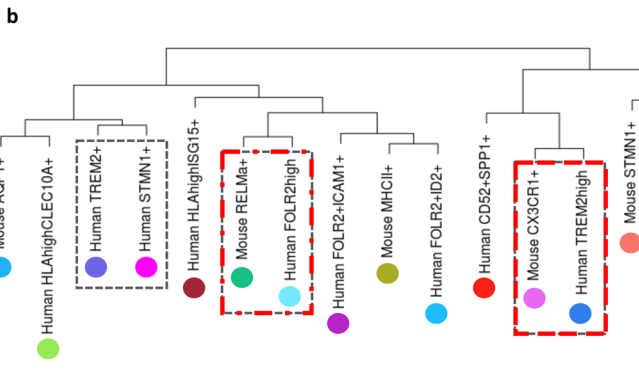
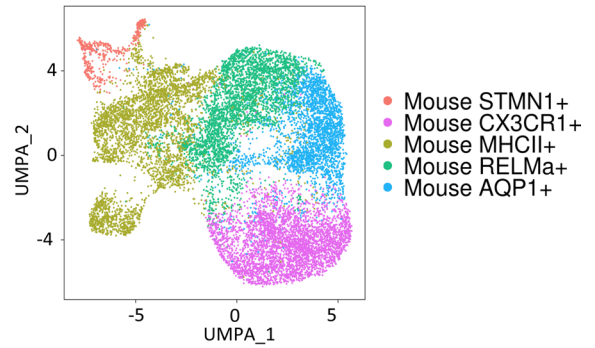
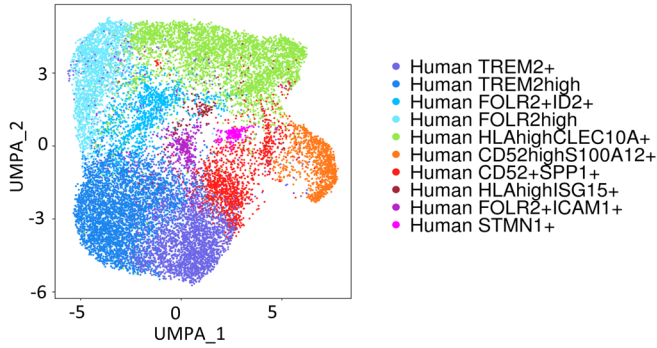
Extended Data Fig. 3 | See next page for caption.

**Extended Data Fig. 3 | Pathway analysis of differentially expressed genes between clusters revealing different effector pathways in STM**

**subpopulations. a**, Heatmap illustrating scaled pseudo-bulk expression of significantly enriched pathways in four MerTK<sup>pos</sup> clusters and **(b)** in four MerTK<sup>neg</sup> clusters and in the MerTK<sup>pos</sup> ICAM1<sup>pos</sup> cluster (Healthy, n = 4; UPA, n = 4; naïve-active RA, n = 5; treatment-resistant RA, n = 6 and RA in remission, n = 6). Rows are genes and columns represent average expression for cells in each cluster by subject group. All genes are significantly expressed in at least 60% of cells in that cluster. DE Genes identified by Seurat function (MAST) were filtered afterwards to ensure that the p-value adjusted by Bonferroni correction is significant ( $p < 0.05$ ). Average log fold change  $\geq 0.25$ . Differentially expressed genes between clusters were used to perform GO and IPA analysis to identify significant cluster specific pathways (Fisher's exact test with Bonferroni correction). Upregulated genes from selected significant pathways of interest are annotated.

**a**  **Healthy**  
Undifferentiated Arthritis (UPA)  
Naïve, Active RA

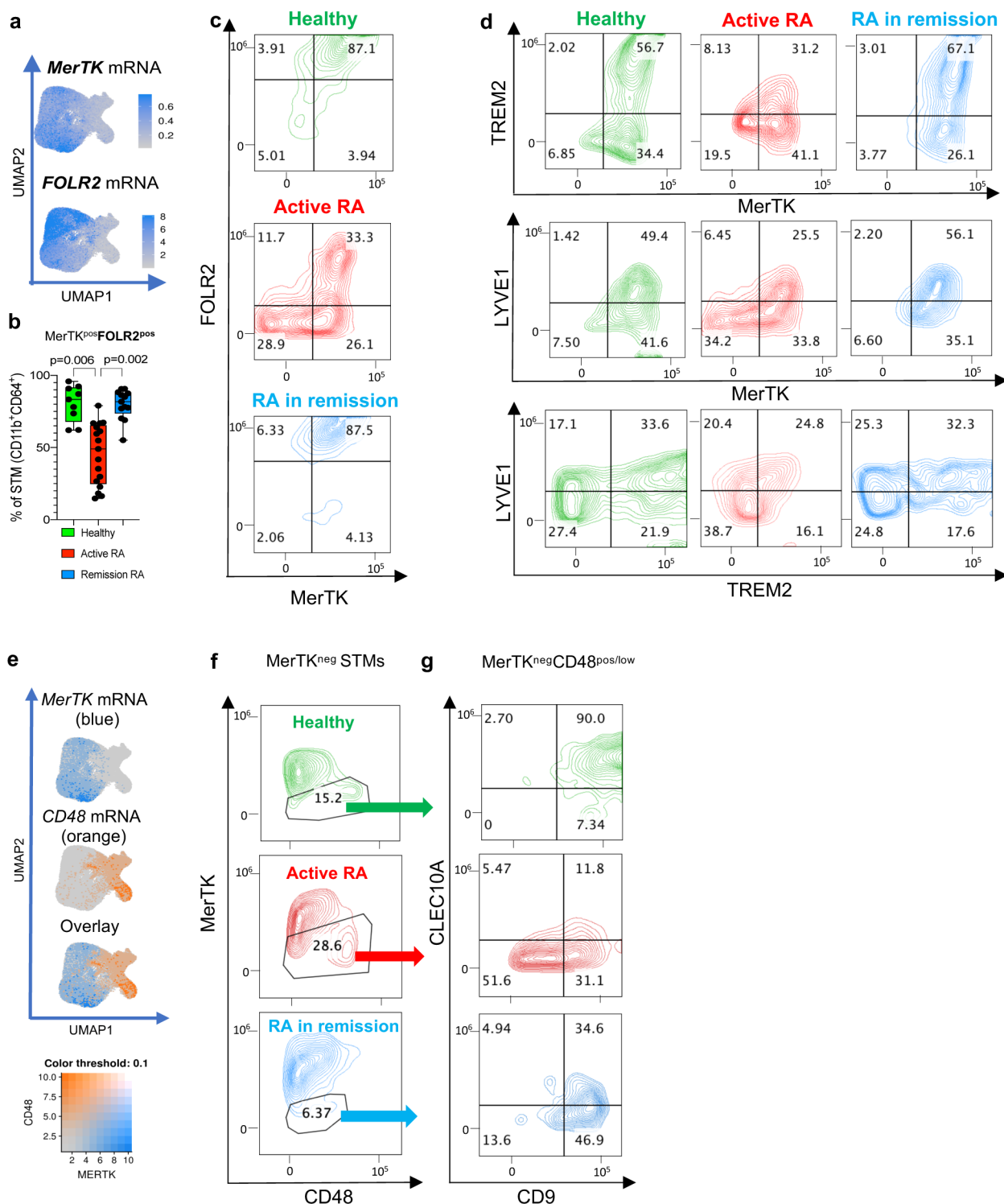
 **Culemann et al. (2019)**  
Steady state  
Day 1, 2 & 5 following serum transfer



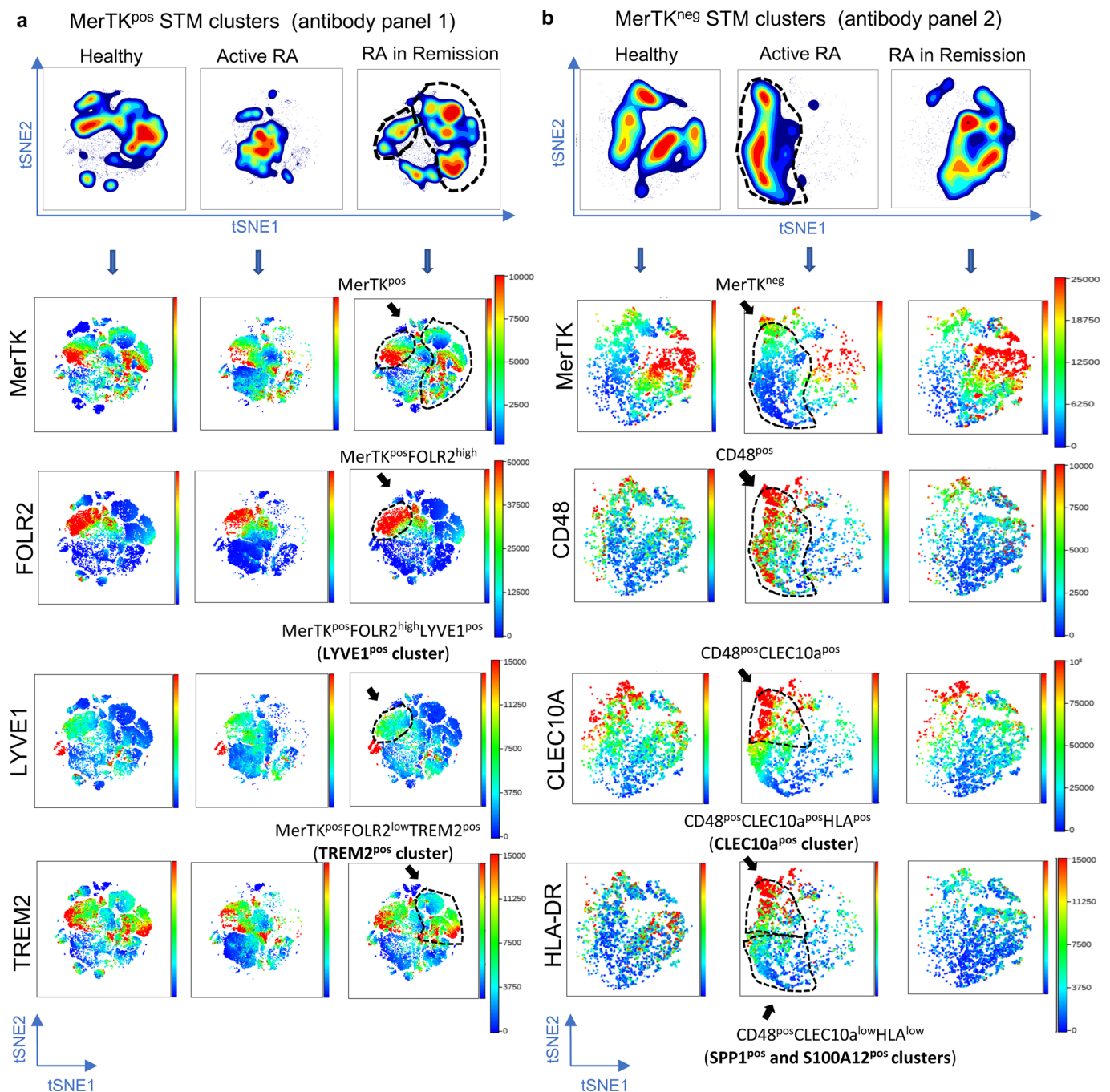
Extended Data Fig. 4 | See next page for caption.

**Extended Data Fig. 4 | Comparison of Human and Mouse (Culemann et al., 2019) single-cell transcriptional profiling of synovial macrophages.** **a**, UMAP projections for human and mouse scRNAseq data analyzed separately. Mouse data clustered at a resolution of 0.3 and UMAP projection represents the top 12 PCs. Human data for this comparison included samples from healthy tissue (n = 4), UPA (n = 5) and naïve-active RA (n = 5) to align with disease conditions modelled in the mouse data (n = 4). **b**, Dendrogram representing the relationship between human macrophage phenotypes and mouse clusters. This plot was generated from the hierarchical clustering of the average expression of orthologous genes by each population. **c-d**, Patients' cohort described in Fig. 2a. Violin plots show log-normalized expression values of STMN, a marker of proliferation; CSF1R, that is the highest in FOLR2<sup>pos</sup>ID2<sup>pos</sup>, and GM-CSFR (CSF2R) that is higher in MerTK negative clusters of human STMs. Shape of the violin represents the density of the data at different expression values with median marked by dot while colour represents unique STM cluster. **d**, MerTK<sup>pos</sup> STMs are enriched in tight-junction proteins. Heatmap illustrating scaled pseudobulk expression of significantly enriched pathways by each patient group within each of identified STM clusters. Rows represent genes with a potential contribution to synovial lining-layer barrier function (GO pathway- involved tight-junction assembly and organization). Columns represent equal average expression for cells in each cluster by subject group. The blue box highlights gene orthologue identified in mouse synovial lining macrophages as tight-junction proteins (Culemann et al). Among them, TJP1 is expressed by human MerTK<sup>pos</sup>TREM2<sup>pos</sup> and MerTK<sup>pos</sup>FOLR2<sup>pos</sup>LYVE1<sup>pos</sup> STMs.



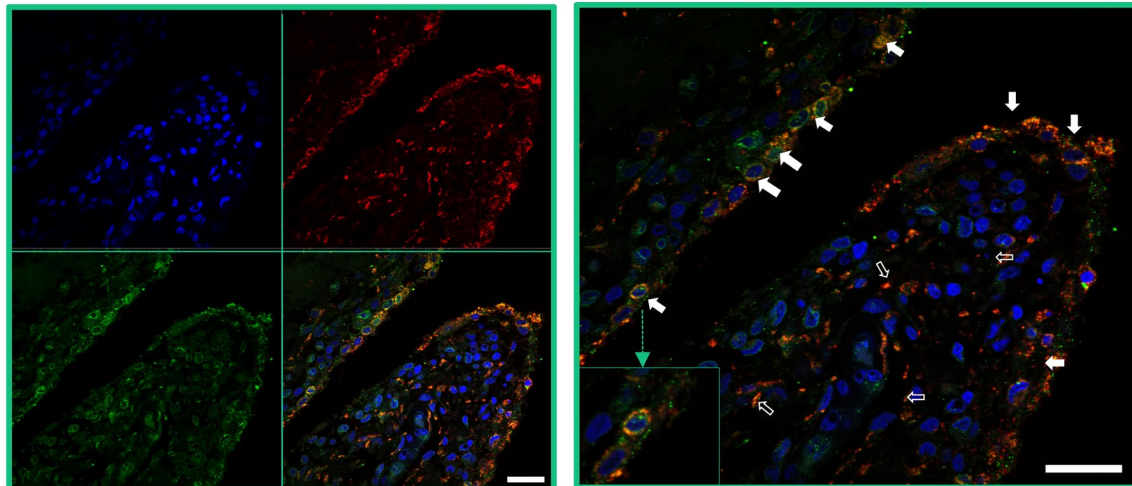


**Extended Data Fig. 5 | Flow-cytometric validation of STM clustering categorized by scRNAseq. a-c**, scRNAseq data (a) (patient cohort described in Fig. 2a) and flow cytometry data (b-c) representing 16 independent experiments with synovial tissue samples from 31 RA patients and 10 Healthy showing that mRNA and protein expression of MerTK and FOLR2 coincide, suggesting that FOLR2 can be used as an alternative marker of MerTK<sup>pos</sup> STMs. **d**, Representative gating strategies for TREM2 and LYVE1 positive STMs in conjunction with MerTK expression in health, active RA and RA in disease remission. The TREM2<sup>pos</sup> cluster is defined by the positive expression of MerTK and TREM2, and the LYVE1<sup>pos</sup> cluster is defined by the positive expression of LYVE1 and MerTK. A proportion of TREM2<sup>pos</sup> STMs are also LYVE1<sup>pos</sup>. The n numbers per staining and quantitative data are provided in Fig. 2i-k. **e-g**, scRNAseq data (e) (patient cohort described in Fig. 2a) and representative gating strategy for MerTK<sup>neg</sup> STMs (f) showing that most of MerTK<sup>neg</sup> STMs are CD48 positive. **g**, Distribution of CD9 and CLEC10a positive cells within MerTK<sup>neg</sup>CD48<sup>low/pos</sup> STMs in health, active RA and RA in disease remission are shown. The MerTK<sup>neg</sup>S100A12<sup>pos</sup> cluster is defined as CD48<sup>low/pos</sup>CD9<sup>neg</sup>CLEC10a<sup>neg</sup>, the MerTK<sup>neg</sup>SPP1<sup>pos</sup> cluster is defined as CD48<sup>pos/low</sup>CD9<sup>pos</sup>CLEC10a<sup>neg</sup>, and the MerTK<sup>neg</sup>CLEC10a<sup>pos</sup> cluster is defined as CD48<sup>low/pos</sup>CD9<sup>pos</sup>CLEC10a<sup>pos</sup>. The n numbers per staining and quantitative data are provided in Fig. 2i-k.

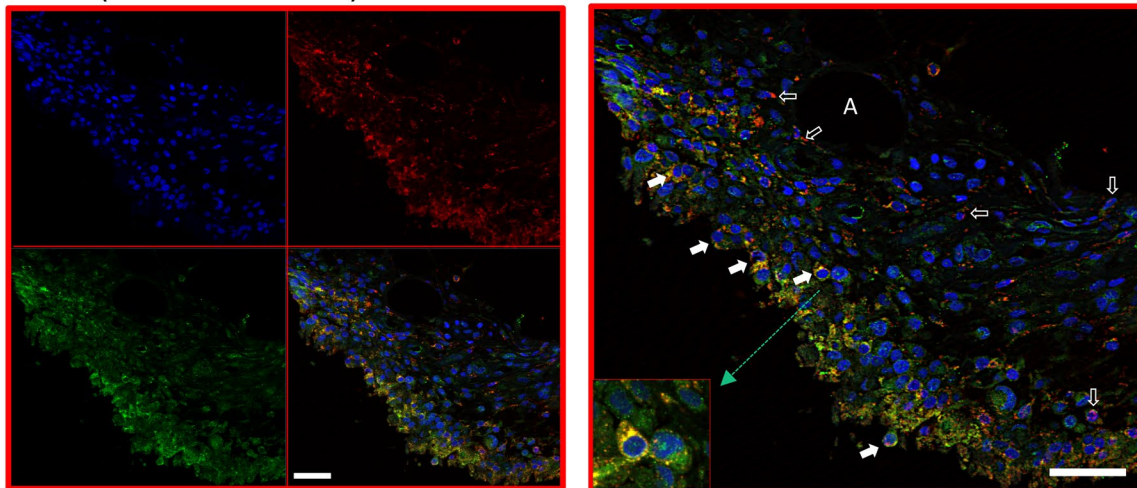


**Extended Data Fig. 6 | High-dimensional characterization of STMs using viSNE dimensionality reduction algorithm. a,b**, STMs in healthy and RA in sustained disease remission show enrichment in MerTK positive clusters ( $\text{TREM2}^{\text{pos}}$  and  $\text{FOLR2}^{\text{high}}\text{LYVE1}^{\text{pos}}$ ) while patients with active RA show an increase in MerTK negative clusters ( $\text{CLEC10A}^{\text{pos}}$ ,  $\text{SPP1}^{\text{pos}}$  and  $\text{S100A12}^{\text{pos}}$  clusters). **a-b**, Single cell synovial tissue digests from healthy controls and RA patients as described in Fig. 2i-k and Extended Data Fig. 5 were stained with panel 1 of 9 antibodies (plus dump panel) to identify MerTK positive clusters (**a**) or with panel 2 of 9 antibodies (plus dump panel) to identify MerTK negative clusters (Supplementary Table 8 and Methods) (**b**). viSNE plots of clustered total STMs ( $\text{CD64}^{\text{pos}}\text{CD11b}^{\text{pos}}\text{lineage}^{\text{neg}}$ ) are displayed for MerTK positive (**a**) and MerTK negative (**b**) STMs, showing cell density of clusters and changes between conditions. The number of cells per condition were normalized to 25K. Bars represent individual expression scale for each marker. Dotted lines demarcate clusters dominant in remission RA/healthy (**a**) or active RA (**b**). **a**, Synovial tissue from Healthy ( $n=9$ ), active RA ( $n=17$ ) and RA in Remission ( $n=13$ ) were used to evaluate  $\text{MerTK}^{\text{pos}}\text{FOLR2}^{\text{pos}}$  STMs; from healthy ( $n=9$ ), active RA ( $n=17$ ) and RA in Remission ( $n=12$ ) to evaluate  $\text{MerTK}^{\text{pos}}\text{TREM2}^{\text{pos}}$  STMs; and Healthy ( $n=9$ ), active RA ( $n=14$ ) and RA in Remission ( $n=9$ ) to evaluate  $\text{MerTK}^{\text{pos}}\text{LYVE2}^{\text{pos}}$  STMs. **b**, Synovial tissue from Healthy ( $n=8$ ), active RA ( $n=13$ ) and RA in Remission ( $n=7$ ) were used to evaluate  $\text{MerTK}^{\text{neg}}\text{CD48}^{\text{pos}}$ ,  $\text{MerTK}^{\text{neg}}\text{S100A12}^{\text{pos}}$  and  $\text{MerTK}^{\text{neg}}\text{CLEC10a}^{\text{pos}}$  STMs; and from Healthy ( $n=7$ ), active RA ( $n=12$ ) and RA in Remission ( $n=7$ ) to evaluate  $\text{MerTK}^{\text{neg}}\text{SPP1}^{\text{pos}}$  STMs.

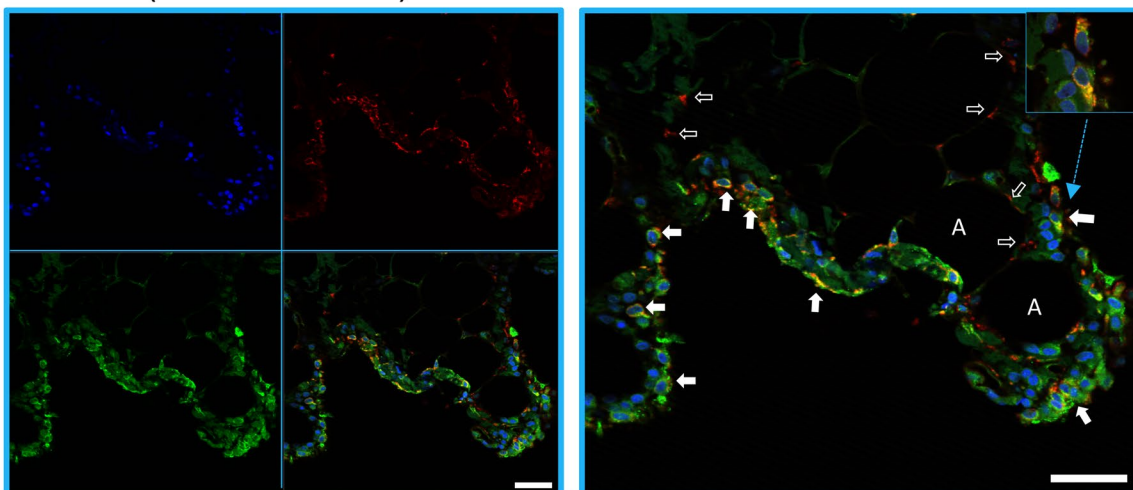
## a Healthy (TREM2/CD68/Nuclei)



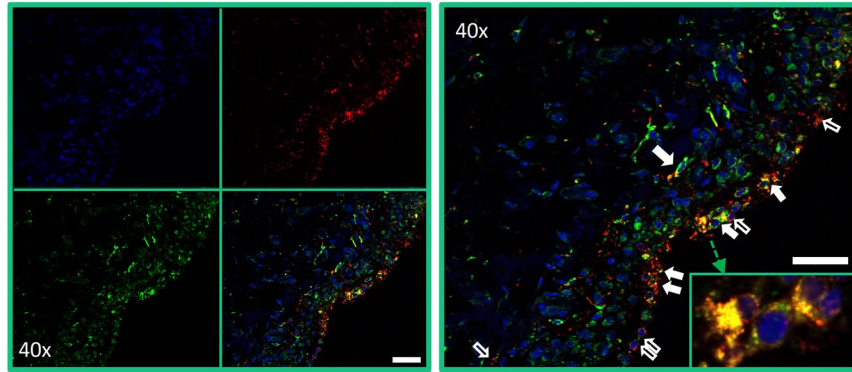
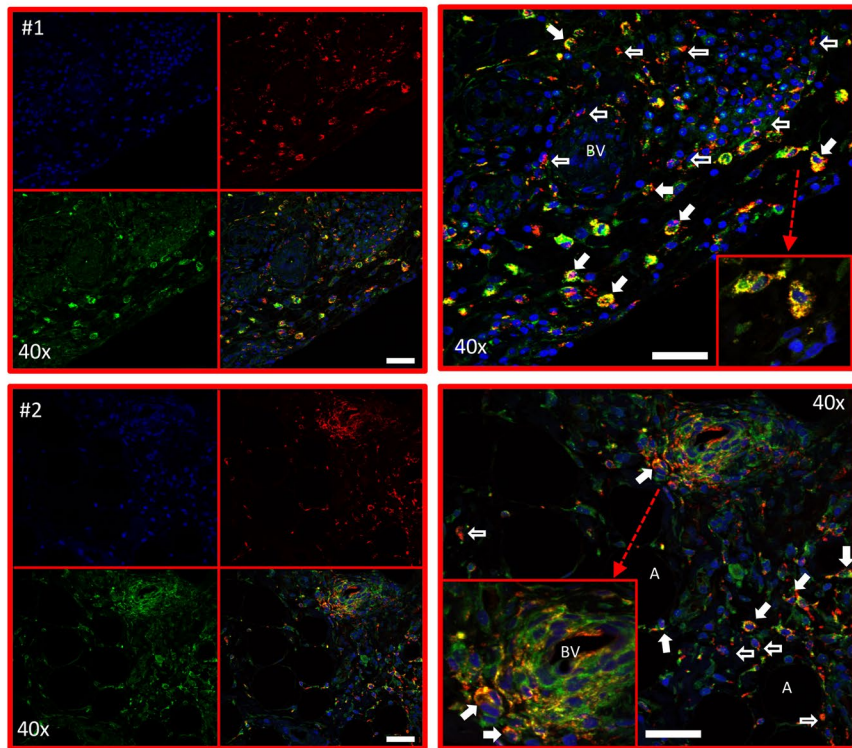
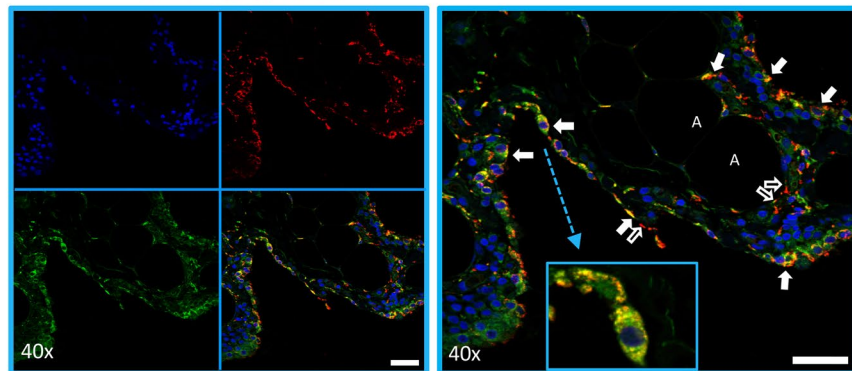
## b Active (TREM2/CD68/Nuclei)



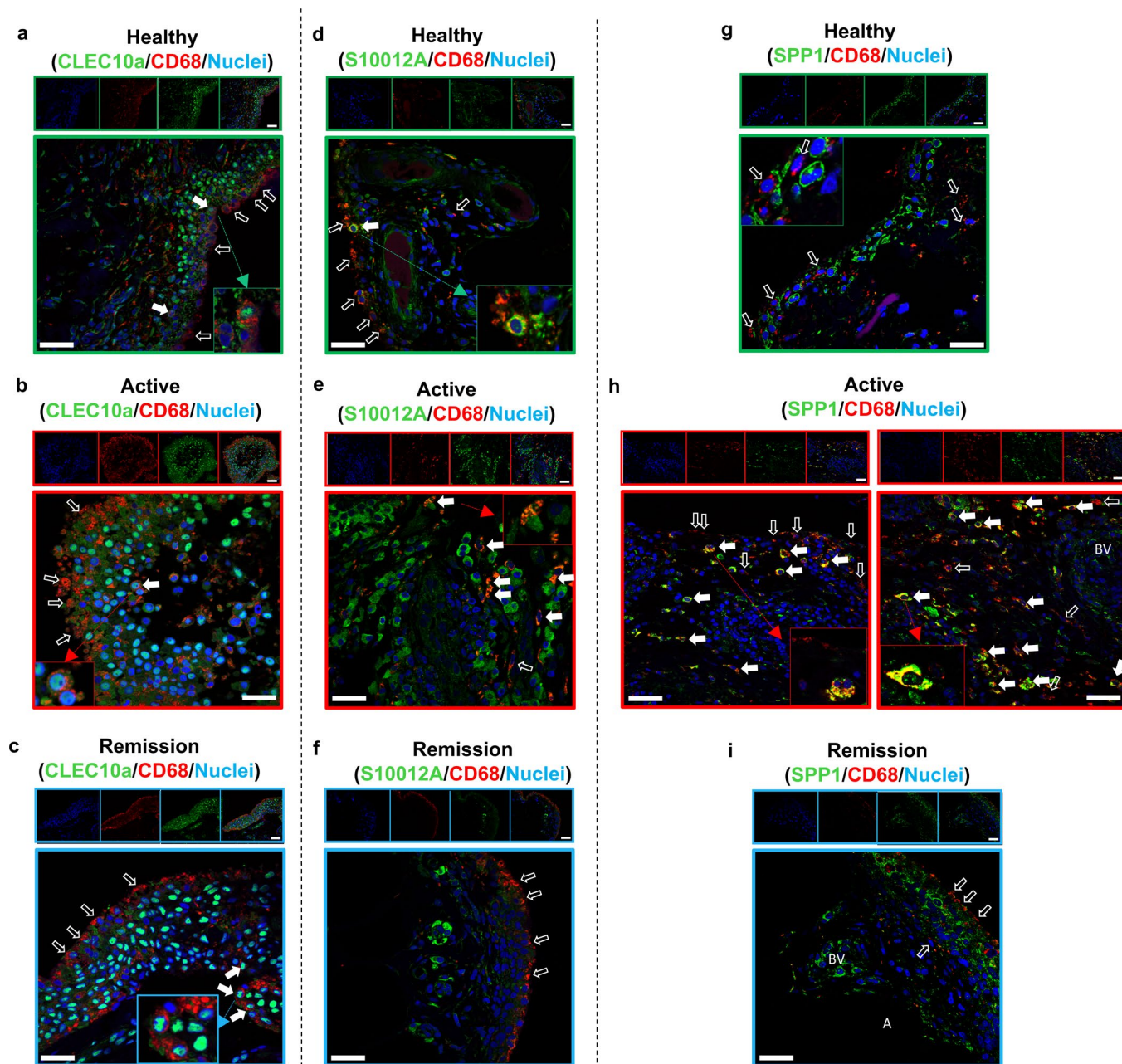
## c Remission (TREM2/CD68/Nuclei)



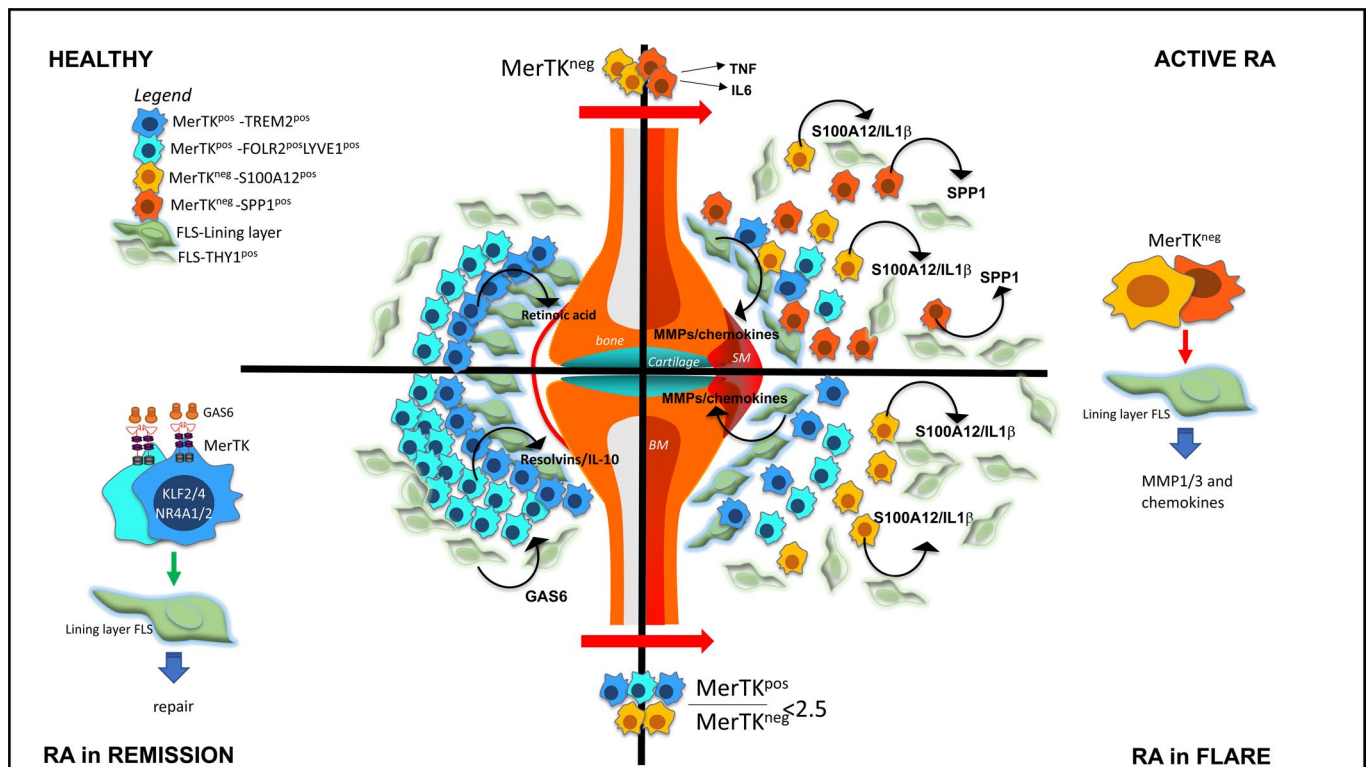
**Extended Data Fig. 7 | TREM2<sup>pos</sup> STMs form a lining-layer in the healthy synovium and in the synovium from RA patients in sustained disease remission.** Representative confocal microscopy images (40 $\times$ ) showing IF staining for TREM2 (green) and macrophage marker CD68 (red) in (a) healthy synovium (b) active RA synovium, and (c) remission RA synovium. These show TREM2<sup>pos</sup>CD68<sup>pos</sup> (solid white arrows) and TREM2<sup>neg</sup>CD68<sup>pos</sup> (hollow white arrows) macrophages. The inset images show TREM2<sup>pos</sup>CD68<sup>pos</sup> cells at higher magnification. Nuclei are stained with DAPI (blue). A, adipocyte. Images representative of synovial tissue of healthy donors (n=5), active RA (n=6) and remission RA (n=6) obtained in 3 independent experiments with similar results are shown. Scale bars = 50  $\mu$ m.

**a Healthy (LYVE1/CD68/Nuclei)****b Active (LYVE1/CD68/Nuclei)****c Remission (LYVE1/CD68/Nuclei)**

**Extended Data Fig. 8 | LYVE1<sup>pos</sup> STMs locate mainly in the synovial lining-layer in health and in remission RA, and predominantly in the interstitium in active RA.** Representative confocal microscopy images (40x) showing IF staining for LYVE1 (green) and macrophage marker CD68 (red) in **(a)** healthy synovium **(b)** active RA synovium (two different patients), and **(c)** remission RA synovium. These show LYVE1<sup>pos</sup>CD68<sup>pos</sup> (solid white arrows) and LYVE1<sup>neg</sup>CD68<sup>pos</sup> (hollow white arrows) macrophages. The inset images show LYVE1<sup>pos</sup>CD68<sup>pos</sup> at higher magnification. Nuclei are stained with DAPI (blue). A, adipocyte; BV, blood vessel. Images representative of synovial tissue of healthy donors (n=5), active RA (n=6) and remission RA (n=6) obtained in 3 independent experiments with similar results are shown. Scale bars = 50 μm.



**Extended Data Fig. 9 | CLEC10a<sup>pos</sup>, S100A12<sup>pos</sup> and SPP1<sup>pos</sup> STMs are located predominantly in the synovial interstitium.** **a–c**, Representative confocal microscopy images (40×) showing IF staining for CLEC10a (green) and macrophage marker CD68 (red) in **(a)** healthy synovium **(b)** active RA synovium, and **(c)** remission RA synovium. These show CLEC10a<sup>pos</sup>CD68<sup>pos</sup> (solid white arrows) and CLEC10a<sup>neg</sup>CD68<sup>pos</sup> (hollow white arrows) macrophages, and CLEC10a<sup>pos</sup>CD68<sup>neg</sup> cells that are not macrophages. Inset images show CLEC10a<sup>pos</sup>CD68<sup>pos</sup> macrophages at higher magnification. **d–f**, Synovial S10012A<sup>pos</sup> STMs are scarce in healthy and remission RA but abundant in the sublining layer in active RA. Representative confocal microscopy images (40×) showing IHC staining for S10012A (green) and macrophage marker CD68 (red) in **(d)** healthy synovium **(e)** active RA synovium, and **(f)** remission RA synovium. These show S10012A<sup>pos</sup>CD68<sup>pos</sup> (solid white arrows) macrophages only in active RA. S100A12A<sup>neg</sup>CD68<sup>pos</sup> (hollow white arrows) macrophages and S100A12A<sup>pos</sup>CD68<sup>neg</sup> cells are located throughout the synovial tissue. Inset images show S10012A<sup>pos</sup>CD68<sup>pos</sup> macrophages at higher magnification. **g–i**, Synovial SPP1<sup>pos</sup> STMs are scarce in healthy and remission RA but abundant in the sublining layer in active RA. Representative confocal microscopy images (40×) showing IF staining for SPP1 (green) and macrophage marker CD68 (red) in **(g)** healthy synovium, **(h)** active RA synovium (two patients), and **(i)** remission RA. These show SPP1<sup>pos</sup>CD68<sup>pos</sup> (solid white arrows) macrophages and SPP1<sup>neg</sup>CD68<sup>pos</sup> (hollow white arrows) macrophages. Inset images show SPP1<sup>pos</sup>CD68<sup>pos</sup> macrophages at higher magnification. The nuclei are stained with DAPI (blue). Images representative of synovial tissue of healthy donors (n=5), active RA (n=6) and remission RA (n=6) obtained in 3 independent experiments with similar results are shown. A, adipocyte; BV, blood vessel. Scale bars = 50 μm.



**Extended Data Fig. 10 | Distinct synovial tissue macrophage subsets regulate inflammation and remission in rheumatoid arthritis.** The **HEALTHY** synovial membrane (SM) contains predominantly MerTK<sup>pos</sup> STMs with two subpopulations: TREM2<sup>pos</sup> and LYVE1<sup>pos</sup>. Their transcriptomics suggest immunoregulatory functions, *for example* production of retinoic acid. In **ACTIVE RA**, the synovial membrane is infiltrated by MerTK<sup>neg</sup>CD48<sup>pos</sup> STMs with two main phenotypes, expressing either S100A alarmins and IL-1 $\beta$ , or osteopontin (SPP1); both are the main source of pathogenic TNF and IL-6, and potent contact-dependent inducers of chemokines and MMPs from synovial fibroblasts (FLS). **RA in REMISSION** is characterized by restoration of MerTK<sup>pos</sup>TREM2<sup>pos</sup> and MerTK<sup>pos</sup>LYVE1<sup>pos</sup> subpopulations. Their transcriptome is characterized by MerTK-dependent transcription factors that are negative-regulators of inflammation. They are low producers of pro-inflammatory cytokines; further downregulated by locally-produced GAS6. Instead they produce resolvins and induce a repair response in FLS. Their relative proportion in remission was indicative of flare after treatment cessation. When the proportion of MerTK<sup>pos</sup> STMs becomes less than 47.5%, (or the ratio of MerTK<sup>pos</sup> to MerTK<sup>neg</sup> becomes less than 2.5) there is a likelihood of **FLARE** after treatment cessation. MerTK<sup>neg</sup> STMs in patients predicted to flare have a CD48<sup>pos</sup>S100A12<sup>pos</sup> phenotype that releases the alarmin S100A12 upon stimulation, suggesting a role in the initiation of flare. BM bone marrow; MMPs, matrix metalloproteinases; KLFs krueppel like factors; NR4As, nuclear receptor subfamily 4 group A; ATF3, cAMP-dependent transcription factor 3; TREM2, triggering receptor expressed on myeloid cells 2; LYVE1, lymphatic vessels endothelial hyaluronan receptor 1; FOLR2, folate receptor beta; GAS6, growth arrest-specific 6; S100A12, S100 calcium-binding protein A12; THY1, CD90.

## Reporting Summary

Nature Research wishes to improve the reproducibility of the work that we publish. This form provides structure for consistency and transparency in reporting. For further information on Nature Research policies, see our [Editorial Policies](#) and the [Editorial Policy Checklist](#).

### Statistics

For all statistical analyses, confirm that the following items are present in the figure legend, table legend, main text, or Methods section.

n/a Confirmed

- The exact sample size ( $n$ ) for each experimental group/condition, given as a discrete number and unit of measurement
- A statement on whether measurements were taken from distinct samples or whether the same sample was measured repeatedly
- The statistical test(s) used AND whether they are one- or two-sided  
*Only common tests should be described solely by name; describe more complex techniques in the Methods section.*
- A description of all covariates tested
- A description of any assumptions or corrections, such as tests of normality and adjustment for multiple comparisons
- A full description of the statistical parameters including central tendency (e.g. means) or other basic estimates (e.g. regression coefficient) AND variation (e.g. standard deviation) or associated estimates of uncertainty (e.g. confidence intervals)
- For null hypothesis testing, the test statistic (e.g.  $F$ ,  $t$ ,  $r$ ) with confidence intervals, effect sizes, degrees of freedom and  $P$  value noted  
*Give  $P$  values as exact values whenever suitable.*
- For Bayesian analysis, information on the choice of priors and Markov chain Monte Carlo settings
- For hierarchical and complex designs, identification of the appropriate level for tests and full reporting of outcomes
- Estimates of effect sizes (e.g. Cohen's  $d$ , Pearson's  $r$ ), indicating how they were calculated

*Our web collection on [statistics for biologists](#) contains articles on many of the points above.*

### Software and code

Policy information about [availability of computer code](#)

#### Data collection

IF image acquisition was done with Zeiss LSM 880 confocal microscope.  
Cells for phenotyping were acquired with Flow cytometry: BD FACSAria III high speed cell sorter with FACSDiva (v8.0.3)  
scRNAseq was performed with scRNAseq 10xGenomics (Chromium controller is GCG-SR-1) and scRNAseq BD Rhapsody Express (633702).  
qPCR data were acquired with 7900 HT TaqMan reader.  
Ultrasound machine used for guided biopsies was Mylab Twice (Esaote).

#### Data analysis

10x Genomics scRNAseq data analysis, including read alignment and generation of count matrices, were performed using the Cell Ranger (2.1) pipeline. Raw base call files (BCL) generated by sequencing were demultiplexed into FASTQ files per sample. The "cellranger count" tool mapped the reads against the Human genome (hg19) and performed UMI counting. QC, Filtering, Integration and Clustering was performed in The Seurat package (3.0.1) in R. Differentially expressed genes were found with MAST package in R. Pathway analysis was performed with StringDB (<https://string-db.org/>) and IPA (v 01-12).  
scRNAseq BD Rhapsody data were analyzed with BD Genomics Rhapsody Analysis Pipeline CWL and The Seurat package (3.1.2) in R. Flow cytometry data were analyzed with FlowJo software version 10.3.0 (Tree Star Inc, OR, USA) and Cytobank ([www.cytobank.org](http://www.cytobank.org)). Confocal microscopy data were analyzed with Zeiss zen black software.  
Statistical analysis of the data other than scRNAseq was performed in Prism version 8.2.1 or in IBM SPSS version 20.0.

For manuscripts utilizing custom algorithms or software that are central to the research but not yet described in published literature, software must be made available to editors and reviewers. We strongly encourage code deposition in a community repository (e.g. GitHub). See the Nature Research [guidelines for submitting code & software](#) for further information.

## Data

Policy information about [availability of data](#)

All manuscripts must include a [data availability statement](#). This statement should provide the following information, where applicable:

- Accession codes, unique identifiers, or web links for publicly available datasets
- A list of figures that have associated raw data
- A description of any restrictions on data availability

Ranked lists of the STM cluster markers (i), condition-specific markers of MerTKpos STM clusters identified by comparison of two clinical conditions (ii), multiple conditions (iii), STM cluster pathway analysis (iv), FLS cluster markers (v), and DEGs of lining layer FLS clusters comparing active and remission synovium (vi) are provided in the Supplementary DataSets.

The list of genes in the custom stromal panel (vii), sample scRNAseq metrics of FLS co-cultured with STM and sequenced with scRNAseq BD Rhapsody system (viii), and the list of DEGs from FLS-MoM co-cultured with MerTK inhibitor (ix) are provided in the Supplementary DataSets.

All raw and processed data of STM scRNAseq, STM-FLS co-culture scRNAseq and MoM-FLS co-culture bulk RNAseq (FLS) were deposited at EMBL-EBI and are available with the following accession numbers: E-MTAB-8322, E-MTAB-8873 and E-MTAB-8316. The Seurat objects and codes used (Jupyter notebook) are available from the corresponding authors upon reasonable request.

## Field-specific reporting

Please select the one below that is the best fit for your research. If you are not sure, read the appropriate sections before making your selection.

- Life sciences       Behavioural & social sciences       Ecological, evolutionary & environmental sciences

For a reference copy of the document with all sections, see [nature.com/documents/nr-reporting-summary-flat.pdf](https://www.nature.com/documents/nr-reporting-summary-flat.pdf)

## Life sciences study design

All studies must disclose on these points even when the disclosure is negative.

### Sample size

No statistical methods were used to predetermine sample size for scRNAseq (n=5-6 patients/per group). We used a pragmatic choice of sample numbers based on the numbers used in the emerging clinical scRNAseq data set literature, for example Villani et al Science 2017. In addition, in the absence or appropriate preliminary data for a power analysis, we designed our study to include discovery and validation scRNAseq patient cohorts to confirm findings (Extended Data Figure 2). All conclusions derived from single-cell sequencing data were subject to subsequent robust validation by flow cytometry and IHC/IF. Below are the exact n numbers for scRNAseq and validation studies.

All synovial tissue samples were obtained from patients with Rheumatoid Arthritis using minimally invasive Ultrasound guided technique at the SYNGem Biopsy unit of the Division of Rheumatology at the Fondazione Policlinico Universitario A. Gemelli IRCCS – Università Cattolica del Sacro Cuore in Rome, Italy. All synovial tissue from healthy donors were obtained from the University of Glasgow from patients attending arthroscopy for meniscal tear or cruciate ligament damage, with normal synovium (MRI and macroscopically).

FACS phenotyping of STMs was performed after fresh synovial tissue biopsies digestion with Liberase (described in Methods) from discrete patient cohorts stratified based on disease phase (n=45 naive to treatment, n=31 resistant to treatment and n=36 in sustained remission respectively). Comparison cohorts were processed with the same protocol (described in Methods) including 10 healthy donors. Phenotyping was performed in at least 22 independent experiments.

For single cell RNA-seq experiments 17 synovial tissues of RA patients (n=5 treatment-naive, n=6 treatment-resistant n=6 in sustained remission, respectively), 4 patients with Undifferentiated Peripheral Arthritis and 4 Healthy controls (described in Methods) were used in the study in 5 independent experiments.

For validation of scRNAseq identified STM clusters with Immune-histochemistry / immuno-fluorescence experiments, 12 synovial tissues of RA patients (n=6 with active disease and n=6 in sustained remission) (described in Methods) and 5 healthy controls were used in 3 independent experiments.

For validation of scRNAseq identified STM clusters by flow cytometry synovial tissues from healthy (n=9), active RA (n=14-17) and remission (n=9-12) were used in at least 16 independent experiments.

For fibroblast-like synoviocytes (FLS) and MerTK/CD206neg and MerTK/CD206pos STM co-culture experiments (n=6), 6 synovial tissues of RA patients (n=3 with active disease and n=3 in sustained remission, respectively) and FLS from 5 RA patients (described in Methods) were used in 3 independent experiments;

For FLS in vitro co-culture with monocyte-derived macrophages experiments, 9 synovial tissue of RA patients (described in Methods) were used in at least 3 independent experiments in 5 independent experiments

To assess the production of GAS6 by FLS in vitro, 15 synovial tissue from RA patients (n=5 naive to treatment, n=5 treatment resistant and n=5 in sustained remission, respectively), were used in 5 independent experiments.

### Data exclusions

We pre-established quality criteria for the samples to be included in the analysis of scRNAseq data. These included 50k reads per cell and number of sequenced macrophages ~500 per sample. Two samples out of 27 did not meet these criteria. Sample SA139 was removed due to low sequencing depth in the macrophages. SA225 was removed due to low number of sequenced macrophages (140). This is described in the



Methods and illustrated in Supplementary Table 4 and Supplementary Fig.8. Similarly in Flow cytometry validation of scRNAseq data, tissues with less than 500 synovial tissue macrophages were excluded from quantitative data analysis.

Replication	We had Discovery and Validation cohorts in scRNAseq experiment with showed similar data. Cell types detected in the synovial tissue were highly reproducible across patients. scRNAseq findings were validated by flow cytometry, IF and functional studies. All In vitro experiments were repeated more than 3 times and showed similar data.
Randomization	The experiments were not randomized. We continued or discontinued the treatment of RA patients in remission based on patients' written consent.
Blinding	The investigators assessing the clinical outcome after treatment discontinuation in RA patients in sustained remission were blinded on the STMs distribution at the time of treatment schedule modification.

## Reporting for specific materials, systems and methods

We require information from authors about some types of materials, experimental systems and methods used in many studies. Here, indicate whether each material, system or method listed is relevant to your study. If you are not sure if a list item applies to your research, read the appropriate section before selecting a response.

### Materials & experimental systems

n/a	Involved in the study
<input type="checkbox"/>	<input checked="" type="checkbox"/> Antibodies
<input checked="" type="checkbox"/>	<input type="checkbox"/> Eukaryotic cell lines
<input checked="" type="checkbox"/>	<input type="checkbox"/> Palaeontology and archaeology
<input checked="" type="checkbox"/>	<input type="checkbox"/> Animals and other organisms
<input type="checkbox"/>	<input checked="" type="checkbox"/> Human research participants
<input checked="" type="checkbox"/>	<input type="checkbox"/> Clinical data
<input checked="" type="checkbox"/>	<input type="checkbox"/> Dual use research of concern

### Methods

n/a	Involved in the study
<input checked="" type="checkbox"/>	<input type="checkbox"/> ChIP-seq
<input type="checkbox"/>	<input checked="" type="checkbox"/> Flow cytometry
<input checked="" type="checkbox"/>	<input type="checkbox"/> MRI-based neuroimaging

## Antibodies

### Antibodies used

Antibodies used for synovial tissue IHC and fluorescent IHC:  
 IgG2a mouse anti human CD68 (clone L26, at 1.2 ug/ml, Leica Biosystem)  
 IgG2a mouse anti-human CD68 (clone 514H12; antibody at 6.7ug/ml) (Leica Biosystem).  
 IgG rabbit anti-human MerTK (clone Y323, Abcam ab205718, dilution 1/1000),  
 Rabbit IgG polyclonal Cy3-coniugated anti-human MerTK, clone 5770, bs-0548R-Cy3, dilution 1/100, (BIOSS)  
 Secondary conjugated antibody fluorescein isothiocyanate (FITC) conjugated goat anti-mouse IgG H&L, #ab6785, (Abcam, dilution 1/1000).

Primary antibodies used to map distinct SMTs in human synovial tissue:  
 Rabbit Anti- human -LYVE1 (1:200 dilution, cat HPA042953/Sigma). This is polyclonal Abs.  
 Rat anti-human -TREM2 (1:50 dilution, cat Ab86491/Abcam plc). This is polyclonal Abs.  
 Rabbit anti-human CLEC10A (1:100 dilution, cat Ab197346/Abcam plc). This is polyclonal Abs.  
 Rabbit anti-human S100A12/ CGRP (1:100 dilution, catAb196740/Abcam plc). This is polyclonal Abs.  
 Rabbit anti-human Osteopontin (SPP1) (1:100 dilution, catAb8448/Abcam plc). This is polyclonal Abs.  
 Mouse anti-human CD68 (1:40 dilution, clone PG-M1, catM087629-2/ Dako).

Secondary antibodies used to map distinct SMTs in human synovial tissues:  
 A-11008/ Goat anti-Rabbit IgG Alexa Fluor 488 (1:100) A-11008/ Goat anti-Rat IgG Alexa Fluor 488 (1:100)  
 A-21055/ Goat anti-Mouse IgG Alexa Fluor 660 (1:100).These are all polyclonal Abs from ThermoFisher Scientific.

Antibodies used for STM phenotyping and STMs/FLS sorting:  
 Brilliant Violet 711 anti-human CD45 Antibody (dilution 1:100, clone HI30, cat 304050/ Biolegend)  
 Alexa Fluor 700 anti-mouse/human CD11b (dilution 1:100, clone M1/70, cat 101222/ Biolegend)  
 Brilliant Violet 510 anti-human CD64 (dilution 1:100, clone 10.1, cat 305028/ Biolegend)  
 Brilliant Violet 421 anti-human CD206 (MMR) (dilution, 1:100, clone 15.2, cat321126/Biolegend) ,  
 Brilliant Violet 785 anti-human HLA-DR (dilution 1:100, clone L243, cat307642/Biolegend)  
 PE anti-human MERTK (dilution 1:100, clone 590H11G1E3, cat 367608/Biolegend)  
 PerCP/Cy5.5 anti-human CD163 (dilution 1:100, clone RM3/1, cat 326512/ Biolegend)  
 APC anti-human Folate Receptor-b (dilution 1:500, clone 94b, cat391706/ Biolegend)  
 PE-Cy7 recombinant-human TREM2 (dilution 1:100, clone 2B5, catNPB1-07101/ Novus)  
 FITC anti-human CD15 (SSEA-1) dump channel (dilution 1:100, clone W6D3, cat323004/ Biolegend)  
 FITC antihuman CD19 dump channel (dilution 1:100, clone HIB19, cat302206/ Biolegend)  
 FITC anti-human CD117 (c-kit) dump channel (dilution 1:100, clone 104D2, cat313232 Biolegend)  
 FITC antihuman CD3 dump channel (dilution 1:100, clone UCHT1, cat300440 Biolegend)  
 FITC anti-human CD56 (NCAM) dump channel (dilution 1:100, clone Mem-188, cat 304604/Biolegend)  
 FITC anti-human CD1c dump channel (dilution 1:100, clone L161, cat 331518/Biolegend)  
 FITC anti-human CD20 dump channel (dilution 1:100, clone 2H7, cat302304/Biolegend)

FITC anti-human CD21 dump channel (dilution 1:100, clone Bu22, cat354910/Biolegend)  
 PE-Cy7-anti-human TIM4 (dilution 1:100, clone 9F4, cat 354005/Biolegend)  
 APC-anti-human Podoplanin (dilution 1:100, clone NZ 1.3, cat 17-9381-42/Life Technologies)  
 Antibodies used for validation of scRNAseq STM clusters with FACS:  
 PE anti-human MerTK (1:100 cat. n.#367608, clone 590H11G1E3, Biolegend)  
 PE/Cy7 Ant-human TREM-2 (2B5) (1:100 cat. n.#NBP1-07101PECY7, clone 2B5, Novus Biologicals)  
 Alexa Fluor 405 LYVE-1 Antibody (ALY7) (1:50 cat. n.#NBP1-43411AF405, clone ALY7, Novus Biologicals)  
 PE/Cy7 anti-human MerTK (1:100 cat. n.#367610, clone 590H11G1E3, Biolegend)  
 PE anti-human CD301 (CLEC10A) (1:100 cat. n.#354704, clone H037G3, Biolegend)  
 Biotin anti-human CD9 (1:500 cat. n.#312112, clone HI9a, Biolegend)  
 Brilliant Violet 421 Streptavidin (1:100 cat. n.#405226, Biolegend)  
 APC anti-human Folate Receptor b (FR-b) (1:200 cat. n.#391706, clone 94b, Biolegend)  
 PE-CF594 Mouse anti-human CD48 (1:100 cat. n.#562717, clone TU145, BDBiosciences)

#### Validation

All antibodies used in this study are commercially available. They have been used in the essays (Flow, IHC/IF) according with manufacturer design detailed in the data-sheets. They have been appropriately validated by manufacturers for a given application and this information is provided on their website and product information data-sheets easily accessible with the catalog number provided in the box above. In addition, all antibodies described here have been further optimized for an appropriate concentration by testing several dilutions and the positivity of the signal controlled by FMO and isotype controls on human tonsil tissues or synovial tissues or monocyte-derived macrophages.

## Human research participants

Policy information about [studies involving human research participants](#)

#### Population characteristics

All synovial tissue samples were obtained from patients with Rheumatoid Arthritis using minimally invasive Ultrasound guided technique at the SYNGem Biopsy unit of the Division of Rheumatology at the Fondazione Policlinico Universitario A. Gemelli IRCCS – Università Cattolica del Sacro Cuore in Rome, Italy. All synovial tissue from healthy donors were obtained from the University of Glasgow from patients attending arthroscopy for meniscal tear or cruciate ligament damage, with normal synovium (MRI and macroscopically). Demographics, clinical and immunological characteristic of different patients' cohorts used in this study are described in Methods and Supplementary Tables. We recorded the following clinical parameters: disease duration expressed in years, disease activity scores (DAS28) and disease in remission duration expressed in years. We recorded the following immunological parameters: sero-positivity and plasma titers of anti-citrullinated peptides antibodies and IgA/IgM Rheumatoid factor. All patients were sero-positive.

#### Recruitment

Human subjects selection for this study was based on identification of patients with Rheumatoid Arthritis or Undifferentiated Peripheral Inflammatory Arthritis undergoing a clinically indicated synovial tissue biopsy procedure who had provided signed informed consent for bio-specimen storage and research use. Patients meeting these criteria were included regardless of age, gender, ethnicity and race. There was no bias in recruitment and this was not a clinical trial.

#### Ethics oversight

All protocols were reviewed and approved by the Institutional Review Board (IRB) at the Università Cattolica del Sacro Cuore, Rome, Italy (6334/15) and by the West of Scotland Research Ethics Committee, Glasgow, UK (19/WS/0111).

Note that full information on the approval of the study protocol must also be provided in the manuscript.

## Flow Cytometry

### Plots

Confirm that:

- The axis labels state the marker and fluorochrome used (e.g. CD4-FITC).
- The axis scales are clearly visible. Include numbers along axes only for bottom left plot of group (a 'group' is an analysis of identical markers).
- All plots are contour plots with outliers or pseudocolor plots.
- A numerical value for number of cells or percentage (with statistics) is provided.

### Methodology

#### Sample preparation

Synovial tissue biopsies were first digested with Liberase at 0.15ug/ml, 0.78 Wunsch units/ml;TM Research Grade, Roche Diagnostics, 00000005401127001, Sigma)at 37°C, 5% CO<sub>2</sub> in a humidified atmosphere for 30-45min rotating on a Miltenyi MACSmix tube-rotator). Cell were then centrifuged at 1800rpm for 10min, resuspended and washed with FACS buffer, and transferred to FACS tubes (BD Biosciences) in a final volume of 3ml FACS buffer (PBS/2%FSC/2mMEDTA). An 80µl aliquot was set aside for live-dead gating (unstained cells). To the rest of the cells, Fixable Viability Dye eFluorTM 780 (eBioscience) was added at 1:1000 in PBS and incubated for 20min at 4°C. Cells were then washed with FACS buffer. Four tubes were labelled: a) unstained, b) live-dead marker only c) Fluorescence Minus One Control (FMO) tube, FMO minus FITC, where cells were stained with antibodies specific for STM but not FITC-antibodies against all other lineage-positive cells d) cells stained with antibodies against STMs and FITC-antibodies against any unwanted lineage. Staining was performed in a final volume of 500µl with antibody dilution 1/100 for 30min on ice. All antibodies are listed in Supplementary Fig.7a. Cells were washed

twice with FACS buffer and resuspended in a final volume of 500µl, filtered through an Easy Strain 100µm cell-strainer and analyzed or sorted with the use of FACS ARIAll sorter (BD Bioscience). Synovial tissue macrophages were gated based on their membrane expression of CD45, CD64, CD11b, and HLA-DR after all other cell lineages (FMO-FITC gating) and cell-doublers were excluded (dump channel). FMO-FITC cells were used to set up a gate to exclude unwanted lineage-positive cells (dump channel). The expression of MerTK, CD163 and CD206 were evaluated on gated CD64posCD11bposHLA-DRpos STMs. List of antibodies and gating strategy is presented in Supplementary Fig.7b-d. Similar approach was used to validate STM cluster found in scRNAseq. We developed antibody panels 1 and 2 (presented in Supplementary Table 8), which were used in conjunction with dump panel antibodies (Supplementary Fig.7a). The clusters were defined in each individual patient by panel 1 and/or panel 2 using FlowJo software (Tree Star Inc, OR, USA). Samples with less than 500 STM acquired were excluded from quantitative data analysis. In addition, the CD64+CD11b+HLADR+ population from each sample was exported and concatenated to make one .fcs file per subject group. These .fcs files were uploaded to Cytobank ([www.cytobank.org](http://www.cytobank.org)) where the viSNE dimensionality reduction algorithm was applied. This allowed for the visualisation of the changes in clusters' distribution between different conditions using the Cytobank software.

Instrument

BD FACSAria™ Flow Cytometer, Serial number P64828200209 Configuration number 51205

Software

BD FACSDiva Version 8.0.1, and Microsoft Windows 7 used for the collection of data while FlowJo software version 10.3.0 (Tree Star Inc, OR, USA) and Cytobank ([www.cytobank.org](http://www.cytobank.org)) were used for data analysis.

Cell population abundance

The abundance of STMs in total synovial tissue digest is ~2-3%. Purity of STMs after sorting was ~100% as evaluated by the recall of the sorted samples.

Gating strategy

Synovial tissue macrophages were gated based on their membrane expression of CD45, CD64, CD11b, and HLA-DR after all other cell lineages (FMO-FITC gating) dead cells, cell-doublers were excluded (via live-Dead marker, FSC-A vs FSC-W plot and dump channel). FMO-FITC cells were used to set up a gate to exclude unwanted lineage-positive cells (dump channel). The expression of MerTK, CD163 and CD206 were evaluated on gated CD64posCD11bposHLA-DRpos STMs. List of antibodies and gating strategy is presented in Supplementary Fig.7b-d. Similar approach was used to validate STM cluster found in scRNAseq. We developed antibody panels 1 and 2 (presented in Supplementary Table 8), which were used in conjunction with dump panel antibodies (Supplementary Fig.7a). The clusters were defined in each individual patient by panel 1 and/or panel 2 using FlowJo software (Tree Star Inc, OR, USA). The gating strategy is presented in Extended Data Fig. 4. Samples with less than 500 STM acquired were excluded from quantitative data analysis. In addition, the CD64+CD11b+HLADR+ population from each sample was exported and concatenated to make one .fcs file per subject group. These .fcs files were uploaded to Cytobank ([www.cytobank.org](http://www.cytobank.org)) where the viSNE dimensionality reduction algorithm was applied. This allowed for the visualisation of the changes in clusters' distribution between different conditions using the Cytobank software.

Tick this box to confirm that a figure exemplifying the gating strategy is provided in the Supplementary Information.